โครงสร้างและสมบัติของพอลิเมอร์อิเล็กโทรไลต์ชนิดแข็ง:
ระบบพอลิ(เอธิลีนออกไซด์)/พอลิ(เอธิลีนไกลคอล)/เกลือ

นางสาว จิตติมา เชาว์ดำรงสกุล

STRUCTURES AND PROPERTIES OF SOLID POLYMER ELECTROLYTES: POLY(ETHYLENE OXIDE)/POLY (ETHYLENE GLYCOL)/SALTS SYSTEMS

Miss Jittima Chaodamrongsakul

A Thesis Submitted in Partial Fulfillment of the Requirements

for the Degree of Master of Science in Chemistry

Suranaree University of Technology

Academic Year 2003

STRUCTURES AND PROPERTIES OF SOLID POLYMER ELECTROLYTES: POLY(ETHYLENE OXIDE)/POLY (ETHYLENE GLYCOL)/SALTS SYSTEMS

Suranaree University of Technology has approved this thesis submitted in partial fulfillment of the requirements for the Master's Degree

Thesis Examining Committee

....

(Asst. Prof. Dr. Malee Tangsathitkulchai)

Chairperson

....

(Asst. Prof. Dr. Visit Vao-Soongnern)

Member (Thesis Advisor)

....
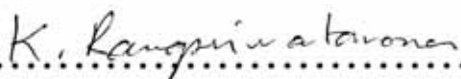
(Asst. Prof. Dr. Kunwadee Rangsriwatananon)

Member

....
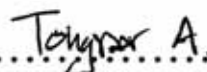
(Asst. Prof. Dr. Anan Tongraar)

Member

....
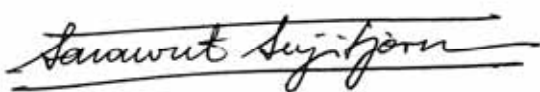
(Assoc. Prof. Dr. Sarawut Sujitjorn)

Vice Rector for Academic Affairs

....

(Assoc. Prof. Dr. Prasart Suebka)

Dean of the Institute of Science

จิตติมา เชาว์ดำรงสกุล: โครงสร้างและสมบัติของพอลิเมอร์อิเล็กโทรไลต์ชนิด
แข็ง: ระบบพอลิ(เอธิลีนออกไซด์)/พอลิ(เอธิลีนไกลคอล)/เกลือ
(STRUCTURES AND PROPERTIES OF SOLID POLYMER
ELECTROLYTES: POLY(ETHYLENE OXIDE)/POLY(ETHYLENE
GLYCOL)/SALTS SYSTEMS)
อาจารย์ที่ปรึกษา: ผศ. ดร. วิสิษฐ์ แววสูงเนิน, 161 หน้า ISBN 974-533-291-7

การวิจัยพอลิเมอร์อิเล็กโทรไลต์ชนิดแข็ง (SPEs) สำหรับประยุกต์เป็นวัสดุเก็บพลังงาน
ชนิดใหม่ได้ศึกษาโดยการทดลอง การคำนวณเชิงทฤษฎีและการจำลองแบบโมเลกุล ระบบที่ศึกษา
คือแผ่นฟิล์มพอลิเอธิลีนออกไซด์อิเล็กโทรไลต์ที่มีองค์ประกอบจากพอลิเอธิลีนออกไซด์/พอลิเอธิ
ลีนไกลคอล/เกลือ (PEO/PEG/salt) โดยพอลิเอธิลีนออกไซด์ พอลิเอธิลีนไกลคอลและเกลือทำหน้า
ที่เป็นพอลิเมอร์หลัก พลาสติไซเซอร์ และประจุไอออนตามลำดับ ตัวอย่างฟิล์มของระบบ
xPEO/PEG/LiCF$_3$SO$_3$ หรือ KSCN เมื่อ x แปรค่าจาก 4 ถึง 20 เตรียมได้จากเทคนิคการฉาบสาร
ละลาย เทคนิคที่ใช้ศึกษาโครงสร้างและสมบัติของระบบนี้คือ ดิฟเฟอเรนเชียลสแกนนิงคาลอริ
มิเตอร์ (DSC) เอกซเรย์ดิฟแฟรกชัน (XRD) ฟูเรียร์แทรนส์ฟอร์มอินฟราเรดสเปกโทรสโกปี
(FT-IR) และเครื่องวัดความต้านทาน DSC และ XRD แสดงให้เห็นว่าเปอร์เซ็นต์ความเป็นผลึกลด
ลงในระบบพลาสติไซ การนำไฟฟ้าที่อุณหภูมิห้องเพิ่มขึ้นจาก 1.33x10^{-8} ซีเมนต์ต่อเซนติเมตร (15
เปอร์เซ็นต์โดยน้ำหนักของ PEG) เป็น 2.15x10^{-8} ซีเมนต์ต่อเซนติเมตร (100 เปอร์เซ็นต์โดยน้ำหนัก
ของ PEG) ค่าการนำไฟฟ้านี้สูงขึ้นมากกว่าระบบ PEO/salt ที่ไม่ได้พลาสติไซ พลาสติไซเซอร์จะมี
บทบาทต่อการเร่งการแตกตัวของเกลือและเพิ่มความเข้มข้นของตัวพาประจุ

ทฤษฎีไอโซเมอร์เชิงโครงรูป ซึ่งตั้งอยู่บนพื้นฐานของอุณหพลศาสตร์เชิงสถิติได้นำมาใช้ตี
ความและทำความเข้าใจสมบัติเชิงโครงรูปของพอลิเมอร์ สมบัติเชิงโครงรูปที่คำนวณได้พบว่าสอด
คล้องกับผลการทดลอง ความสัมพันธ์ระหว่างการนำไฟฟ้าเชิงไอออนต่อความเข้มข้นของเกลือได้
ศึกษาจากวิธีเชิงทฤษฎีโดยใช้แบบจำลองเอนโทรปีเชิงโครงรูปของอดัม-กิบส์ นอกจากนี้ยังนำแบบ
จำลองอุณหพลศาสตร์เชิงโมเลกุลจากพื้นฐานของทฤษฎีฟลอรี-ฮักกินส์เพื่อแสดงแผนภูมิวัฏภาค
ของ PEO/LiCF$_3$SO$_3$ และกำหนดจุดยูเทคติกของระบบนี้

สาขาวิชาเคมี   ลายมือชื่อนักศึกษา ....จิตติมา เชาว์ดำรงสกุล...............
ปีการศึกษา 2546   ลายมือชื่ออาจารย์ที่ปรึกษา ....

JITTIMA CHAODAMRONGSAKUL: STRUCTURES AND PROPERTIES OF SOLID POLYMER ELECTROLYTES: POLY (ETHYLENE OXIDE)/POLY(ETHYLENE GLYCOL)/SALTS SYSTEMS THESIS ADVISOR: ASST. PROF. DR. VISIT VAO-SOONGNERN, Ph.D., 161 PP. ISBN 974-533-291-7

The research in solid polymer electrolytes (SPEs) for an application as novel energy storage materials was performed by experimental, theoretical and molecular modeling approaches. The system of interest was the plasticized Poly(ethylene oxide), PEO based electrolyte film of various compositions PEO/Poly(ethylene glycol), PEG/salt where PEO, PEG and salt acted as a polymer host, plasticizer and ionic charge, respectively. The film samples from the system xPEO/PEG/ $LiCF_3SO_3$ or KSCN, where x was varied from 4 to 20 were prepared by solution casting technique. Differential Scanning Calorimeter (DSC), X-Ray Diffraction (XRD), Fourier Transform Infrared Spectroscopy (FT-IR) and high resistance meter were employed to study the structures and properties of these materials. Both DSC and XRD indicated a decrease in the percent of crystallinity for the plasticized system. Room temperature conductivity increased from 1.33×10^{-8} S cm^{-1} (15 %wt PEG) to 2.15×10^{-8} S cm^{-1} (100 %wt PEG). The conductivity was much higher than in similar PEO/salt systems that were not plasticized. The plasticizer seemed to play a catalytic role in dissociating salt and increasing the carrier concentration.

The Rotational Isomeric State (RIS) theory based on statistical thermodynamics was employed to interpret and to understand polymer conformational dependent properties. From calculated results, the conformational dependent properties were in reasonable agreement with experimental findings. The dependence of ionic conductivity on salt concentration was investigated theoretically by using Adam-Gibbs configurational entropy model. In addition, a molecular thermodynamic model based on Flory-Huggins theory gave the predicted phase diagram of $PEO/LiCF_3SO_3$ and the eutectic point of this system was identified.

School of Chemistry   Student's Signature ... Jittima Chaodamrongsakul ...

Academic Year 2003   Advisor's Signature .... Visit Vsw ...

ACKNOWLEDGMENT

First of all, I would like to express my sincerest thanks to my thesis advisor Assist. Prof. Dr. Visit Vao-soongnern for his guidance and for making many extensive and valuable comments throughout the entire thesis. I am also very thankful for his patience in reading the thesis and especially for his constant encouragement, which always kept me going, and for his support throughout the writing of the thesis.

In addition, I am very grateful to the thesis examining committee for their valuable help and many helpful suggestions. I also would like to thank Assoc. Prof. Dr. Saowanee Rattanaphani for aluminum plate for coat sample. A deep gratitude is extended to all staffs at the Center for Scientific and Technological Equipment for their scientific advice, assistance and service on the XRD, FT-IR and DSC. I would like to thank the Department of Polymer Engineering for assistance and service on the high resistance meter. I would also like to thanks all members in Department of Chemistry whom I have shared this experience with, who have shared their knowledge and made this a fun time. Our friendship has been an unexpected and wonderful gift. Especially, members in Computational Chemistry research group for their timely help and support me with available computer and printer. Last, but certainly not least, I am deeply grateful to my parents for their support, understanding, encouragement, and love.

Jittima Chaodamrongsakul

CONTENTS

CONTENTS (CONTINUED)

CONTENTS (CONTINUED)

CONTENTS (CONTINUED)

LIST OF TABLES

LIST OF TABLES (CONTINUED)

LIST OF FIGURES

LIST OF FIGURES (CONTINUED)

LIST OF FIGURES (CONTINUED)

LIST OF FIGURES (CONTINUED)

LIST OF FIGURES (CONTINUED)

LIST OF FIGURES (CONTINUED)

LIST OF ABBREVIATIONS

SPEs	Solid polymer electrolytes
PEG	Poly(ethylene glycol)
PEO	Poly(ethylene oxide)
$LiCF_3SO_3$	Lithium trifluoromethanesulfonate
Tf or triflate	Trifluoromethanesulfonate
KSCN	Potassium Thiocyanate
PC	Propylene carbonate
EC	Ethylene carbonate
XRD	X-Ray Diffraction
DSC	Differential Scanning Calorimeter
FT-IR	Fourier Transform Infrared
NMR	Nuclear Magnetic Resonance
RIS	Rotational Isomeric State
MM	Molecular Mechanics
VTF	Vogel-Tammann-Fulcher
σ	Ionic conductivity
$S\ cm^{-1}$	Siemen/centimeter
I	Current
V	Voltage
R	Resistance

LIST OF ABBREVIATIONS (CONTINUED)

T_g	Glass transition temperature
T_m	Melting temperature
$\langle r^2 \rangle_o$	Mean square unperturbed end-to-end distance
$\langle r^2 \rangle_o / nl^2$	Characteristic ratio
C_n	Characteristic ratio
$\langle s^2 \rangle_o$	Mean-square radius of gyration
$\langle s^2 \rangle_o / nl^2$	Mean-square unperturbed radius of gyration ratio
$\langle \mu^2 \rangle_o / nm^2$	Mean-square unperturbed dipole moment
t	Trans
g^+	Gauche$^+$
g^-	Gauche$^-$
Z	Conformational partition function
U	Statistical weight matrix
$E_i(\phi_i)$	Single bond energy
$\langle \ldots \rangle$	Ensemble average for all possible conformations
G	Super generator matrix
I	Identity matrix
$\otimes$	Direct product
θ	Bond angle

LIST OF ABBREVIATIONS (CONTINUED)

ϕ	Torsion angle
$[\eta]$	Intrinsic viscosity
η_{rel}	Relative viscosity
η_{red}	Reduced viscosity
η_{inh}	Inherent viscosity
$\overline{W}$	Probability for cooperative rearrangement
$\Delta\mu$	Potential energy hindering the cooperative rearrangement per monomer unit
S_c	Configurational entropy at temperature T
S_c^*	Critical configurational entropy $\left(\approx k_B \ln 2\right)$
k_B	Boltzmann constant
SV_j	Specific volume of component j
MW_j	Molecular weight of component j
r_1	Relative molar volume of component 1; $r_1 = 1$ for salt
r_2	Relative molar volume of component 2; $r_2 = SV_2 MW_2 /\left(SV_1 MW_1\right)$
λ_s	Degree of specific interactions between salt ions and the base group in polymer

LIST OF ABBREVIATIONS (CONTINUED)

ϕ_i	Volume fraction of component i
χ_{FH}	Flory-Huggins interaction parameter
ΔH_m	Heat of melting
% wt	Percent weight
K	Degree Kelvin
°C	Degree Celcius
Å	Angstrom
et al.	et alia (and other)

CHAPTER I

INTRODUCTION

The rapid development of portable electronic devices and electric/hybrid vehicles has increased the demand for compact, lightweight, high capacity batteries. Polymers are widely studied due to their significant potential as Solid Polymer Electrolytes (SPEs) for an application as a medium in rechargeable batteries. Wright first reported that SPEs exhibit significant ionic conductivity (Wright, 1975). The potential use of SPEs in batteries applications was first suggested by Armand (Armand et al., 1979).

SPEs consist of salts dissolved in solid high molecular weight polymer. These compounds are solid state coordination compounds and as such sit between coordination chemistry and conventional solid state chemistry. Polymer, which can dissolve salt must be comprise of O, N or S atoms because these atoms can interact with cation, and make decompositive salt to have a better ionic conductivity.

Poly(ethylene oxide) (PEO) is the most interesting base material because of its high chemical and thermal stability. PEO can also solvate a wide variety of salts, even at very high salt concentrations (Bruce, 1995; Preechatiwong et al., 1996; Chintapalli, 1996; Mendolia et al., 1995; Quartarone et al., 1998; Song et al., 1999). The solvation of salts occurs through the association of the metallic cations with the oxygen atoms in the backbone. Although PEO has been by far the most common systems studied, several other polymers or copolymer are regarded as possible fruitful alternatives.

Examples include poly(propylene oxide) (PPO), poly(vinyl chloride) (PVC), polyether-urethanes and many more. However, none of these appears to have the same ability to solvate salts as PEO (Johansson, 1998).

Pure PEO is a semicrystalline polymer, possessing both an amorphous and a crystalline phase at room temperature. The multi-phase nature of PEO is most often regarded as a major problem in real working systems, since the ionic conduction has been shown to take place mainly in the amorphous phase. Furthermore, the same is true for the study of specific properties, where the effect of a variable can be concealed by the changes in the relative amounts of each phase.

Many investigations have been done to reduce the crystalline content, via various approaches such as using blends, copolymers, comb-branch polymers and cross-linked polymer networks (Mendolia et al., 1995; Quartarone et al., 1998; Song et al., 1999; Sukeshini et al., 1998). The most dramatic improvement in the ionic conductivity of SPEs, with reduction of their crystalline content, is the addition of a low molecular weight or plasticizer. Plasticizer can result in greater ion dissociation which allows greater numbers of charge carriers for ionic transport. In several previous studies (Song et al., 1999; Sukeshini et al., 1998), the ionic conductivity of SPEs was increased by the addition of low-molecular-weight poly(ethylene glycol), (PEG), which has the same repeating unit as PEO. PEG gives a higher conductivity due to a lower viscosity and a higher concentration of hydroxyl groups. Both features help to enhance the mobility of the ions, to reduce crystallinity, to decrease the glass transition temperature (T_g) and the activation energy for ion conduction. In addition, it helps to increase the proportion of amorphous region and consequently enhance the conductivity. From these reason, PEG is selected as a plasticizer.

It is commonly accepted that the knowledge about the polymer conformation should contribute to an understanding of the ion-polymer interaction which plays an important role to ion conduction mechanism in SPEs. Theoretical studies based on statistical thermodynamics have been extensively performed for macromolecules in order to interpret and to understand their physical properties which strongly depend on the spatial arrangement of chain molecules. The Rotational Isomeric State (RIS) theory is an excellent calculation technique to predict the conformation-dependent physical properties of polymeric chains. The theory assumes that each skeletal bond has a small number of discrete rotational states and considers interactions between atoms on a chain separated by only a small number of bonds (short-range interactions). Interaction appearing upon a rotation around a single bond and two consecutive bonds is called *the first-order interaction* and *the second-order interaction*, respectively. These interactions are then parameterized and grouped into the matrix called *the statistical weight matrix*. Then the conformation-dependent physical properties can be computed from these statistical weight matrices. The most frequently calculated properties are the mean-square end-to-end distance $\langle r^2 \rangle_0$, the characteristic ratio (C_n) and the mean-square radius of gyration $\langle s^2 \rangle_0$.

Thermal and electrical behavior of PEO-salt systems can be better understood by characterization of the crystalline and amorphous phases presented in the complex. The construction of phase diagrams has been quite useful in understanding the conductivity, stability and mechanical properties over a wide range of compositions and temperature. Stainer et al. (1984) and Robitaille et al. (1987) constructed the phase diagram for the PEO/NH$_4$SCN system and PEO/NaSCN system. In addition to

derive a phase diagram from an experiment, theoretical models can also be employed to explain the phase diagram characteristics. A molecular thermodynamic model based on an extended Flory-Huggins theory which consider both ion-polymer interactions and ion-ion interactions is used to interpret the liquidus curves in the resulting phase diagram of polymer/salt systems (Kim et al., 1999). Adam and Gibbs analyzed the WLF-type (Williams, Landel and Ferry) behavior in terms of configurational entropy, using some simplified arguments. The Adam-Gibbs configurational entropy model is generally used for describing the dependence of conductivity (σ) on temperature. Kim and coworker (Kim et al., 1998) established the phase diagrams of PEO/MnBr$_2$, PEO/MnI$_2$ and compared their experimental results with the developed thermodynamic model.

In this research work, we will study the effect of adding PEG on the structure and ionic conductivity of SPEs based on PEO host polymer at various plasticizer content and salt concentrations. The study will involve experiment, molecular modeling and theory.

Research Objectives

1. To develop the Rotational Isomeric State (RIS) model capable of describing the conformational characteristics of PEO and compare their conformation-dependent properties with those obtained from experiment.

2. To study the effect of adding salt on the structures, crystallinity and ionic conductivity in PEO complex.

3. To study the effect of adding plasticizer (PEG) on the structures and ionic conductivity in PEO/PEG/salt complexes.

Scope and Limitation of the Studies

 Experimental Part

In this research work, structures and properties of thin film based on PEO/PEG/salts complexes at various salt concentrations and percent plasticizer will be investigated. The experimental techniques employed in this study were as follows:

- Viscometry: to determine the intrinsic viscosity.

- Nuclear Magnetic Resonance (NMR) Spectroscopy: to study the structures and dynamics of PEO chain in solution with and without salt.

- Fourier Transform Infrared Spectroscopy (FT-IR): to monitor an ionic association and to study the interaction between PEO and salt.

- X-Ray Powder Diffraction (XRD): to characterize crystallinity structure of sample.

- Differential Scanning Calorimeter (DSC): to obtain the melting point, percent crystallinity and to construct the phase diagram of this material.

- Conductivity measurement: to determine the ionic conductivity.

Computational and Theoretical Part

The RIS model will be employed to predict the conformational dependent properties of PEO such as mean-square end-to-end distance $\langle r^2 \rangle_o$, characteristic ratio (C_n) and mean-square radius of gyration $\langle s^2 \rangle_o$, by using statistical weight matrices as input. The elements of the matrices can be estimated from the conformational energy calculations for small representative segment of polymer molecules by Molecular Mechanics (MM) calculation.

The theoretical treatment for this work is composed of two main parts. First, the Adam-Gibbs configurational entropy model will be modified to predict the dependency of an ionic conductivity on salt concentration. Second, an extended Flory-Huggins theory will be employed to correlate the phase behavior of this complex.

CHAPTER II

LITERATURE REVIEW

2.1 Solid Polymer Electrolyte (SPEs)

Solid Polymer Electrolytes (SPEs) consist of salts dissolved in solid high molecular weight polymer. Polymer, which can dissolve salt must be comprise of O, N or S atoms because these atoms can interact with cation, and make decompositive salt to have a better ionic conductivity. A considerable scientific effort has been dedicated to exploring and understanding the characteristics of these electrolyte systems. Many investigations have focused on developing SPEs with high ionic conductivities (10^{-3} S cm^{-1} or higher) at ambient temperature. In majority of reported systems (Chintapalli, 1996; Bruce, 1995), an alkali or alkaline earth metal salt is solubilized in polymer, generally through complex formation with ion-chelating monomer units or with pendant moieties of the macromolecule. One of the earliest example involved complexes of alkali salts with poly(ethylene oxide) (PEO) studied in detail by Wright and co-workers (Fenton et al., 1973; Wright, 1975). However, it was particularly Armand and co-worker who pointed out and explored the usefulness of ion-conducting polymer electrolytes in high energy density storage device (Armand et al., 1979).

Two general types of polymer electrolytes have been intensively investigated, SPEs and polyelectrolytes. A typical SPEs consists of a coordinating polymer, usually

a polyether, in which a salt, e.g. LiClO$_4$, is dissolved (Figure 2.1a). Both anions and cations can be mobile in these types of electrolytes. By contrast, polyelectrolytes contain charged groups, either cations or anions, covalently attached to polymer, Figure 2.1(b), so only the counterion is mobile.

Several advantages result from replacing the aqueous electrolytes of conventional batteries with SPEs. First, polyethers have good chemical stability and are generally unreactive with lithium, which is a very attractive battery anode because of its high reducing power and low equivalent weight. Second, SPEs can be used as thin layer, thus, the battery volume and weight devoted to the electrolyte are decreased. In addition, their mechanical properties are very attractive: Polymer electrolytes are deformable, flexible, and easily fabricated by conventional manufacturing processes. The typical polymer-based battery is a layered thin-film structure in which a thin polymer electrolyte (~20-50 mm thick) is sandwiched between a lithium anode and an intercalation cathode (e.g., V$_6$O$_{13}$) (Figure 2.2). The entire cell can be produced as a continuous tape and can be rolled or folded into its finished shape (Mendolia et al., 1995).

(a) (b)
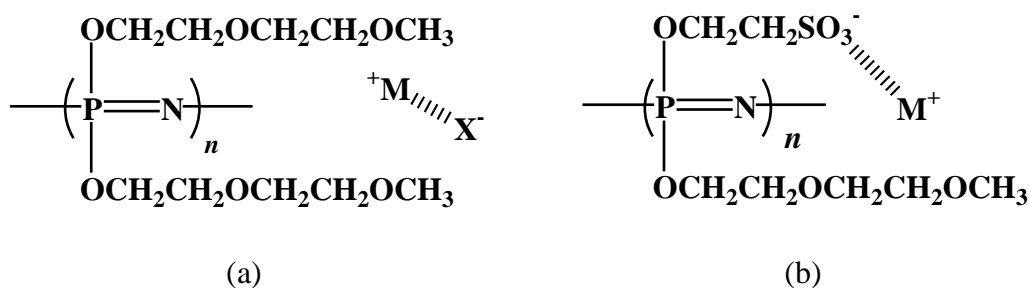
Figure 2.1 Example system to illustrate the contrast between (a) SPEs containing a salt MX and (b) polyelectrolyte in which the anion is attached to the polymer (Bruce, 1995).
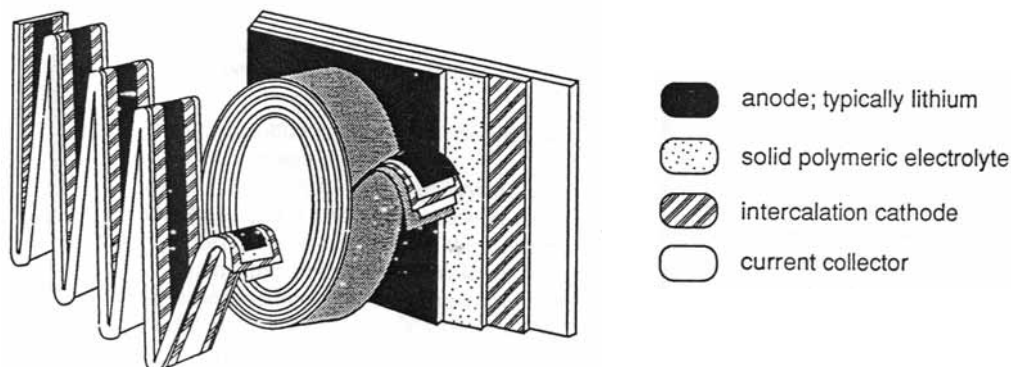
Figure 2.2 Schematic of polymer-based batteries. The thin-film composites are very flexible and can be folded or rolled into various geometries (Mendolia et al., 1995).

When salt is dissolved into polymer matrix, solid polymer electrolyte, SPE, is formed. To make these SPEs, the salts used are often of low-lattice energy and the polymer matrix must be polar, at least locally. The free energy change of dissolving a salt can be written:

$$\Delta G_m \quad = \quad \Delta H_m - T\Delta S_m \tag{2.1}$$

where $\Delta G_m \langle \; 0$ denotes to a spontaneous reaction. The mixing entropy, ΔS_m, consists of two main components: translational entropy and configurational entropy. The introduction of salt reduces the freedom of the polymer chain motion, *via* the formation of cation-polymer bonds, and therefore causes a reduction in translational entropy. The flexibility of the polymer on the other hand, provides the possibility to adopt several conformations suitable for multidentate cation

coordination which may contribute with a positive configurational entropy. At first, it was believed that the total entropy of solvation was always likely to be positive. However, SPEs have been observed to behave in an opposite way to most liquid electrolytes as a function of temperature. Salt precipitation has been observed when increasing the temperature, an indication of a negative entropy contribution to the solvation. The mixing enthalpy, ΔH_m, includes the starting components, lattice energies, the coulombic ion-ion interaction energy and the ion solvation energy. A spontaneous solvation, *i.e.* a negative ΔG_m, often requires a salt of low lattice energy which can be overcome by the ion-solvent interactions. In an ideal SPE, the dissolved cations bind electrostatically to the polymer backbone and the anions are believed to diffuse more or less freely in the matrix. In non-ideal materials ion-pairs or more complex species might form (Figure 2.3).

This is also a general goal in the search for good SPEs - high transport numbers for the cation being of primary importance, local cell concentrations are avoided to ensure a high ionic conductivity. The ion conduction mechanisms of the anion and cation clearly differ; the anion diffuses more or less freely, while the cation is believed to "hop" between polymer chains and between "hops" use the segmental motion of the polymer while temporarily bonded. The possible conformations of the polymer in the cation-polymer complexes locally obtained are of importance for the solvation as stated above in Eq. (2.1), as well as for the cation conduction mechanism.
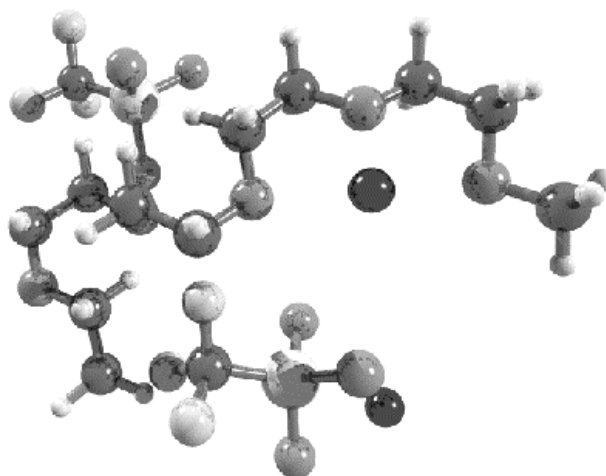
Figure 2.3 Schematic representation of possible local interactions in a polymer electrolyte.

2.2 Poly(ethylene oxide), PEO

Intial investigations of ionically conductive polymers were principally focused on poly(ethylene oxide), PEO. PEO can dissolve at room temperature in many common solvents such as acetonitrile, dichloromethane, carbon tetrachloride, tetrahydrofuran and benzene. The strong interaction between high-molecular-weight PEO and inorganic salts was first reported more than 20 years ago (Fenton et al., 1973), and it is now know that PEO can solvate a wide variety of salts, even at very high salt concentrations. The solvation of salts occurs through the association of the metallic cations with the oxygens in the polyether backbone (Figure 2.4). The solvated ions can be quite mobile in the polymeric solvent, and thus give rise to significant bulk ionic conductivities.
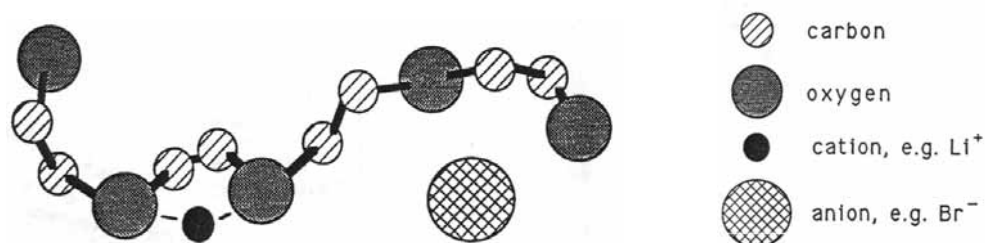
Figure 2.4 Solvation of a salt by a PEO chain. The primary interaction is between the ether oxygens and the cation.
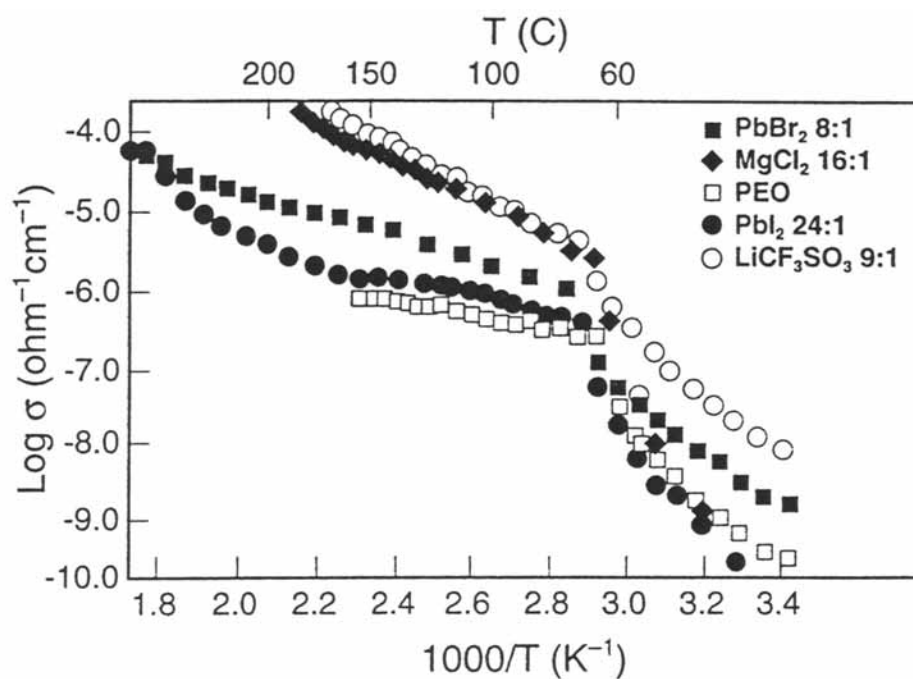
Figure 2.5 Conductivities of various PEO-based electrolytes containing divalent cations. The composition of each system is indicated as a molar ratio of polymer repeat units to salt. The Knee in the curves at around 60°C is attributed to the melting of crystalline PEO (Mendolia et al., 1995).

Pure PEO is a semicrystalline polymer, possessing both an amorphous and a crystalline phase at room temperature. Significant ionic transport occurs only within the amorphous phase. This feature explains the dramatic decrease in ionic conductivity seen in many PEO-based systems for temperatures below the melting point of pure crystalline PEO ($T_m \sim 66°C$) (Figure 2.5); the crystalline PEO regions are non-conductive and serve to hinder bulk ionic transport. Clearly, the inherent crystallinity of PEO is not very attractive for applications in solid electrolytes.

The use of PEO relies on the solvating power of the -CH_2CH_2O- units and its high chemical and thermal stability. PEO itself is stable up to 350°C in the absence of O_2 (Jones et al., 1990). The PEO polymer chain is highly flexible, *i.e.* it contains no double bonds, and it can therefore coordinate various alkali-metal, alkaline-earth-metal, transition-metal and lanthanide ions in a remarkably tight fashion by the ether oxygens' electron lone pairs (Bruce et al., 1993). The concentration of the electron lone pairs ($\sim 10^{22}$ cm^{-3}) and the polarisability of the ether groups gives it properties resembling those of water (Baril et al., 1997). However, when acting as a ligand the coordination strength of the polyether might be expected to be enhanced due to the multidentate nature and the flexibility of the polymer chain. Several low energy conformations can be adopted, exact appearances and relative amounts depending on the cation coordinated.

However, the flexibility, which clearly governs some of the highly desirable properties of this polymer, does have the disadvantage that PEO based systems are prone to crystallization (Takahashi et al., 1973), which is prominent in pure PEO, and reaches a crystallinity maximum of ~ 95 % for $M_w = 6000$ Daltons (Brown et al., 1982). Above this M_w the long range disorder entanglement efficiently prevents the

same magnitude of crystallization. The multi-phase nature of PEO is most often regarded as a major problem in real working systems, since the ion conduction has been shown to take place mainly in the amorphous phase (Berthier et al., 1983). Furthermore, the same is true for the study of specific properties, where the effect of a variable can be concealed by the changes in the relative amounts of each phase.
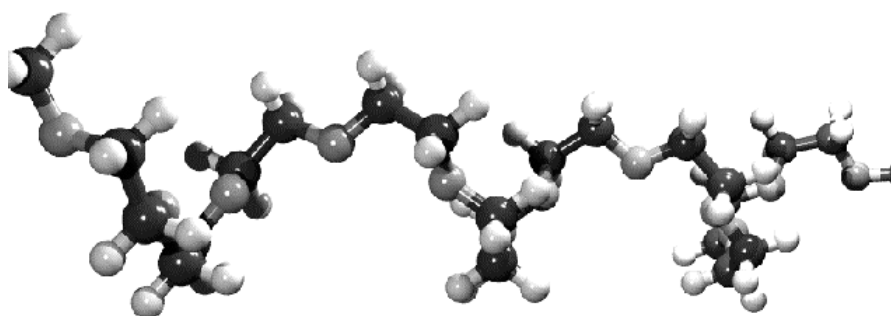
Figure 2.6 PEO viewed perpendicular to the crystalline helix.

Several crystal structures of alkali-metal complexes $MXPEO_n$ have been determined, all with high salt concentrations (n = 3, 4) (Chatani et al., 1987; Lightfoot et al., 1992; Chatani et al., 1990; Lightfoot et al., 1994; Thomson et al., 1996) and also the crystal structure of long chain PEO itself (Takahashi et al., 1973). All crystallise in helical structures, with the geometry and chain conformation varying both depending on the nature of the cation and anion. Some general tendencies are evident from these studies; the anion never interacts directly with the polymer chain in any of these structures, nor does any cation coordinate to more than one PEO helix strand. No cation has a higher coordination number (CN) than 7 and for lithium CN is equal to 5.

However, little is known of the "structure" in the amorphous phase; a notable exception is the study of amorphous $LiCF_3SO_3PEO_3$ by Frech (Frech et al., 1997). This is especially true for lower salt concentrations (higher O/M ratios), which more closely resemble real working systems. For these most of the structural work has been done indirectly using vibrational spectroscopy (Berson et al., 1995; Wendsjo et al., 1992) and NMR (Berthier et al., 1983; Johansson et al., 1992).

2.3 Salts

When review the field of SPEs, the dominant use of lithium salts is obvious. The reason is the proposed use of these salts in all solid-state thin-film batteries where lithium provides the largest possible potential window. Also it is the lightest of all metals, providing high gravimetric Coulombic density despite the low transition number of one electron per lithium atom. For the reaction:

$$2Li \quad + \quad F_2 \quad \leftrightarrow \quad 2LiF$$
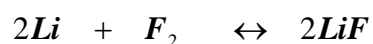
the cell voltage is theoretically $\sim$ 6 V (Aylward et al., 1994). In practice other components than F_2 are used, but still a cell voltage above 3 V is easily reached. The anode, previously often pure lithium metal, now is often a carbon-based intercalation compound which prevents some mortal phenomena to occur i.e. dendrite growth of lithium which would result in a short-circuit. Lithium is the obvious choice of cation, although work considering sodium have also received attention (Doeff et al., 1995).

The ionic conductivity, σ, for a dilute homogenous system at a given temperature, can generally be expressed as:

$$\sigma \;=\; \sum n_i q_i \mu_i \tag{2.2}$$

where n_i is the number of charge carriers i, q_i their charge and μ_i their mobility. The ionic conductivity should thus increase with salt concentration, if all dissolved species were to carry charge at the same rate as for lower concentrations. However, this is not true in SPEs as increasing the concentration leads to formation of neutral ion-pairs which are insensitive to the applied field (reduced n_i) and in addition higher aggregates, *e.g.* triplets, although charged, should move slower due to their higher mass. At the same time, the cations that coordinate the ether oxygens of the polymer chains cause the polymer chains to "stiffen". This decreases the number of free sites along the chains available for further coordination, which decreases μ_i. Furthermore, Eq. (2.2) is valid when the system is dilute.

One way to enhance the ionic conductivity, is by using anions that do not easily form ion-pairs, which results in a large number of solvated charge carriers, even at modest concentrations. The salt used still must have a low enough lattice energy to fulfill Eq. (2.1).

The charge density of the anion should be low to reduce the number of ion-pairs with lithium. The ion conductivity increases for a given cation (*i.e.* lithium) in the series (Bakker, 1995).

$$F^- < Cl^- < Br^- < I^- < ClO_4^- < CF_3SO_3^- \text{ (triflate)} < [(CF_3SO_2)_2N]^- \text{ (TFSI)}$$

Because of the need for even more non-coordinating anions the current attention is mainly focused on large anions with an extensively delocalised negative charge. These are in many cases derived from the triflate anion and their lithium salts provide even higher ionic conductivities.

2.4 Optimizing Polymeric Electrolytes

The previous discussion shows that unmodified PEO is not ideal polymer host for ambient-temperature solid electrolytes; for example, its crystalline nature alone is a great hindrance to ionic transport. In attempts to improve the performance of PEO-salt systems, researchers have sought alternate polymeric media based on the following criteria:

1. The polymer host should be completely amorphous because crystalline phases are nonconductive.

2. A polymer with a lower T_g should result in greater ionic mobilities at room temperature.

3. The system should promote a high level of salt dissociation so that the number of charge carriers is large.

4. The system should facilitate cationic transport.

5. The electrolyte should have good bulk mechanical properties.

In general, PEO-salt electrolytes have satisfactory mechanical properties, except at high temperature at which they begin to flow. Good mechanical properties in polymers can be ensured through several mechanisms: by keeping at least one component of the electrolyte below its T_g, by incorporating crystalline domains into the system, by the use of inert fillers, or by cross-linking the polymer. Clearly, methods of improving mechanical properties sometimes do so at the expense of ionic conductivity. The various polymeric electrolyte systems that have been investigated over the years can be divided into seven categories: (1) various simple homopolymers, (2) networks, (3) copolymers and comb-branch polymers, (4) polyelectrolytes, (5) polymer blends, (6) polymers with inert fillers and (7) plasticized polymers. In each category, some improvement over simple PEO-salt systems has been attained. The plasticized systems will be much more interest because these systems have been most successful in achieving significant conductivities at room temperature.

2.5 Enhancement conductivity of SPEs

Plasticized Systems

The most dramatic improvements in the ionic conductivity of polymer electrolytes have been achieved through the use of plasticizers. The conductivities were enhanced by producing systems with less crystallinity and lower glass-transition temperatures than found in simple PEO-salt systems. Plasticizers, in addition to reducing the crystalline content and increasing the polymer segmental mobility, can

result in greater ion dissociation, thus allowing large numbers of charge carriers for ionic transport; in addition, the cationic transport may be enhanced.

In several studies (Hardy et al., 1985; Spindler et al., 1986; Ito et al., 1987; Takeoka et al., 1991; Iwatsuki et al., 1992), the ionic conductivity of polymer electrolytes was increased by the addition of low molecular weight poly(ethylene glycol), PEG, which has the same repeat unit as PEO. The conductivity increases as the molecular weight of the PEG plasticizer decrease and as its content increase (Ito et al., 1987). The PEG aids in ionic transport mainly by reducing crystallinity and increasing the free volume of the system.

PEO-based electrolytes plasticized with PEG can possess extremely high conductivities, into the range of 10^{-3} S cm^{-1} at 25°C (Ito et al., 1987), but they are not practical for lithium battery applications because the hydroxy end groups of the PEG molecules react with lithium. To avoid this problem, researchers have eliminated the troublesome end groups of PEG by either lithiating them (Wahg et al., 1990) or replacing the hydroxy groups with less reactive methoxy ones (Kelly et al., 1985; Sandner et al., 1992). However, the resulting systems, though electrochemically stable, are about an order of magnitude less conductive.

2.6 General Concepts of Electrically and Ionically Conducting Polymers

The range of electrical conductivity in materials is one of the largest vibrations in any material property (Blythe, 1979). While one tend to regard polymers primarily as insulators, it has been recognized that polymer could be a conductive material even

at low level. The conductivity, σ, of material is defined by Duke and Gibson (1978) as in Eq. (2.3).

$$J = \underline{\sigma}E \tag{2.3}$$

where J is the steady-state current density in A cm^{-2} and induced by an applied electric field (E) in V cm^{-1}. Both J and E are vectors. As a consequence, $\underline{\sigma}$ is a tensor. By assuming that the induced current flows parallel to the imposed fields, Gutmann and Lyons (1976) and Duke and Gibson (1978) stated that a tensor, $\underline{\sigma}$, can be treat as a scalar and simply expressed as the general conduction process contributing from several types of charge carriers as Eq. (2.2).

Here, conductivity (σ) is the charge transport across a unit cross-sectional area per second per unit electric field applied. q_i is the charge on ith species having the concentration, or density, n_i per cubic centimeter and mobility of the μ_i. The latter parameter is the velocity which the carrier moves under unit electric field, i.e., under potential gradient of 1 volt cm^{-1}. It dimension is cm^2 volt^{-1} sec^{-1}. Therefore, the unit of conductivity is given as ohm^{-1} cm^{-1} or Siemen cm^{-1}, where Siemen = ohm^{-1}. High ionic conductivity is a result of ions being able to diffuse though an electrolyte medium. Since it is difficult for ions to move freely in a crystal lattice, electrolytes are rarely used below their melting, T_m, or glass transition, T_g, temperatures where ion mobility is hindered. The relationship of the conductivity of a homogeneous electrolyte can be described by an Arrhenius type equation called the Vogel-Tammann-Fulcher (VTF) Eq. (2.4).

$$\sigma(T) = A\exp\left(-E_a/(T - T_0)\right) \tag{2.4}$$

Here A is the pre-exponential factor and is related to the number of charge carriers and E_a is the apparent activation energy for ion transport. T_o is the temperature at which the conductivity is zero and is usually taken to be 50 K lower than T_m or T_g. The larger the difference between T_o and the use temperature, T, the higher the conductivity (Stowe, 2001).

Measuring Ionic Conductivity

Ohm's law, Eq. (2.5), describes the current (I) as a function of the applied voltage (V) and the resistance (R) of electrolyte.

$$R = \frac{V}{I} \tag{2.5}$$

Conductivity (σ) is directly related to Ohms in that σ (in S cm^{-1}) is defined as the reciprocal of resistivity (ρ) in Ω cm unit, as shown in Eq. (2.6).

$$\sigma = \frac{1}{\rho} \tag{2.6}$$

and

$$\rho \;=\; R\!\left(\frac{A}{l}\right) \tag{2.7}$$

Where A (in cm^2) is the area and l (in cm) is the length of the electrolyte sample. It follows then that

$$\rho \;=\; \frac{1}{RA} \tag{2.8}$$

In order to characterize the conductive properties of the electrolyte alone, it is necessary to minimize the resistive components of the electrode materials. In practice, electrodes of highly electronically conductive and inert material, such as stainless steel or platinum, are used in place of actual working electrode materials. Here, in the intercalation of ion and reactions with the electrode surface are minimized and hence, only the resistive components of the electrolyte are measured (Stowe, 2001).

2.7 Phase Diagrams

Thermal and electrical behavior of PEO-salt systems can be better understood by characterization of the crystalline and amorphous phases present in the complex. The construction of phase diagrams has been quite useful in understanding the behavior of these materials over a wide range of compositions and temperatures. At high temperature or in systems with no crystallization the ions are solvated by the polymer to form a homogeneous polymer-salt solution. However, in PEO-based

complexes crystallization occurs, leading to the formation of spherulites of well-defined PEO-salt stoichiometries. The amorphous regions within the spherulitic material often have a different stoichiometry and these electrolytes are therefore heterogeneous at room temperature. Phase diagrams have been established for a number of polymer electrolytes based on information obtained from Differential Scanning Calorimetry (DSC), optical microscopy, Nuclear Magnetic Resonance (NMR), X-Ray Diffraction (XRD) and conductivity studies. It is essential to know the microscopic structure and morphology of polymer electrolyte systems that form crystalline phases, as ionic conduction takes place only in the amorphous phase (Berthier et al., 1983). The characterization of phase behavior for the PEO-salt systems is qualitative as these systems often consist of several phases, which greatly influence their properties. While phase diagrams can be used to interpret the dependence of the conductivity on concentration and temperature. The relative amounts of each phase in turn depend on the type of polymer and salt used polydispersity and purity of the polymer, thermal history of the system and preparation procedures.

Due to the occurrence of crystallization kinetics in polymers at low temperatures, often it is only possible to approach of thermal equilibrium. Thus the determination of phase diagrams for the polymer-salt systems often becomes complicated. Amorphous phases coexist with crystalline phases and can dissolve salts up to a saturation limit, which may not appear in the phase diagram. The thermal history affects the nature of the crystal spherulites, which will be reflected in the phase-diagram. The presence of impurities such as water, solvent and low molecular weight fractions could also have a significant effect on the phase behavior. The phase

diagrams have to be therefore interpreted carefully. However, a general description of macroscopic structure upon cooling of an amorphous electrolyte can be sought from the phase diagram.

The phase diagrams for PEO-LiCF$_3$SO$_3$, PEO-LiClO$_4$, PEO-LiAsF$_6$, PEO-LiI and PEO-NaI systems have been reported by Fauteux and co-workers based on microscopy, x-ray diffraction, conductivity and DSC studies (Robitaille et al., 1986; Fauteux et al., 1987). All these systems show the presence of a eutectic and at least one salt-rich crystalline intermediate compound with n = 3 stoichiometry. The PEO-LiClO$_4$ and PEO-LiAsF$_6$ systems exhibit the formation of a second isomorphous, crystalline intermediate compound of n = 6 stoichiometry. Phase diagrams have also been reported for other PEO-salt systems such as PEO-NH$_4$SCN (Iwamoto et al., 1968), PEO-KSCN (Lee et al., 1986) and PEO-NaSCN systems (Lee et al., 1986; Robitaille et al., 1987), PEO-Cu(CF$_3$SO$_3$)$_2$ (Chatani et al., 1990) and PEO-Pb (CF$_3$SO$_3$)$_2$ (Lightfoot et al., 1992).

The crystal structures of polymer-salt complexes provide insight into the structure of polymer-salt complexes. The crystal structures of (PEO)$_3$NaI (Chatani et al., 1987) and (PEO)$_3$NaSCN (Chatani et al., 1990) were obtained from stretched oriented fibers. The crystal structure of (PEO)$_3$NaClO$_4$ was obtained for the first time using powder X-ray diffraction (Lightfoot et al., 1992). Recently, the crystal structures of the polymer electrolyte, (PEO)$_3$LiCF$_3$SO$_3$ (Lightfoot et al., 1993), as well as that of (PEO)$_4$KSCN, (PEO)$_4$NH$_4$SCN and (PEO)$_4$ RbSCN were determined by Bruce et al. Using powder diffraction techniques (Bruce et al., 1992; Bruce, 1995; Lightfoot et al., 1994). The crystal structure of (PEO)$_3$NaClO$_4$ is shown in Figure 2.7. The PEO chains are wrapped around the Na$^+$ ions and each Na$^+$ ion is coordinated to

four ether oxygens of the polymer chain and two oxygens each from a different ClO_4^-.

Every ClO_4^- unit bridges two neighbouring Na^+ ions by each donating an oxygen to

the coordination sphere of each Na^+ ion. The structure of $(PEO)_3NaI$ is similar to that

of $(PEO)_3NaClO_4$.

In the $(PEO)_4MSCN$ complexes ($M = K^+$, NH_4^+ or Rb^+) the cations are seven

coordinate with five ether oxygens and two nitrogens form the SCN^- anions. In the

case of $(PEO)_3LiCF_3SO_3$, the Li^+ is five coordinate with three ether oxygens and one

oxygen from each of two triflate units. It has been shown recently that the local

structure in the compound does not change significantly even upon heating to high

temperature. Thus, the crystal structures of polymer-salt complexes can provide

insight into the structure of amorphous polymer-salt complexes and the ion-transport

thereafter.
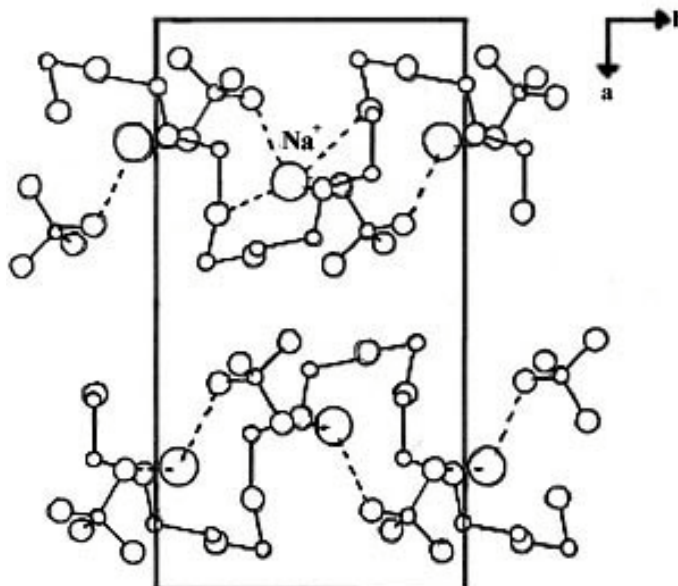
Figure 2.7 Crystal structure of the $(PEO)_3NaClO_4$ complex (Lightfoot et al., 1992).
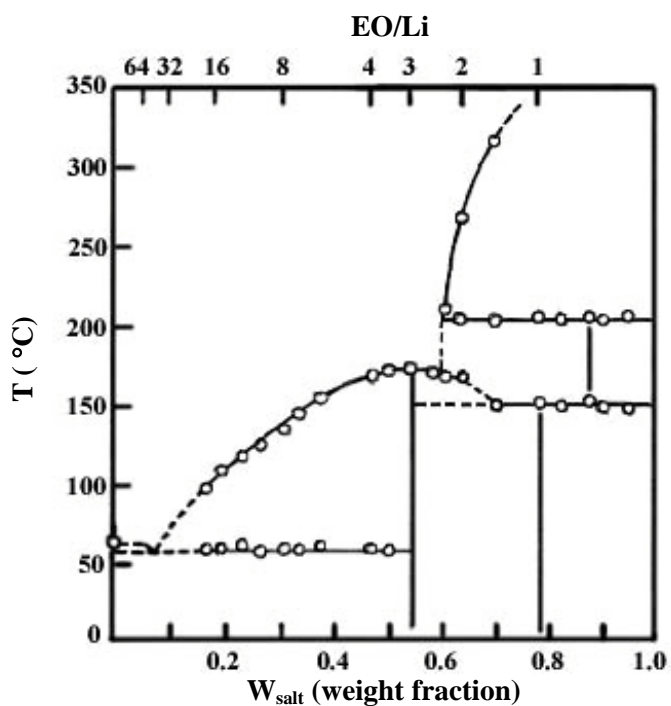
Figure 2.8 Phase diagram of the PEO-LiCF$_3$SO$_3$ system (Vallee et al., 1992).
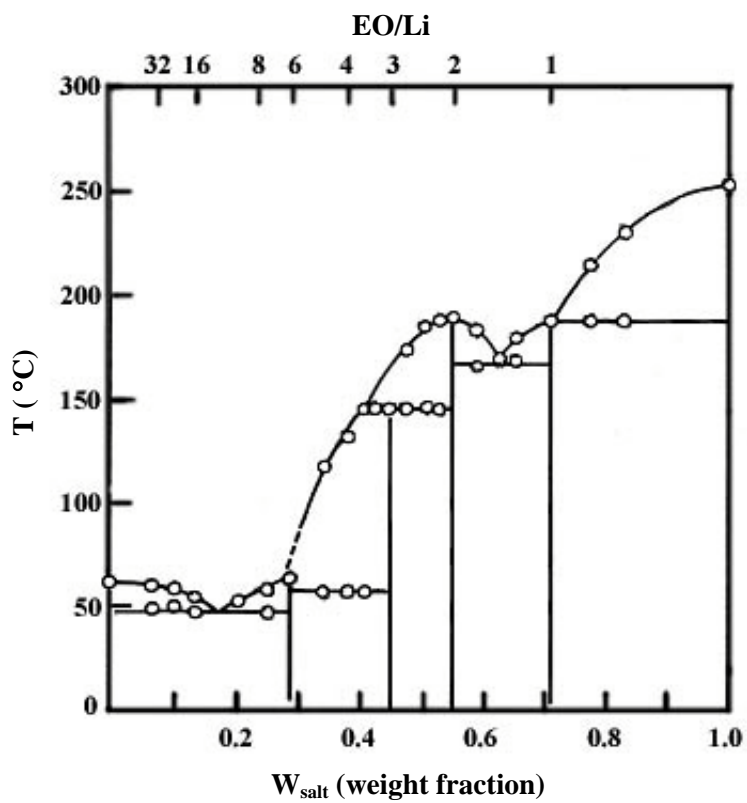
Figure 2.9 Phase diagram of the PEO-LiClO$_4$ system (Vallee et al., 1992).

2.8 The Rotational Isomeric State (RIS) Theory

A polymer consists of macromolecules, molecules differ from small molecules is in the enormous number of conformations that they populate at ordinary temperatures. A variety of models have been developed for averaging conformational dependent properties over the enormous number of conformations accessible to a macromolecule. Theoretical studies based on statistical thermodynamics have been extensively performed for macromolecules in order to interpret and to understand their physical properties which strongly depend on the spatial arrangement of chain molecules. The RIS theory is a powerful method for relating an atom-based model for the local structure of a chain to its conformation-dependent physical properties.

The application of rotational isomeric state techniques to polymers is not new. This approach was first adapted almost 50 years ago (Volkenstein, 1951) in the mathematical treatment of the Ising representation of a linear array of neighbor-dependent magnetic dipoles. Also, the generator matrix technique employed in RIS calculations was invented a decade earlier, for another purpose (Kramers et al., 1941). The special strength of the model is the ability of constructing a formalism based on the detailed informations about the covalent structure (bond lengths, bond angles, torsion angles, and torsion potential energy functions) and evaluating it quickly by the use of generator matrices without the need of enormous computational power. A decade after the first adaptation of the model, there was a strong increase in the use of the RIS model. Flory's classic book (Flory, 1969) appeared on 1969 as a first example of literature on its applications to macromolecules. Since the first appearance of Flory's book, formulations have been simplified and generalized, and

new formulations for the treatment of additional properties have been created. The technique has also become popular among chemical synthesists who try to understand the way in which the physical properties of macromolecules are determined by the monomer units in the chains.

CHAPTER III

RESEARCH METHODOLOGY

3.1 Apparatus and Materials

- Glassware for SPE preparation and viscosity measurement

- Magnetic stirrers and magnetic bars

- Oven and vacuum oven for drying salt and removing solvent

- Glass plate 30 x 20 cm for sample casting.

- Cannon-Ubbelohde Viscometer no. 150.

- Digital temperature controller, capable of maintaining 10-100°C $\pm$ 0.01°C.

- Poly(ethylene oxide) (PEO MW 4 x 10^6), Aldrich.

- Poly(ethylene glycol) (PEG MW 600 and 20,000), Fluka.

- Lithium trifluoromethanesulfonate ($LiCF_3SO_3$), Fluka.

- Potassium Thiocyanate (KSCN), APS Finechem.

- Methanol (CH_3OH), Analytical Reagent, Merck

- Benzene (C_6H_6), Analytical Reagent, Merck

3.2 Computational Part

3.2.1 Polymer Conformation and RIS Theory

RIS theory based on statistical approaches have been extensively performed for macromolecules in order to interpret and understand their physical properties which strongly depend on the spatial arrangements of chain molecules, designated by the term "configuration". A macromolecule that often comprises tens of thousands of atoms may adopt an enormous amount of configurations, thus, it would be almost impossible to consider each of them individually in a reasonable time interval. This leads to the necessity of adopting a statistical approach by which the properties can be deduced as averages over the total population of configuration which differ from one another by the angles of rotation about the bonds of the structure and also, by the bond lengths and bond angles. According to the RIS theory, the continuous ranges of rotation angles accessible to a given bond of a polymer chain are replaced by discrete rotational states that are often three in number and chosen to coincide with one of most stable states having potential minima. Fluctuations about the minima are random and therefore compensatory in their effect on the average properties. The geometrical parameters defining bond lengths and bond angles are thermally fluctuating with narrow ranges and therefore can be kept constant at their mean values. As a result, the number of configuration variables is reduced significantly and thus the number of admissible configurations. The "configurational" search for the most stable states becomes a "conformational" search (the term "conformation" is referred to as the class of configurations generated by executing rotations about single bonds).

RIS theory successfully describes the conformational characteristics of a single polymer chain in its unperturbed state. The basic idea from this model is to determine the torsional rotations about the bonds of the backbone as discrete states. In the RIS scheme, the configurational partition function may be written as

$$Z = \sum_{\phi_1}...\sum_{\phi_n} \exp\left[-E(\phi_1...\phi_n)/RT\right] \tag{3.1}$$

When nearest neighbor dependence is taken into account, the weight associated with a given conformation is

$$\prod_i \exp\left[-E(\phi_{i-1},\phi_i)/RT\right] \tag{3.2}$$

The statistical weight for a bond pair in a given conformation is then given by

$$u_i(\phi_{i-1},\phi_i) = \exp\left[-E(\phi_{i-1},\phi_i)/RT\right] \tag{3.3}$$

The partition function can then be expressed as the sum over all rotational states of the product of these weights. That is

$$Z = \sum_{\phi_i}...\sum_{\phi_n} \prod_i u_i(\phi_{i-1},\phi_i) \tag{3.4}$$

In the matrix form, this can be rewritten as

$$Z = \prod_i \mathbf{U}_i \tag{3.5}$$

where U_i is the statistical weight matrix associated with bond i. It has *m* rows and *n* columns, corresponding to the *m* rotational states of bond (i-1) and the *n* rotational states of bond i.

The conformational properties, *A*, are assumed to be a function only of dihedral angles in the chain backbone. According to statistical mechanics, the average value, $\langle A \rangle$, is approximated as a sum over the discrete rotational states by

$$< A >= Z^{-1} \int ... \int \exp[-E(\phi_1...\phi_n)/RT]A(\phi_1...\phi_n)d\phi_1...d\phi_n \tag{3.6}$$

The statistical weights may then be used to calculate conformational properties by the following expression

$$< A_0 > = Z^{-1} \prod_i \mathbf{G}_i \tag{3.7}$$

where $\mathbf{G_i}$ are "super" generator matrices defined by

$$\mathbf{G}_i = (\mathbf{U}_i \otimes \mathbf{E}_s)\|\mathbf{F}_i\| \tag{3.8}$$

Here $\otimes$ indicates a direct matrix product, $\|\mathbf{F}_i\|$ is the diagonal array of generator matrices $\mathbf{F_i}$, and $\mathbf{E_s}$ is the identity matrix of the same order as $\mathbf{F_i}$. Some conformational

dependent properties can be estimated from the RIS model such as the mean-square end-to-end distance $\langle r^2 \rangle_o$, mean-square radius of gyration $\langle s^2 \rangle_o$, mean-square dipole moment $\langle \mu^2 \rangle_o$.

Conformational dependent Properties Calculated from RIS Theory

RIS theory is excellent for the rapid analysis of conformation-dependent physical properties of chain molecules. The most frequently calculated property is the mean square end-to-end distance, $\langle r^2 \rangle_o$ (subscript zero designates the unperturbed state). The other properties susceptible to rapid computation include the mean-square radius of gyration $\langle s^2 \rangle_o$, and the mean-square dipole moment $\langle \mu^2 \rangle_o$. Next, illustrate the methodology used in RIS for taking $\langle r^2 \rangle_o$ as follows:

To begin, an arbitrary conformation of a linear polymer chain is considered. Beginning at one end of the chain, the backbone atoms are identified by labels ranging from 0 to n for a chain consisting of n backbone bonds. Let each bond be characterized by a vector $\boldsymbol{b}_i$ (Figure 3.1). By convention, bond i connects backbone atoms i-1 and i. For a specific conformation, the squared end-to-end distance of the chain is

$$r^2 \quad = \quad \left(\boldsymbol{b}_1 + \boldsymbol{b}_2 + ... + \boldsymbol{b}_n\right)^2$$

$$= \quad \sum_{i,j=1}^{n} \boldsymbol{b}_i \boldsymbol{b}_j \quad = \quad \sum_{i=1}^{n} \boldsymbol{b}_i^2 + 2\sum_{i\langle j} \boldsymbol{b}_i \boldsymbol{b}_j \tag{3.9}$$

Following Flory (Flory, 1988), let a coordinate system be associated with each backbone bond (excluding the first) as illustrated in Figure 3.1. For bond i, the x_i axis is collinear with the bond, with the origin at backbone atom i-1. The y_i axis is in the plane defined by bond i and i+1 with its positive direction chosen such that its projection on the x_{i-1} axis is positive. The direction of the z_i axis is chosen so that it completes a right-handed coordinate system. Note that a bond vector b_i is expressed in its own coordinate frame as the column vector
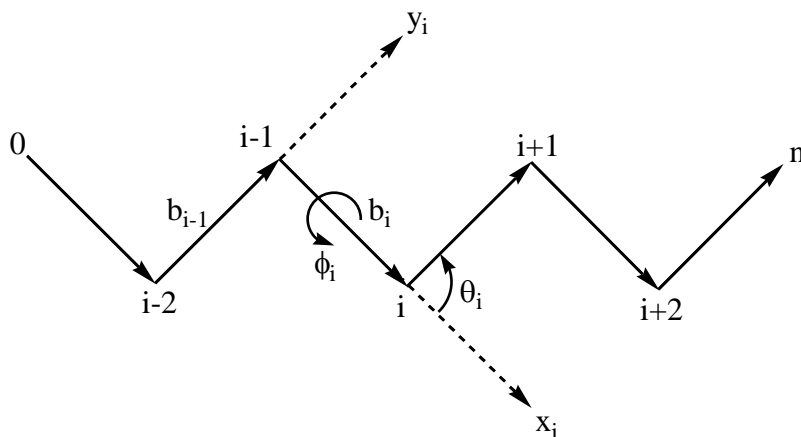
Figure 3.1 Chain representation and coordinates used in the RIS calculation.

$$ b_i \quad = \quad \begin{bmatrix} b \\ 0 \\ 0 \end{bmatrix} \tag{3.10} $$

A vector in the coordinate frame of bond i+1 can be expressed in the coordinate frame of bond i by making use of the transformation matrix T_i.

$$ v^{(i)} \quad = \quad T_i v^{(i+1)} \tag{3.11} $$

where, using the dihedral and valence angles as defined in Figure 3.2, the transformation matrix is given by

$$\boldsymbol{T}_i \;=\; \begin{bmatrix} \cos\theta & \sin\theta & 0 \\ \sin\theta\cos\phi & -\cos\theta\cos\phi & \sin\phi \\ \sin\theta\sin\phi & -\cos\theta\sin\phi & -\cos\phi \end{bmatrix} \tag{3.12}$$

The subscript i on the left-hand side means that the θ and ϕ values within the matrix are those for bond i. Note that θ_i is defined to be the supplement of bond angle i. The value of ϕ_i in $\boldsymbol{T}_i$ is that for the specific conformation being considered. By convention, ϕ_i is 180° when the bond is in the planar trans conformation, and deviations from 180° are measured in right-handed sense (i.e., a positive rotation is one that would "unscrew" the bond if it were a right-handed screw). RIS theory normally assumes that the value of θ_i is conformation independent, but relaxing this assumption does not significantly complicate calculations of chain properties. A bond vector $\boldsymbol{b}_j$, as expressed in its own coordinate frame, can be transformed into coordinate frame i as follows (for $j > i$):

$$\boldsymbol{T}_i \boldsymbol{T}_{i+1}...\boldsymbol{T}_{j-1}\boldsymbol{b}_j \tag{3.13}$$

Henceforth, bond vector $\boldsymbol{b}_i$ are understood to be expressed in their own coordinate frames. Using Eqs. (3.9) and (3.13), the expression for r^2 becomes

$$r^2 \quad = \quad \sum_{i=1}^{n} b_i^2 + 2\sum_{i<j} b_i^T T_i T_{i+1}...T_{j-1} b_j \tag{3.14}$$

This can be expressed in the matrix form as

$$r^2 \quad = \quad F_1 F_2 ... F_n \tag{3.15}$$

where the *generator matrix* F for a given bond is

$$F_i \quad \equiv \quad \begin{bmatrix} 1 & 2b^T T & b^2 \\ 0 & T & b \\ 0 & 0 & 1 \end{bmatrix}_i \tag{3.16}$$

except for the first and last bonds of the chain. Note that some of the members of F_i are themselves matrices of vectors, making F_i a 5×5 matrix. The superscript T denotes the transpose of a matrix or vector.

For terminal bonds, the F matrices take on a special form. Form the first bond, the matrix is

$$F_1 \quad \equiv \quad \begin{bmatrix} 1 & 2b^T T & b^2 \end{bmatrix}_1 \tag{3.17}$$

and for the last bond,

$$F_n \equiv \begin{bmatrix} b^2 \\ b \\ 1 \end{bmatrix}_n \tag{3.18}$$

The easiest way to see that Eqs. (3.14) and (3.15) are indeed equivalent is to explicitly perform the matrix multiplication in Eq. (3.15) for chains of two, three, and four bonds and observe the pattern that emerges.

Equation (3.15) gives the squared end-to-end distance for a specific conformation, but many different conformations are possible. We require a suitably weighted average of this quantity over all conformations. It is at this point that the statistical weights are introduced.

Let the statistical weight matrix for an interior bond of the chain be written as

$$U_i = \begin{bmatrix} u_{\alpha'\alpha} & u_{\alpha'\beta} & \cdots \\ u_{\beta'\alpha} & u_{\beta'\beta} & \cdots \\ \vdots & \vdots & \ddots \end{bmatrix}_i \tag{3.19}$$

where $\alpha', \beta', \ldots$ represent states of bond $i-1$, and $\alpha, \beta, \ldots$ represent states of bond i. Then let a new generator matrix G_i be defined as

$$G_i \equiv \begin{bmatrix} u_{\alpha'\alpha}F(\alpha) & u_{\alpha'\beta}F(\beta) & \cdots \\ u_{\beta'\alpha}F(\alpha) & u_{\beta'\beta}F(\beta) & \cdots \\ \vdots & \vdots & \ddots \end{bmatrix}_i \tag{3.20}$$

As was the case for the $\boldsymbol{F}$ matrices, the $\boldsymbol{G}$ matrices at the chain ends take on special forms:

$$\boldsymbol{G}_1 \equiv \begin{bmatrix} \boldsymbol{F}_1 & 0 & 0 & \cdots & 0 \end{bmatrix} \tag{3.21}$$

and

$$\boldsymbol{G}_n \equiv \begin{bmatrix} \boldsymbol{F}_n \\ \boldsymbol{F}_n \\ \vdots \\ \boldsymbol{F}_n \end{bmatrix} \tag{3.22}$$

Observe that with the above definitions, the matrix product

$$\boldsymbol{G}_1\boldsymbol{G}_2 \ldots \boldsymbol{G}_n \tag{3.23}$$

generates all possible serial products, $F_1F_2 \ldots F_n$, corresponding to all possible chain conformations. Each of these products is multiplied by its overall statistical weight (itself a product of bond statistical weights). It only remains to normalize Eq. (3.23) in order to obtain the mean-squared end-to-end distance.

The normalization factor is simply the serial product of the statistical weight matrices, otherwise known as the configurational partition function:

$$\boldsymbol{Z} = U_1U_2 \ldots U_n \tag{3.24}$$

where, as usual, terminal matrices have a special form:

$$U_1 \equiv \begin{bmatrix} 1 & 0 & \cdots & 0 \end{bmatrix} \tag{3.25}$$

and

$$U_n \equiv \begin{bmatrix} 1 \\ 1 \\ \vdots \\ 1 \end{bmatrix} \tag{3.26}$$

the number of entries in these vectors being determined by the dimensions of the neighboring weights matrices.

Thus, the final expression for the mean-squared end-to-end distance of the chain is

$$\langle r^2 \rangle_0 = Z^{-1} G_1 G_2 \ldots G_n \tag{3.27}$$

This is quite a remarkable result. In this expression, an average over an enormously large number of conformations has been reduced to a simple serial product of matrices, while still accounting for the specific geometry and chemical makeup of the chain. Other conformational properties are also calculated in a similar way as $\langle r^2 \rangle_o / nl^2$.

3.2.2 RIS Parameters from Molecular Mechanics (MM) Technique

There are various methods on obtaining the RIS parameters. The classical techniques are usually based on an assumption of unknown variables denoted as statistical weights for each conformation. These parameters are then parameterized with some selected conformational dependent properties deriving from experiments. This classical method has been done in the past and works reasonably well. Unfortunately, there are some limitations on employing this technique due mainly to a difficulty on assigning the conformational states as well as lack of experimental data to verify the model.

The RIS model derived from the computational method provides an alternative and a convenient way to solve those problems. Molecular Mechanics is the calculation technique based on the approximated potential model, which can be divided into two terms

$$V(r) = V_{bond} + V_{non-bond} \tag{3.28}$$

$$\textbf{\textit{where}} \qquad V_{bond} = V(r)_{stretch} + V(\theta)_{bend} + V(\chi)_{torsion} \tag{3.29}$$

$$V_{non-bond} = V(r)_{van-der-Waals} + V(r)_{electrostatic} \tag{3.30}$$

The collective set of the parameters called "force field" can be obtained basically by spectroscopies such as IR, Raman, NMR, and X-ray and by higher level

ab initio quantum simulations. Molecular optimization is then performed to find the minimum energy state of a molecule for each conformer. The structure obtained by the energy minimization exists at the deep well of the potential function satisfying following conditions.

$$\frac{\partial V(r)}{\partial r} = 0 \quad \text{and} \quad \frac{\partial^2 V(r)}{\partial r^2} > 0 \tag{3.31}$$

To find the minimized structure, many efficient search algorithms have been developed, such as Newton-Raphson and conjugate gradient method. In this work, we adopt the default force field and search algorithm provided by Chem3D software (CambridgeSoft Corporation). The conformational energies are obtained by rotating the dihedral angles and should correspond to the minimized structure at each pair of dihedral angle (ϕ_i, ϕ_j). The increment in dihedral angle for ϕ_i and ϕ_j (at C-C, C-O or O-C bond) is set to 10° (rotation from 0° to 360°). Three short segments of PEO chain used in the computation are presented in Figure 3.2.
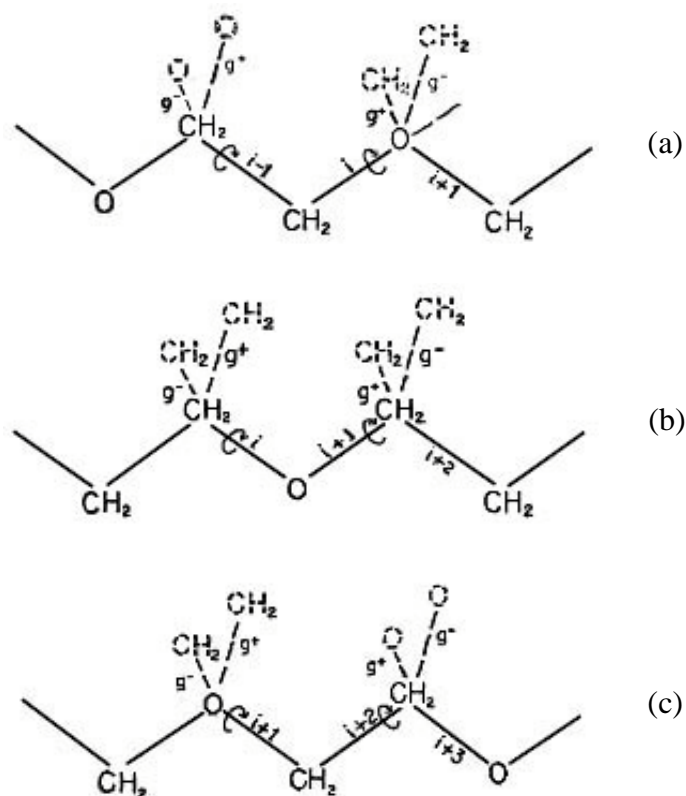
Figure 3.2 Schematic representation of three short segments of PEO chain

(a) C-C, C-O bond pair (b) C-O, O-C bond pair (c) O-C, C-C bond pair.

The model assumes three states (trans, gauche$^+$ and gauche$^-$, abbreviated as t, g^+ and g^-, for each rotatable bond). The statistical weight $\left(U_{\phi_i \ \phi_j}\right)$ can be defined as:

$$U_{\phi_i \ \phi_j} = \frac{\displaystyle\sum_{\phi_i}\sum_{\phi_j} \exp\!\left[-V\!\left(\phi_i,\phi_j\right)/RT\right]}{\displaystyle\sum_{10^0}^{360^o}\sum_{10^0}^{360^0} \exp\!\left[-V\!\left(\phi_i,\phi_j\right)/RT\right]} \tag{3.32}$$

Where $V(\phi_i, \phi_j)$ is a conformational energy (kcal mol^{-1}) at ϕ_i and ϕ_j, R is the gas constant and T is the absolute temperature (K). Then, the statistical weight matrix for each bond pair is of the form:

$$
\begin{bmatrix}
U_{tt} & U_{tg^+} & U_{tg^-} \\
U_{g^+t} & U_{g^+g^+} & U_{g^+g^-} \\
U_{g^-t} & U_{g^-g^+} & U_{g^-g^-}
\end{bmatrix}
\tag{3.33}
$$

To test the quality of parameters obtained from MM method, some conformational dependent properties and fraction of bond conformation can be calculated using the RIS scheme and then compared with results obtained from experiments.

3.3 Theoretical Part

3.3.1 Adam-Gibbs configuration entropy model

In this section Continuum quasi-thermodynamic theories (the free volume and the configurational entropy models) are considered for the interpretation of the conductivity behavior of solid polymer electrolytes as a function of stoichiometry and temperature.

The Free Volume Models

Doolittle's empirical relation between the fluidity of simple hydrocarbons and their free volume (υ_f) is as follows:

$$\phi \;=\; A\exp\!\left[-b\upsilon_o/\upsilon_f\right] \tag{3.34}$$

where A and b are constants and υ_o is the van der Waals volume of the molecule.

As with the same form of Doolittle's Eq. (3.34), Cohen and Turnbull developed a relation between the diffusion constant D in a liquid of hardspheres and the free volume. This derivation is based on the concept that the statistical redistribution of the free volume occasionally opens up voids large enough for a diffusive displacement. The relation is:

$$D \;=\; A\exp\!\left[-\gamma\upsilon^*/\upsilon_f\right] \tag{3.35}$$

where A $\left(= ga^*u\right)$ is a proportionality factor that is related to a geometric factor (g), the molecular diameter (a^*), and the gas kinetic velocity (u). γ is a numerical factor between 0.5 and 1.0 that is introduced to correct for the overlap of the free volume. υ^* is the minimum required volume of the void. To test the applicability of Eq. (3.35) to real liquids, Cohen and Turnbull assume that the free volume is equivalent to the total thermal expansion at constant pressure. Then

$$\upsilon_f \;=\; \upsilon_o \left\{ \exp\left[\int_{T_o}^{T} \alpha \; dT \right] - 1 \right\} \;=\; \alpha \overline{\upsilon}_m \left(T - T_o \right) \tag{3.36}$$

where α is the thermal expansion coefficient, $\overline{\upsilon}_m$ is the mean value of the molecular volume $\left(\upsilon_o \right)$, T is temperature, and T_o is the temperature at which the free volume disappears. Substituting Eq. (3.36) into Eq. (3.35) gives

$$D \;=\; ga^*u \; \exp\left[\frac{-\gamma \upsilon^*}{\upsilon_m \alpha \left(T - T_o \right)} \right] \tag{3.37}$$

From the Nernst-Einstein relationship $\sigma \;=\; \left(nq^2 / k_B T \right) D$ between conductivity $\left(\sigma \right)$ and diffusivity $\left(D \right)$, where n is the carrier concentration, q is the carrier charge, and k_B is the Boltzmann constant, Eq. (3.37) results in the Vogel-Tamman-Fulchur (VTF) form:

$$\sigma(T) \;=\; A \exp\left[\frac{-B}{T - T_o} \right] \tag{3.38}$$

where A and B are constants.

The Configurational Entropy Models

Adam and Gibbs constructed the partition function for the fraction of the overall system that can or cannot undergo a configurational transition, and then evaluate the overall entropy in terms of the configurational entropy of oligomer subunit. For the probability $\overline{W}$ of a mass-transporting cooperative rearrangement, this yields:

$$\overline{W} \;=\; \overline{A}\exp\!\left[-\frac{\Delta\mu S_c^*}{k_B T S_c^{Total}}\right] \tag{3.39}$$

where $\overline{A}$ is a constant, $\Delta\mu$ is the potential energy hindering the cooperative rearrangement per monomer unit, S_C^* is a critical configurational entropy, k_B is the Boltzmann constant, T is the absolute temperature, and S_c^{Total} is the total molar configurational entropy at temperature T. To evaluate the temperature dependence of S_c^{Total}, we can write

$$S_C^{Total}(T) \;-\; S_C^{Total}(T_o) \;=\; \int_{T_o}^{T}\frac{\Delta C_p}{T}dT \;=\; \Delta C_p\ln(T/T_o) \tag{3.40}$$

with ΔC_p the difference in a specific heat between the equilibrium melt and the glass at $T_o\left[S_C^{Total}(T_o)=0\right]$. From substituting Eq. (3.40) into (3.39), we obtain

$$\overline{W} = A\exp\left[\frac{-\Delta\mu S_C^*}{k_B T \Delta C_p \ \ln(T/T_o)}\right] \qquad (3.41)$$

From the assumption, $\ln(T/T_o) \approx (T-T_o)/T_o$ and $T/T_o \approx 1$, Eq. (3.41) can be written as the same form of the VTF Eq. (3.38) with $\overline{B} = \Delta\mu S_c^*/k_B \Delta C_p$.

$$\overline{W} = \sigma(T) = A\exp\left[\frac{-B}{T-T_o}\right] \qquad (3.42)$$

In this study, a configurational entropy model as a function of isothermal composition will be applied to the conductivity results obtained in experiment. The primary exposition of theory is concerned with amorphous polymer/salt systems. Then, the model is extended to semicrystalline polymer/salt systems. Using Flory's lattice treatment of polymer solutions. At the outset, the molar entropy corresponding to a number of different arrangements of polymer and salt ion in mixing is

$$S_1 = -k\left[\frac{\phi_1}{r_1}\ln\phi_1 + \frac{\phi_2}{r_2}\ln\phi_2\right] \qquad (3.43)$$

where ϕ_1, ϕ_2, r_1 and r_2 are the volume fractions and relative molar volumes of components 1 and 2, respectively. r_2 is defined by

$$r_2 = \frac{\upsilon_2 MW_2}{\upsilon_1 MW_1} \qquad (3.44)$$

where υ_1, υ_2, MW_1 and MW_2 are specific volumes of salt and polymer, and molecular weights of salt and polymer, respectively; $r_1 = 1$ for the salt ion. The mixing entropy does not take into account the difference between the salt cation and the salt anion.

The disorientation of polymer contributes to the entropy equal to

$$S_2 \;=\; k\left[\frac{\phi_1}{r_1}(r_2 - 1)\ln\frac{z-1}{e}\right] \tag{3.45}$$

where z is the lattice coordination number taken as 6 in this study. Flory proposed that the configurational entropy of amorphous polymer/solvent system (or amorphous polymer/salt system) should be expressed as $S_1 + S_2$. However, in a solid polymer electrolyte system, a drop of chain flexibility with an increase of salt concentration should be considered (i.e., the configurational entropy loss). Hence, the entropy introduced to correct for a drop of chain flexibility is

$$S_3 \;=\; k_B f(\phi_1)\ln\frac{z-1}{e} \tag{3.46}$$

$$f(\phi_1) \;=\; \lambda_s\phi_1 \tag{3.47}$$

where λ_s is a degree of specific interaction between the salt ion and the base group of polymer, which is inversely proportional to temperature, $\lambda_s\phi_1$ is associated with the length of coordinated chain. The entropy $k_B\ln\left[(z-1)/e\right]$ arises from the fact that the

segment location relative to that of the immediate predecessor is not predetermined in the lattice.

The total molar configurational entropy (S_c^{Total}) of the amorphous polymer/salt system is obtained by combining Eqs. (3.43), (3.45), and (3.46).

$$S_C^{Total}/k_B \quad = \quad -\frac{\phi_1}{r_1}\ln\phi_1 - \frac{\phi_2}{r_2}\ln\phi_2 + \frac{\phi_2}{r_2}(r_2-1)\ln\frac{z-1}{e} + \lambda_s\phi_1\ln\frac{z-1}{e} \qquad (3.48)$$

If the semicrystalline polymer/salt system was considered, the deduction of $S_4 = k_B f(\phi_C)\ln(z-1/e)$ should be taken into account, where ϕ_C is the volume fraction of the crystalline unit in the polymer.

By substituting Eq. (3.48), and $S_c^* = k_B\ln 2$ into Eq. (3.39), a new configurational entropy model as a function of isothermal composition can be obtained as following.

$$\overline{W} \quad = \quad \sigma(\phi) \quad = \quad A\exp\left[\frac{-B'}{S_C^{Total}/k_B}\right] \qquad (3.49)$$

where constant B' is defined by

$$B' \quad = \quad \frac{\Delta\mu\ln 2}{k_B T} \qquad (3.50)$$

From Eqs. (3.48-3.50), the dependence of conductivity on salt composition and the chain length can be described and used to predict the maximum of the conductivity for amorphous polymer/salt systems.

3.3.2 Flory-Huggins theory

When we consider a salt effect of the free energy of mixing, we assume that the salt is a particle, and the consequential decrease of entropy should be corrected in the interaction energy term (χ).

Correlating Equations

For a binary polymer/salt system, the Flory-Huggins expression for the molar Gibbs energy of mixing ΔG at a temperature T is given by

$$\frac{\Delta G}{RT} \;=\; \frac{\phi_1}{r_1}\ln\phi_1 + \frac{\phi_2}{r_2}\ln\phi_2 + \chi_{FH}\phi_1\phi_2 \tag{3.51}$$

where R is the gas constant; ϕ_1, ϕ_2, r_1 and r_2 are volume fractions and relative molar volumes of components 1 and 2, respectively, and χ_{FH} is the Flory-Huggins interaction parameter. Recently, Qian and coworker (Qian et al., 1991) suggested a semiempirical form for χ. They replaced χ_{FH} by $g(T,\phi_2)$, a function of temperature and concentration. The Gibbs free energy of mixing and chemical potentials in terms of the new interaction parameter χ from the relation, $\chi \;=\; g - \phi_1 g'$, are given by

$$\frac{\Delta G}{RT} \;=\; \frac{1-\phi_2}{r_1}\ln(1-\phi_2)+\frac{\phi_2}{r_2}\ln\phi_2+\phi_2\int_{\phi_2}^{1}\chi(T,\phi)d\phi \tag{3.52}$$

$$\frac{\Delta\mu_1}{RT} \;=\; \ln(1-\phi_2)+\phi_2\left(1-\frac{r_1}{r_2}\right)+\chi(T,\phi_2)r_1\phi_2^2 \tag{3.53}$$

$$\frac{\Delta\mu_2}{RT} \;=\; \ln\phi_2+(1-\phi_2)\left(1-\frac{r_2}{r_1}\right)$$

$$-r_2\phi_1\phi_2\chi(T,\phi_2)+r_2\int_{\phi_2}^{1}\chi(T,\phi)d\phi \tag{3.54}$$

Qian and coworker proposed that χ was given by the product of a temperature-dependent term, $D(T)$, and a concentration dependent term, $B(\phi)$:

$$\chi(T,\phi) \;=\; D(T)B(\phi_2) \tag{3.55}$$

Following Flory (Flory, 1953) and Qian (Qian et al., 1991) suggest

$$D(T) \;=\; d_o+\frac{d_1}{T}+d_2\ln T \tag{3.56}$$

where d_o, d_1 and d_2 are constants for a given binary system. For the concentration-dependent term, they use

$$B(\phi_2) \;=\; 1+b_1\phi_2+b_2\phi_2^2 \tag{3.57}$$

where b_1 and b_2 are constants for a given binary system.

In this study, we use simple functions of temperature and composition reported elsewhere (Kim et al., 1998):

$$D(T) = d_0 + \frac{d_1}{T} \qquad (3.58)$$

$$B(\phi_2) = 1 + b\phi_2 \qquad (3.59)$$

where d_0, d_1 and b are adjustable model parameters.

The Melting Point Depression Theory

In a semicrystalline system, the condition of equilibrium between crystalline polymer and the polymer unit in the solution may be described as follows:

$$\mu_u^c - \mu_u^0 = \mu_u - \mu_u^0 \qquad (3.60)$$

where μ_u^c, μ_u and μ_u^0 are chemical potentials of crystalline polymer segment unit, of liquid (amorphous) polymer segment unit and chemical potential in the standard state, respectively. Now the formal difference appearing on the left-hand side is expressed as follows:

$$\mu_u^c - \mu_u^0 \;=\; -\Delta H_u \left(1 - T/T_m^0\right) \tag{3.61}$$

where ΔH_u is the heat of fusion per segment unit, T and T_m^0 are the melting temperature of the species in a mixture and of the pure phases, respectively. The right-hand side of Eq. (3.60) can be restated as follows:

$$
\begin{aligned}
\mu_u - \mu_u^o \;=\; RT \frac{V_u}{V_1} \Bigg[& \frac{r_1}{r_2} \ln \phi_2 + \left(1 - \phi_2\right)\left(\frac{r_1}{r_2} - 1\right) \\
& - r_1 \phi_1 \phi_2 \left(d_o + \frac{d_1}{T_{m,2}}\right)\left(1 + b\phi_2\right) \\
& + r_1 \left(d_o + \frac{d_1}{T_{m,2}}\right)\left(1 + \frac{b}{2} - \phi_2 - \frac{b}{2}\phi_2^2\right) \Bigg]
\end{aligned}
\tag{3.62}
$$

where V_u and V_1 are the molar volumes of the polymer repeating unit and of salt ions, respectively. By substituting Eqs. (3.61) and (3.62) into Eq. (3.60) and replacing T by $T_{m,2}$, the equilibrium melting temperature of the mixture is given by

$$
\begin{aligned}
\frac{1}{T_{m,2}} - \frac{1}{T_{m,2}^o} \;=\; -\frac{R}{\Delta H_u}\frac{V_u}{V_1} \Bigg[& \frac{r_1}{r_2} \ln \phi_2 + \left(1 - \phi_2\right)\left(\frac{r_1}{r_2} - 1\right) \\
& - r_1 \phi_1 \phi_2 \left(d_o + \frac{d_1}{T_{m,2}}\right)\left(1 + b\phi_2\right) \\
& + r_1 \left(d_o + \frac{d_1}{T_{m,2}}\right)\left(1 + \frac{b}{2} - \phi_2 - \frac{b}{2}\phi_2^2\right) \Bigg]
\end{aligned}
\tag{3.63}
$$

The subscripts 1, 2 and u refer to the salt ion, the polymer and the polymer segment unit, respectively. Similarly, we obtain

$$\frac{1}{T_{m,1}} - \frac{1}{T_{m,1}^o} = -\frac{R}{\Delta H_1}\left[\ln(1-\phi_2)+\phi_2\left(1-\frac{r_1}{r_2}\right)\right.$$

$$\left.+\left(d_o+\frac{d_1}{T_{m,1}}\right)(1+b\phi_2)r_1\phi_2^2\right] \tag{3.64}$$

From Eqs. (3.63) and (3.64), we can predict liquidus curves in the phase diagram of binary polymer/salt systems.

3.4 Experimental Part

3.4.1 Preparation of PEO/PEG/salts complexes

PEO (MW 4 x 10^6 g mol^{-1}) and PEG (MW 600g mol^{-1}) were used as received. The salts were dried in the vacuum oven at ~ 100-140 °C for 48 hours and then stored in a glove box or alternatively in a dessicator. Stoichiometric amount of PEO and the desired salt (different salt concentration and percent plasticizer) were dissolved in methanol and stirred continuously for 24 hours at room temperature. A set up of tools was shown in Figure 3.3a. After continuous stirring, the solution was allowed to stand at room temperature for 24 h to facilitate degassing. To obtain thin film of the sample, the gelatinous polymer solution was cast on the glass plate (Figure 3.3b). The films were dried in vacuum oven at 50 °C for 24 hours to remove solvent.

The concentration of salt in polymer-salt complexes was expressed in terms of molar ratios of the ether oxygen in the polymer to metal cation of salt (O:M). The O:M ratios could be converted to molal concentrations (moles of salt per kg of polymer) or to weight ratios (w) of salt to polymer using Eqs. (3.65) and (3.66) respectively.

$$Molal = (M:O) \times (1000/MW_{per\ oxygen}) \tag{3.65}$$

$$w = W_{salt}/W_{polymer} = (M:O) \times (MW_{salt}/MW_{per\ oxygen}) \tag{3.66}$$

where $Mw_{per\ oxygen} = MW_{polymer}/(n+1)$. The amount of PEG was expressed as a weight percent (wt %) of the PEO present, followed by

$$y\% = [Wt(PEG)/Wt(PEO)] \times 100 \tag{3.67}$$
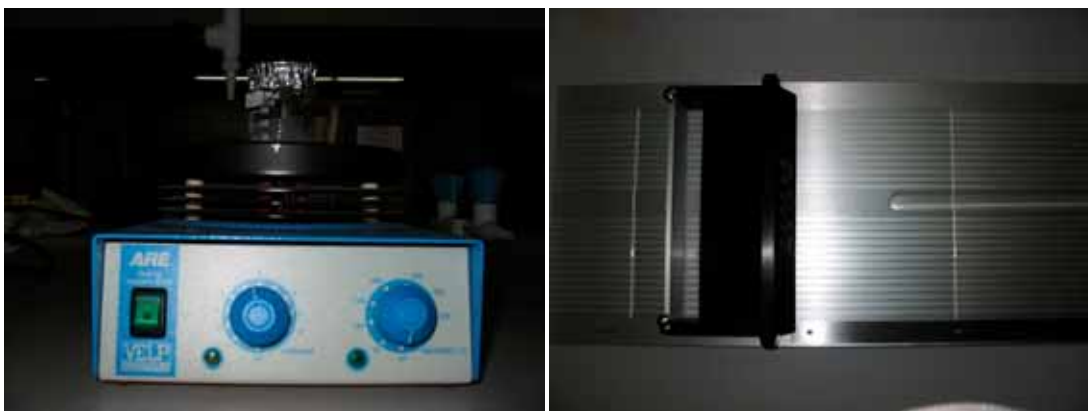
(a)   (b)

Figure 3.3 Preparation of SPEs films (a) sets up of tool for mix sample and
(b) aluminum plate for cast sample.

3.4.2 Characterization

3.4.2.1 Viscometry

The intrinsic viscosities, $[\eta]$, of PEO was measured using a Cannon-Ubbelohde capillary viscometer No 150 (Figure3.4). Polymer solution was prepared directly by dissolving a known weight of PEO in benzene. Viscosities of benzene and PEO solution were measured at 25, 30, 40, 50 and 60 °C. Concentrations were expressed in g dl^{-1} of solution. A constant temperature bath was used to maintain the temperature of the solutions. The bath was thermostatted to ± 0.1 °C in order to measure the intrinsic viscosity.

Figure 3.4 A Cannon Ubbelohde capillary viscometer No 150.

The capillary viscometers used for dilute solution measurements are made of glass. They were operated by filling with a suitable volume of liquid, drawing the liquid level to a point above the upper mark on the bulb, and measuring the time required for the liquid meniscus to fall from the upper mark to the lower

mark. The flow time is related to the viscosity of the liquid and is determined by the driving pressure, using an equation known as Poiseuille's Law,

$$\eta = \frac{\pi R^4 P}{8lQ} = \frac{\pi R^4 Pt}{8lV} \tag{3.68}$$

where R is the radius of the capillary, P is the pressure driving the fluid through the capillary, l is the length of capillary, $Q = V/t$ is the volumetric flow rate, V is the volume of liquid, and t is the time of flow. However, there are many sources of error in capillary viscometry depending upon the viscosity level, the nature of the fluid, and the geometric design of the capillary viscometer. Several corrections are important for dilute solutions of polymers.

The Poiseuille equation, after a kinetic energy correction and an entrance correction, has the form

$$\eta = A\rho t - \frac{B\rho}{t} = A\rho t \left(1 - \frac{B}{At^2} \right) \tag{3.69}$$

where η is the viscosity of the liquid, ρ is the liquid density, and A and B are constants for the particular viscometer. A and B can be obtained graphically by plotting $\eta/\rho t$ versus $1/t^2$. The intercept of the line though the data point gives A and the slope gives $(-B/A)$.

The relative viscosity, η_{rel}, is measured first and can be calculated by an equation

$$\eta_{rel} \equiv \frac{\eta}{\eta_0} = \frac{\rho t\left(1 - B/At^2\right)}{\rho_0 t_0\left(1 - B/At_0^2\right)} \tag{3.70}$$

where the subscript 0 refers to the pure solvent.

In dilute solution, the ratio ρ/ρ_0 is usually closed to unity, so that

$$\eta_{rel} = \frac{t\left(1 - B/At^2\right)}{t_0\left(1 - B/At_0^2\right)} \tag{3.71}$$

If the viscometer has an outflow time greater than 100 sec for the pure solvent, the kinetic energy correction B/At^2 are negligible compared to unity, and then

$$\eta_{rel} = \frac{t}{t_0} \tag{3.72}$$

The relative viscosity is used to calculate the reduced viscosity, (η_{red}), and the inherent viscosity, (η_{inh}). For given polymer solution, the reduced viscosity and inherent viscosity calculated according to the following equations.

$$\eta \equiv \frac{\eta_{sp}}{c} = \frac{\eta_{rel} - 1}{c} \tag{3.73}$$

$$\eta \equiv \frac{\ln \eta_{rel}}{c} \tag{3.74}$$

where η_{sp} is $\eta_{rel} - 1$ and c is the polymer concentration (g/dl).

After that, $[\eta]$ can be determined by using the Huggins and Kraemer Equation, which is the viscosity number (the reduced viscosity) or the logarithmic viscosity number (the inherent viscosity), extrapolated to c = 0. It is shown as follows:

$$[\eta] \equiv \lim_{c \to 0}\left(\frac{\eta_{sp}}{c}\right) = \lim_{c \to o}\left(\frac{\ln \eta_{rel}}{c}\right) \quad (3.75)$$

The unit of $[\eta]$ is g/dl .

An extrapolation to infinite dilution requires a measurement of the viscosity at several concentrations. The sample concentration should not be too large because additional effects may then arise from intermolecular forces and entanglements between chains. The Huggins and Kraemer Equation are used for this extrapolation.

The Huggins Equation is

$$\frac{\eta_{sp}}{c} = [\eta] + k'[\eta]^2 c \quad (3.76)$$

and the Kraemer Equation is

$$\frac{\ln \eta_{rel}}{c} = [\eta] + k''[\eta]^2 c \quad (3.77)$$

where both k' and k'' are constants.

Furthermore, the intrinsic viscosity is related to $\langle r^2 \rangle_0$, which can be predicted by RIS theory. The relation is equated as follows:

$$[\eta] \;=\; \Phi \left[\frac{\langle r^2 \rangle_0}{M} \right]^{3/2} \tag{3.78}$$

where Φ is the hydrodynamic factor (2.6×10^{21}) and M is the average molecule weight.

3.4.2.2 Nuclear Magnetic Resonance (NMR) Spectroscopy

The ^{1}H and ^{13}C-NMR experiments were performed on a Varian Unity INOVA NMR spectrometer operating at 300 MHz. The spectra were collected on 5% wt of PEO in D_2O solution with and without salt (K_2SO_4). ^{1}H and ^{13}C-NMR spin lattice relaxation times (T_1) were measured using a 180°-τ-$90^{\,o}$ pulse sequence. The temperature was varied from an ambient temperature to ca. 80 °C to study the effect of temperature changes on the properties of PEO solutions.

3.4.2.3 FT-IR Spectroscopy

Infrared spectroscopy is an important technique in organic chemistry. It is an easy way to identify the presence of certain functional groups in a molecule.

Also, one can use the unique collection of absorption bands to confirm the identity of a pure compound or to detect the presence of specific impurities.

The interactions between PEO/PEG/salt complexes and salt association were investigated by FTIR. The study was carried out with FT-IR spectrometer Perkin-Elmer model: spectrum GX as shown in Figure 3.6. The numbers of scans were 4 at the resolution of 4 cm^{-1}. The range of measurement was between 4000 cm^{-1} and 400 cm^{-1}.

Figure 3.5 300 MHz Unity Inova NMR spectrometer.

Figure 3.6 FTIR spectrometer Perkin-Elmer model: spectrum GX.

3.4.2.4 X-ray Power Diffraction (XRD)

X-ray diffraction is an important instrumental technique to the materials scientist. With many materials, this technique provides a quick and easy way to figure out what is happening after they are synthesized or reacted. Of course this is limited to crystalline materials, but with exceptions of solids such as gels, glasses and polymers above their glass transition temperature, some degree of order is demonstrated. This allows a determination of what it is that we are dealing with at an atomic level, it gives a chance to model intermediate phases, and design ways to make out come suit our needs.

The sources of the x-rays are from the excitation of a Cu target (other metals can be used but, this was used in all of these experiments so it will be focused on here) that causes the removal of an electron from the atomic core. Upon relaxation of the atom by dropping an electron from an outer shell into the core, there is the

emission of a photon. For the success of this, the electron used to excite the copper target much contain a high amount of kinetic energy. When the copper target is used, the process occurring is the removal of an electron in the 1s shell which is replenished by an electron dropping from the 2p orbital. The x-ray produced by this is termed K_α emission. K_β emission is when the replenishing electrons are provided by the 3d orbital. This occurs, but it is not so favorable as the K_α, which is more intense. Therefore, the x-ray from the target is filtered through nickel prior to hitting the sample to absorb the K_β the nickel can dispose of this energy as non-radiative decay.

A Bruker D5005 X-ray generator was used to give Cu K_α radiation. The diffraction patterns were recorded at room temperature between 2θ values 10° to 60°.

Figure 3.7 Bruker, model D5005 X-ray diffractometer with Ni-filtered Cu K_α

3.4.2.5 Differential Scanning Calorimeter (DSC)

The melting temperature, T_m and the percentage crystallinity of PEO and SPEs films were investigated using a PerkinElmer PYRIS (Diamond) Differential Scanning Calorimeters (DSC) as shown in Figure 3.8. Indium sample was employed to calibrate the machine. The amount of sample used in the study was about 10 mg, loaded using aluminum pans, the range of testing temperature was from 25 °C to 200 °C with the heating ramp 10 °C min^{-1} under an inert gas atmosphere.

Figure 3.8 PerkinElmer PYRIS (Dimond) Differential Scanning Calorimeters (DSC).

3.4.2.6 Conductivity measurement

Conductivity measurement was performed using a Hewlett-Packard 4339B high resistance meter (Figure 3.9). The samples were sandwiched between the stainless steel blocking electrodes in sample holder (4 cm in diameter). A potential difference of 1 volt was applied to the sample. Electrification time as 60 second was used for measurement.

Figure 3.9 Hewlett-Packard 4339B high resistance meter.

CHAPTER IV

RESULTS AND DISCUSSION

4.1 Computational Part

4.1.1 Conformational Energy from Molecular Mechanics Calculation

RIS model was employed to predict the conformational dependent properties of PEO using statistical weight matrices as the input. The elements of these matrices were estimated from the conformational energy map for small representative segment of polymer molecules calculated by Molecular Mechanics (MM) technique at 300 K. Model of PEO chain was represented by four skeletal bonds or pairs of dihedral angles (ϕ_i, ϕ_j). To find the minimized structure, the default force field was adopted with the search algorithm provided by Chem3D software. The conformational energies were obtained by rotating the dihedral angles and the optimized structure should be corresponded to the energy minimum structure for each pair of dihedral angles. An increment of dihedral angles (ϕ_i, ϕ_j) was set to $10°$ (rotation from $0°$ to $360°$). Model of PEO used in the computation are defined by three short segments according to each skeleton bond as follows: C-C, C-O and O-C bond.
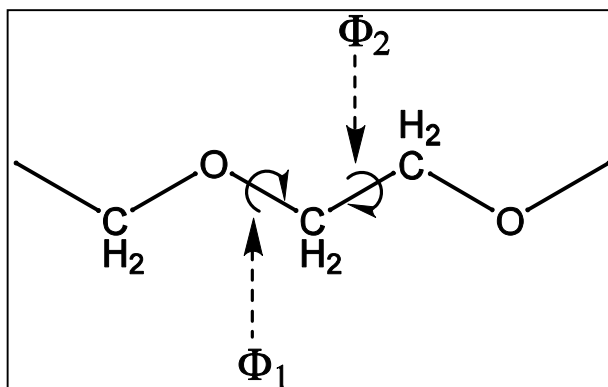
Figure 4.1 Schematic representation of PEO model with O-C and C-C (ϕ_1, ϕ_2) bond pair.
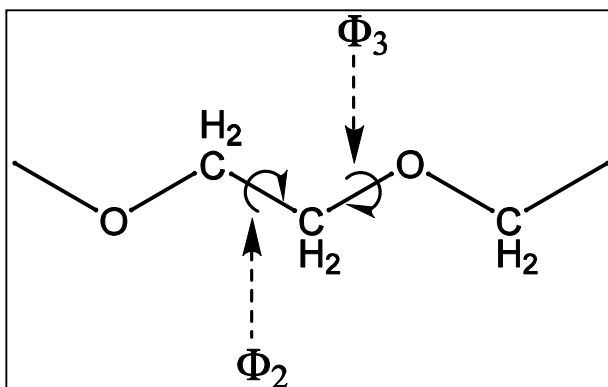
Figure 4.2 Schematic representation of PEO model with C-C and C-O (ϕ_2, ϕ_3) bond pair.
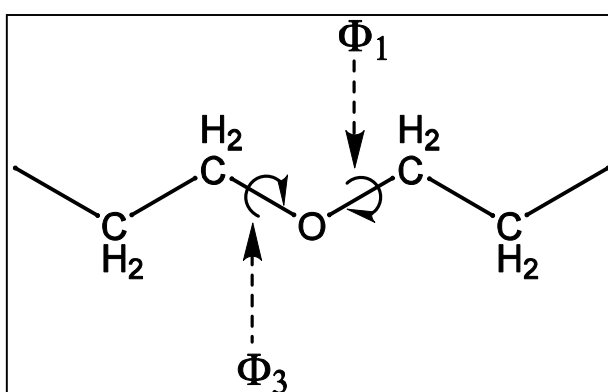
Figure 4.3 Schematic representation of PEO model with C-O and O-C (ϕ_3, ϕ_1) bond pair.

The skeletal bond conformations can be treated according to the rotational isomeric state model. The model assumes three discrete states: trans, gauche$^+$ and gauche$^-$, abbreviated as t, g^+ and g^-. The nine pair-wise dependent rotational isomeric states $(tt, tg^+, tg^-, g^+t, g^-t, g^+g^+, g^-g^+, g^+g^-, g^-g^-)$ and conformational energy contour maps for each bond pair of PEO model are plotted in Figure 4.4 - 4.6. The positions and magnitudes of the energy minima on the resulting energy-contour maps yield the values of the preferred rotational angles and their associated statistical-weights for each two-bond sequence. The conformational properties for the whole polymer chain can then be calculated from the properties of individual two-bond sequences using matrix multiplication technique.

$g^+ g^+ = 70°, 70°$

$g^+ t = 70°, 180°$

$g^+ g^- = 70°, 290°$

$t g^+ = 180°, 70°$

$t t = 180°, 180°$

$t g^- = 180°, 290°$

$g^- g^+ = 290°, 70°$

$g^- t = 290°, 180°$

$g^- g^- = 290°, 290°$

● = O atom   ○ = H atom   ◔ = C atom
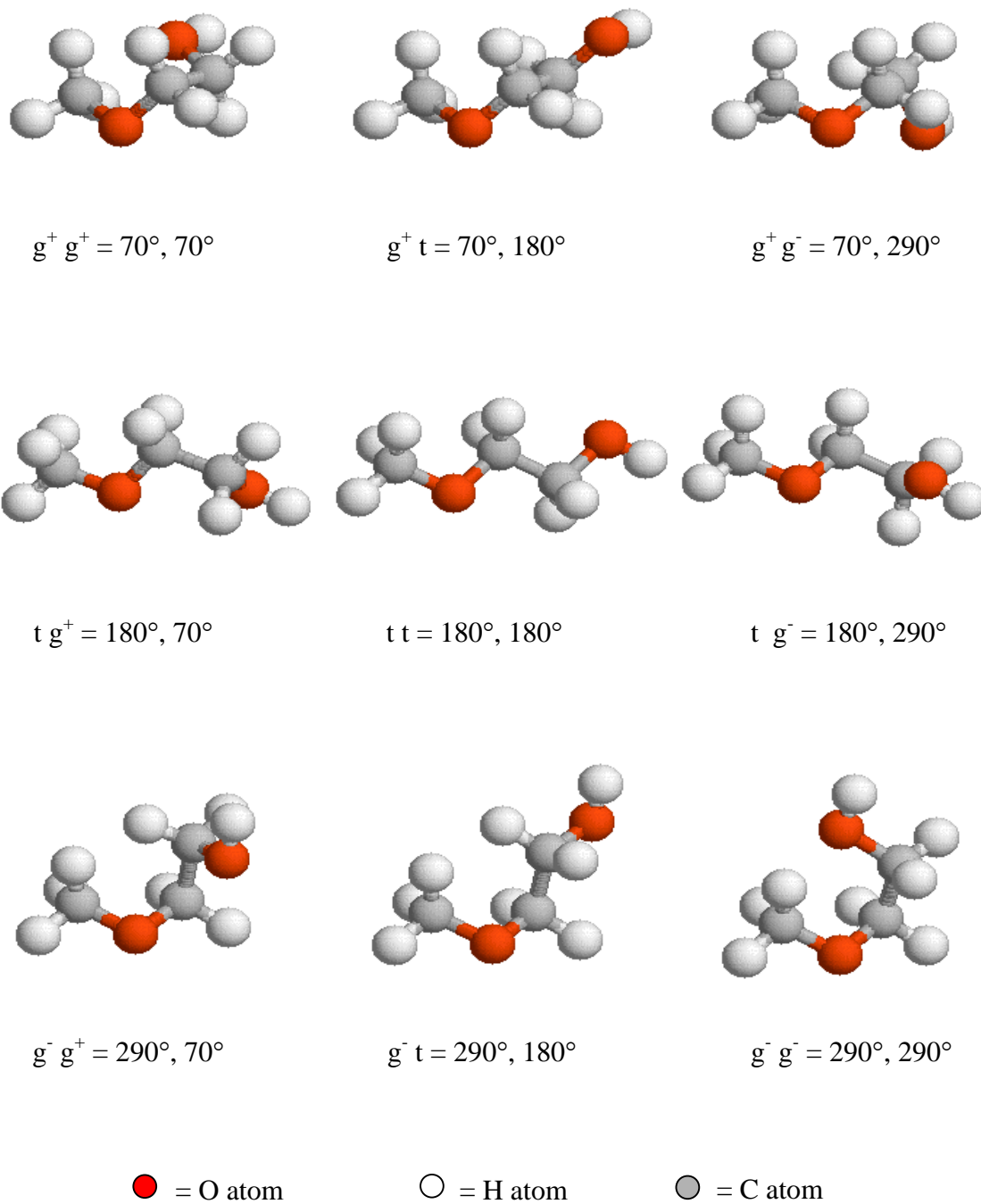
Figure 4.4a The nine pair-wise dependent rotational isomeric states of the

optimized PEO model with O-C and C-C (ϕ_1, ϕ_2) bond pair.
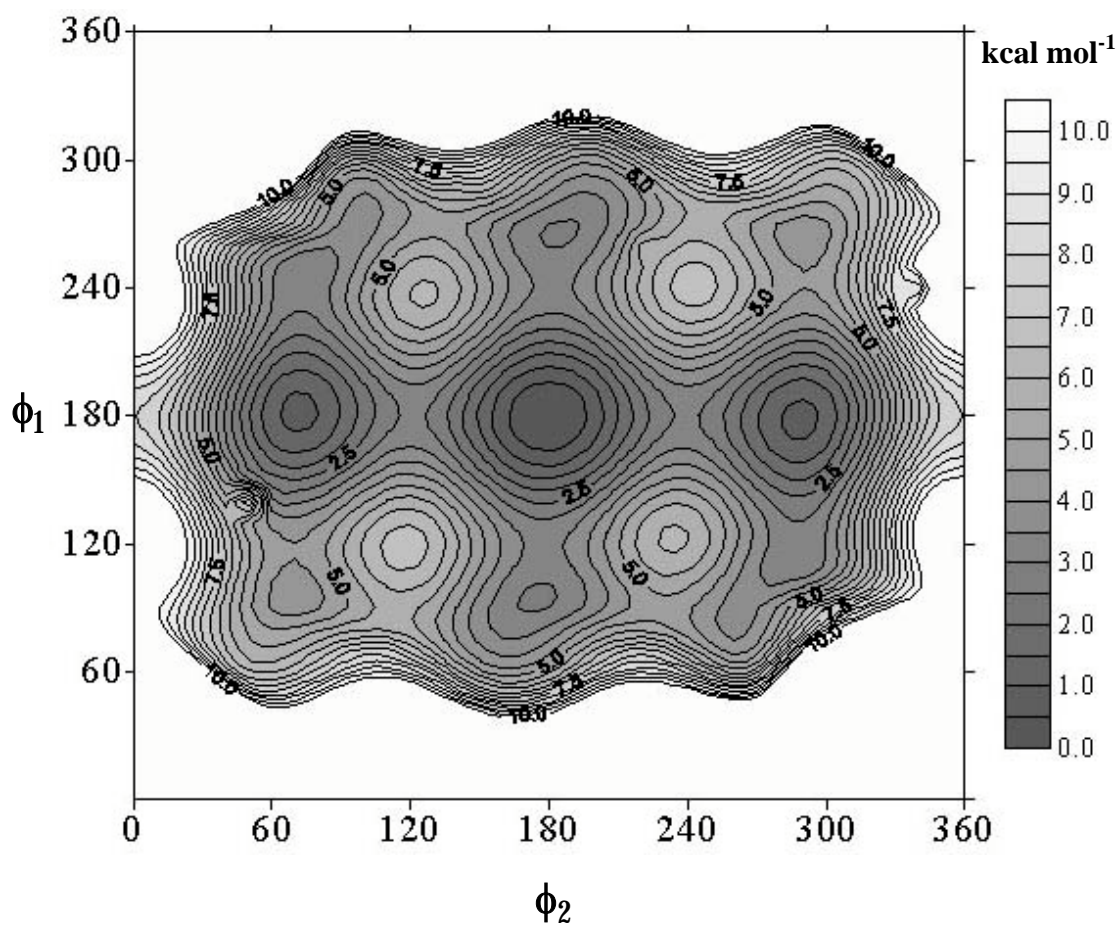
Figure 4.4b The conformational energy contour map (kcal mol^{-1}) for the

optimized PEO model with O-C and C-C (ϕ_1, ϕ_2) bond pair.

$g^+ g^+ = 90°, 90°$ $g^+ t = 90°, 180°$ $g^+ g^- = 90°, 270°$

$t g^+ = 180°, 90°$ $t t = 180°, 180°$ $t g^- = 180°, 270°$

$g^- g^+ = 270°, 90°$ $g^- t = 270°, 180°$ $g^- g^- = 270°, 270°$

● = O atom   ○ = H atom   ◯ = C atom
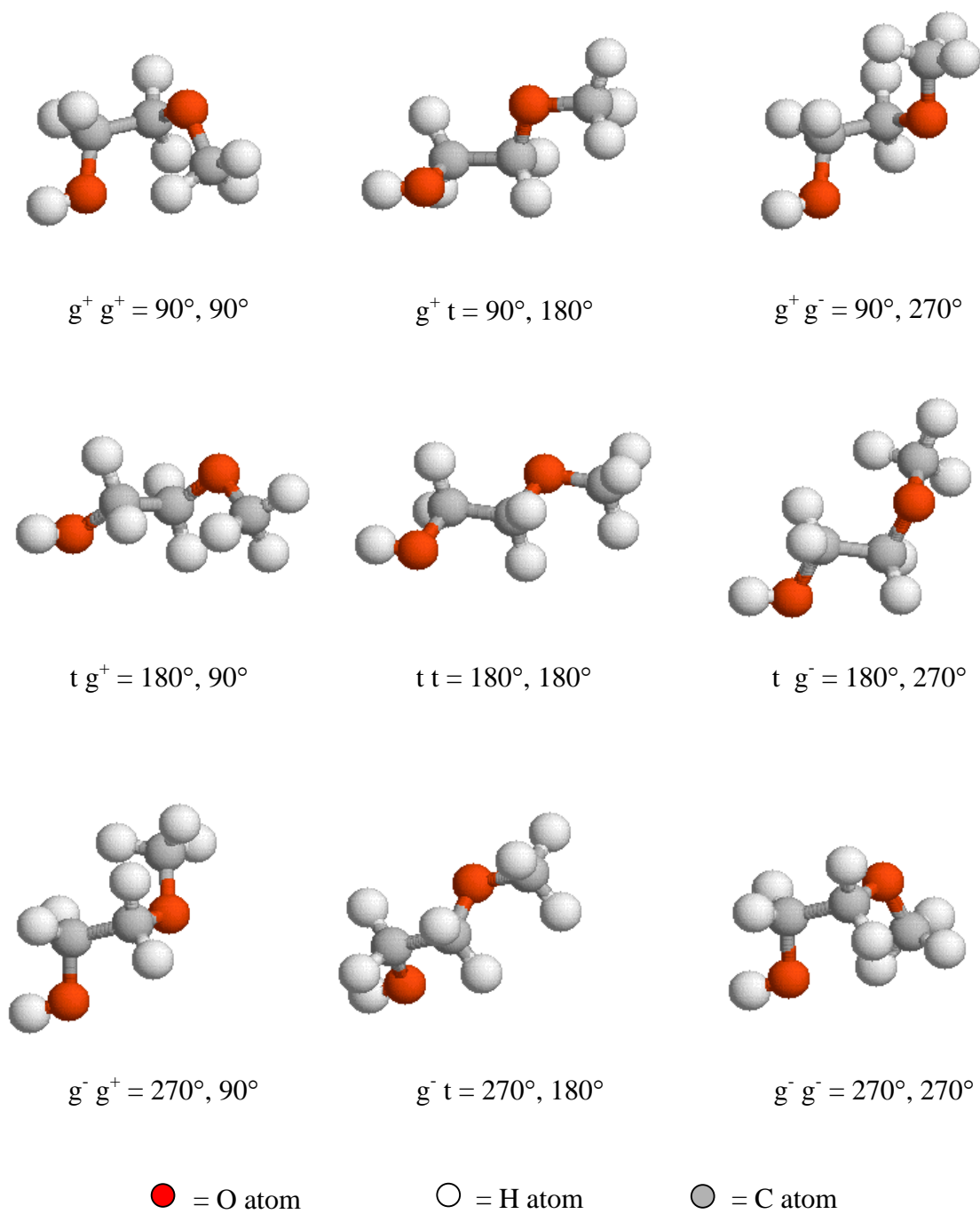
Figure 4.5a The nine pair-wise dependent rotational isomeric states of the optimized PEO model with C-C and C-O (ϕ_2, ϕ_3) bond pair.
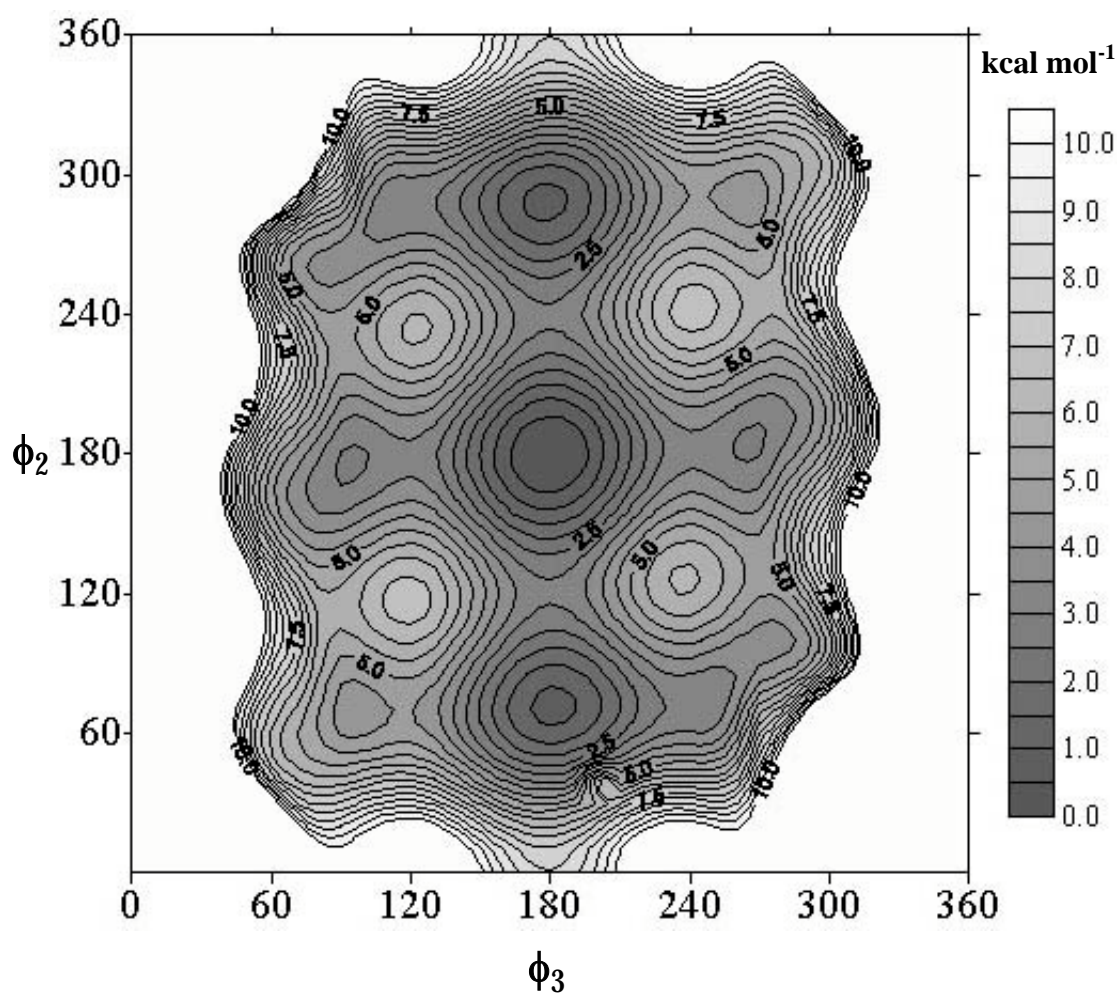
Figure 4.5b The conformational energy contour map (kcal mol^{-1}) for the

optimized PEO model with C-C and C-O (ϕ_2, ϕ_3) bond pair.

$g^+ g^+ = 90°, 90°$

$g^+ t = 90°, 180°$

$g^+ g^- = 90°, 270°$

$t g^+ = 180°, 90°$

$t t = 180°, 180°$

$t g^- = 180°, 270°$

$g^- g^+ = 270°, 90°$

$g^- t = 270°, 180°$

$g^- g^- = 270°, 270°$

● = O atom   ○ = H atom   ◯ = C atom
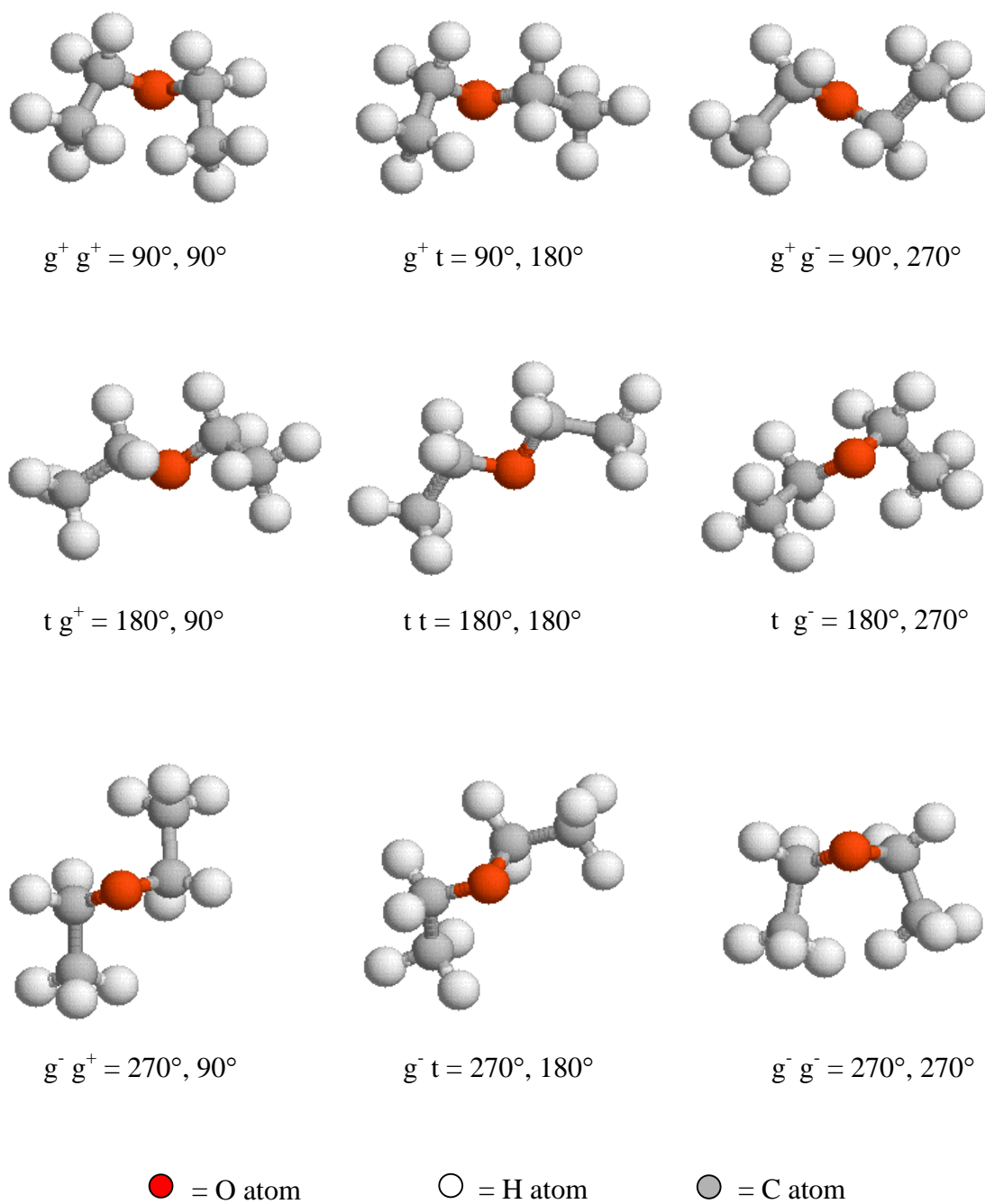
Figure 4.6a The nine pair-wise dependent rotational isomeric states of the

optimized PEO model with C-O and O-C (ϕ_3, ϕ_1) bond pair.
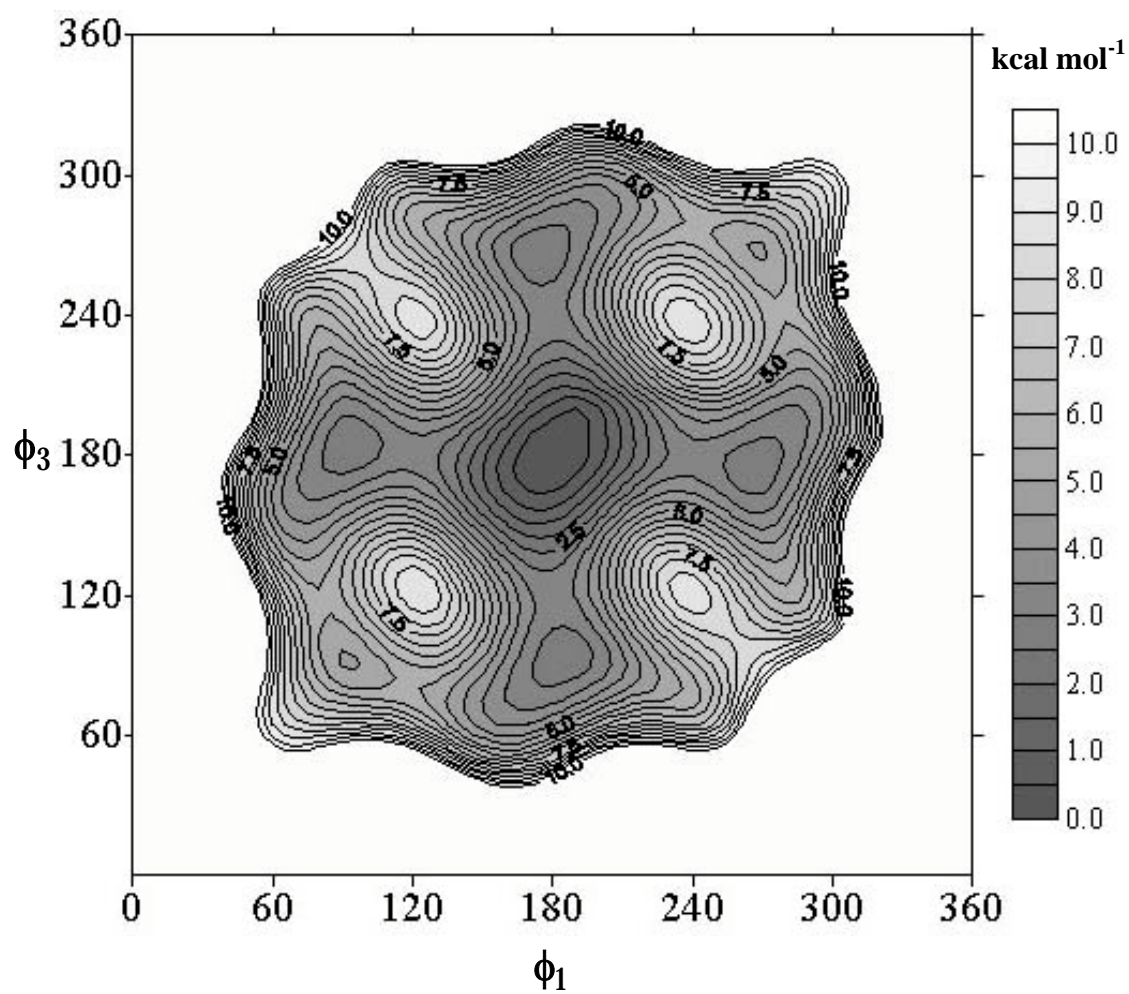
Figure 4.6b The conformational energy contour map (kcal mol^{-1}) for the optimized PEO model with C-O and O-C (ϕ_3, ϕ_1) bond pair.

4.1.2 Statistical Weight Matrices of PEO

The bond lengths, bond angles, torsion angles and dipole moment vectors used in this calculation are listed in Table 4.1.

Table 4.1 Geometrical parameters used in the RIS model

Bond length (Å)	Bond angle (°)	Torsion angle (°)			
			t	g^+	g^-
C-C 1.512	$\angle$CCO 110.7				
C-O 1.431	$\angle$COC 106.8	C-C	180	70	290
O-C 1.431	$\angle$OCC 110.7	C-O	180	90	270
		O-C	180	90	270

The conformational energies estimated from MM calculation are parameterized and grouped into the matrix by Eq. (3.32). The statistical weight matrices of (O-C, C-C), (C-C, C-O) and (C-O, O-C) bond pairs are as follows:

$$U_{OC-CC} \quad = \quad \begin{matrix} & g^+ & t & g^- \\ g^+ & \begin{pmatrix} 0.9315 & 0.9690 & 0.8611 \\ t & 0.9927 & 1.0000 & 0.9903 \\ g^- & 0.8540 & 0.9607 & 0.8835 \end{pmatrix} \end{matrix}$$

$$
U_{CC\text{-}CO} \quad = \quad
\begin{array}{c}
\\
g^+ \\
t \\
g^-
\end{array}
\begin{array}{ccc}
g^+ & t & g^- \\
\left(\begin{array}{ccc}
0.9313 & 0.9928 & 0.8536 \\
0.9687 & 1.0000 & 0.9604 \\
0.8609 & 0.9903 & 0.8833
\end{array} \right)
\end{array}
$$

$$
U_{CO\text{-}OC} \quad = \quad
\begin{array}{c}
\\
g^+ \\
t \\
g^-
\end{array}
\begin{array}{ccc}
g^+ & t & g^- \\
\left(\begin{array}{ccc}
0.9221 & 0.9750 & 0.8315 \\
0.9741 & 1.0000 & 0.9672 \\
0.8314 & 0.9678 & 0.8742
\end{array} \right)
\end{array}
\qquad (4.1)
$$

4.1.3 Conformational Dependent Properties of PEO

The RIS model is excellent for the rapid analysis of conformation-dependent properties of chain molecules in their 'unperturbed' state. The most frequently calculated property is the mean square unperturbed end-to-end distance, $\langle r^2 \rangle_o / nl^2$ (subscript zero designates the unperturbed state or θ point). Other properties susceptible to rapid computation include the mean-square dipole moment, $\langle \mu^2 \rangle_o / nm^2$, and the mean-square radius of gyration, $\langle s^2 \rangle_o / nl^2$. The viscosity of dilute polymer solution in θ condition can be estimated from $\langle r^2 \rangle_o / nl^2$ via the equivalent sphere model for hydrodynamic properties.

This section present an application of the RIS model to estimate the mean square unperturbed dimension and compare it to experimental result. Values of $\langle r^2 \rangle_o / nl^2$, $\langle s^2 \rangle_o / nl^2$ and $\langle \mu^2 \rangle_o / nm^2$, were computed for PEO chain using the RIS model with geometrical parameters listed in Table 4.1. The statistical weight matrices used in this calculation are from Eq (4.1). The results are summarized in Table 4.2.

Table 4.2 $\langle r^2 \rangle_o / nl^2$, $\langle s^2 \rangle_o / nl^2$ and $\langle \mu^2 \rangle_o / nm^2$ for PEO as estimated from the RIS model and experiments.

Properties	RIS calculation (300K)	Experimental result
$\langle r^2 \rangle_o / nl^2$	3.608	4.0[a] (313 K) 3.3[b] (298 K)
$\langle s^2 \rangle_o / nl^2$	5.412	-
$\langle \mu^2 \rangle_o / nm^2$	0.635	0.62[c] (293 K)

[a] Mark and Flory, 1965. [b]Intrinsic viscosity. [c]Bak, Elefante and Mark, 1967.

Conformational-dependent properties from the RIS model are in excellent agreement with those values from experimental results. For example, $\langle r^2 \rangle_o / nl^2$ from the previous literature measurement is 4.0 ± 0.4 at 313 K (Mark et al., 1965) and 0.62 at 293 K for $\langle \mu^2 \rangle_o / nm^2$ (Bak et al., 1967). The concurrence of these values with experimental results proposes that the conformation energy obtained from molecular

mechanic (MM) calculation by the default force field in Chem3D software can be used to construct an appropriated RIS model to predict other conformational-dependent properties.

Temperature Coefficients

The temperature coefficient of statistical properties such as the unperturbed, random-coil dimension $\langle r^2 \rangle_o$ assumes particular importance in the study of the configurations of chain molecules. In such configurational analyses, the temperature coefficient, $d \ln \langle r^2 \rangle_o / dT$, are interpreted using RIS theory to yield chain conformational energies, which, in turn, may be used to interpret and even predict values of other configuration-dependent properties of the molecule. The results are shown in Table 4.3 from RIS calculation of the temperature coefficient for PEO. The result thus obtained, $10^3 \, d \ln \langle r^2 \rangle_o / dT = 0.12 \, K^{-1}$, is comparable to the previous reported value of $0.23 \pm 0.02 \, K^{-1}$ (Bluestone et al., 1974).

Table 4.3 Temperature coefficients $d \ln \langle r^2 \rangle_o / dT$, of PEO.

	$d \ln \langle r^2 \rangle_o / dT \ (10^3 \, K^{-1})$
RIS calculation	0.12
Bluestone et al., 1974	0.23 ± 0.02^{a}

[a] determined in benzene.

Intrinsic Viscosity Measurement

Intrinsic viscosities of PEO in benzene were measured at 25°, 30°, 40°, 50° and 60 °C. At least four concentrations were investigated for each polymer solution. Intrinsic viscosities, $[\eta]$, were obtained in the usual manner by extrapolation of η_{sp}/c to infinite dilution. According to Eq. 3.75.

Table 4.4 Intrinsic viscosities of PEO in benzene.

Temperature	Intrinsic viscosities $[\eta]$ (g dl^{-1})	
(°C)	MW = 600 g mol^{-1}	MW = 20,000 g mol^{-1}
25	0.0316	0.3507
30	0.0114	0.3099
40	0.0946	0.2097
50	0.0307	0.1792
60	0.0192	0.0756

The intrinsic viscosities of PEO in benzene at 25 °C were 0.0316 (MW = 600 g mol^{-1}) and 0.3507 g dl^{-1} (MW = 20,000 g mol^{-1}) for two PEO samples. These results give molecular weights equal to 590 and 19,709 g mol^{-1}, respectively, according to the relationship (Bluestone et al., 1974).

$$[\eta] \;=\; 3.97 \times 10^{-4} \quad M_v^{\,0.686} \tag{4.2}$$

where $\boldsymbol{M}_v$ is a viscosity average molecular weight. Our finding seems to be reasonable as there are close to the molecular weight provided by the manufacture (600 and 20,000 g mol^{-1}). The dependence of ln $[\eta]$ on temperature for these two samples is shown in Figure 4.7. The results are well represented by the linear correlation as straight lines with covariance equal 0.966 and 0.961. The slopes of the lines give 10^3 d ln $\langle\eta\rangle_o/\boldsymbol{dT}$ = -0.070 and -0.041 K^{-1} for 600 and 20,000 g mol^{-1}, respectively. These values are comparable in magnitude to range of values –1.2 to –2.0 K^{-1} obtained by de Candia and coworker on four PEO fractions having viscosity-average molecular weights $\boldsymbol{M}_v$ in the interval 400-4,000 g mol^{-1} in the thermodynamically good solvents (Candia et al., 1972).

The result of temperature coefficient from RIS theory rarely gives agreement with experimental result. Among the reasons for this are following:

1. An energy minimization is equivalent to a zero-temperature calculation, whereas the chain statistics are desired at finite temperature.

2. The energy is calculated in vacuum, yet statistical weights can be affected by solvent, by other chain in the system, and by far-removed atoms in the same chain. This may seems surprising given that RIS theory by design applies only to θ chains.

3. The force field used might not be sufficiently accurate. Even a small error in, e.g., the energy of a *gauche* state relative to a *trans* state can have a large effect on the calculated conformational statistics of a chain. Although high-quality force fields and quantum methods exist, good first-principles predictions of chain statistical require accuracies on the order of 0.1 kcal mol^{-1} for the energy difference between accessible conformations.
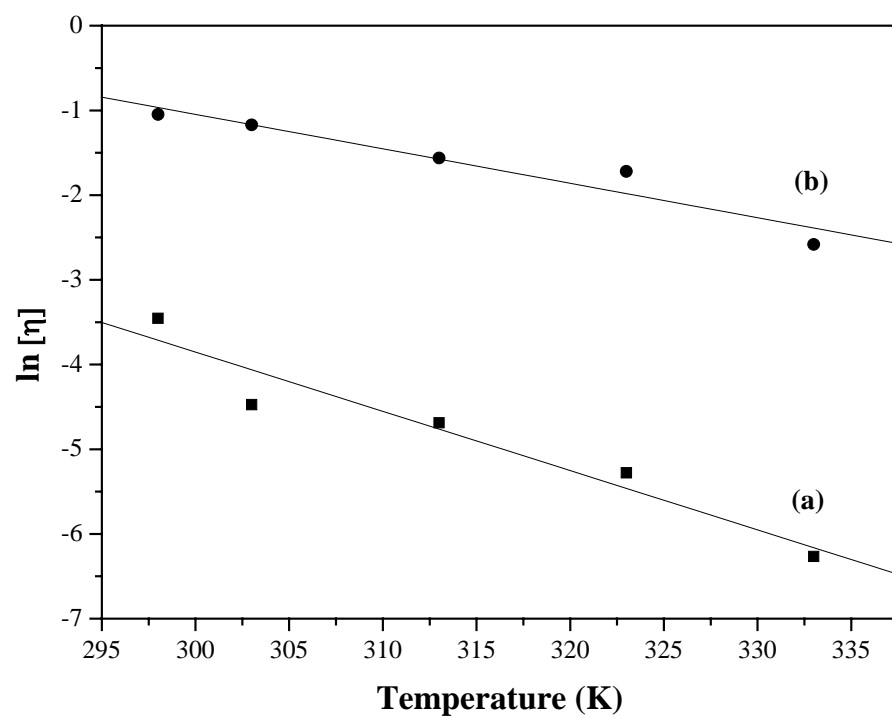
Figure 4.7 Intrinsic viscosity vs. temperature for PEO in benzene; the

molecular weights of the two samples are (a) 600 and (b) 20,000 g mol^{-1}

4.2 Experimental Part

4.2.1 Nuclear Magnetic Resonance (NMR) Spectroscopy

NMR spectroscopy is the most effective and significant method for observing the structure and dynamics of polymer chain both in solution and in the solid state. This part deals with solution NMR spectroscopy. Corresponding information may be obtained mainly by ^{1}H and ^{13}C spectroscopy.

Figure 4.8 shows the 300 MHz ^{1}H NMR spectra for 5% wt of PEG in D$_2$O solution recorded at 25.0 °C just below the melting temperature of PEO. From the spectra obtained the absorption signal only for PEG protons around 3.7 ppm and 4.8 ppm. Based on these results, the peak at 3.7 ppm is a typical NMR signal for the methylene proton on PEG and at 4.8 ppm owing to OH in chain end PEG.
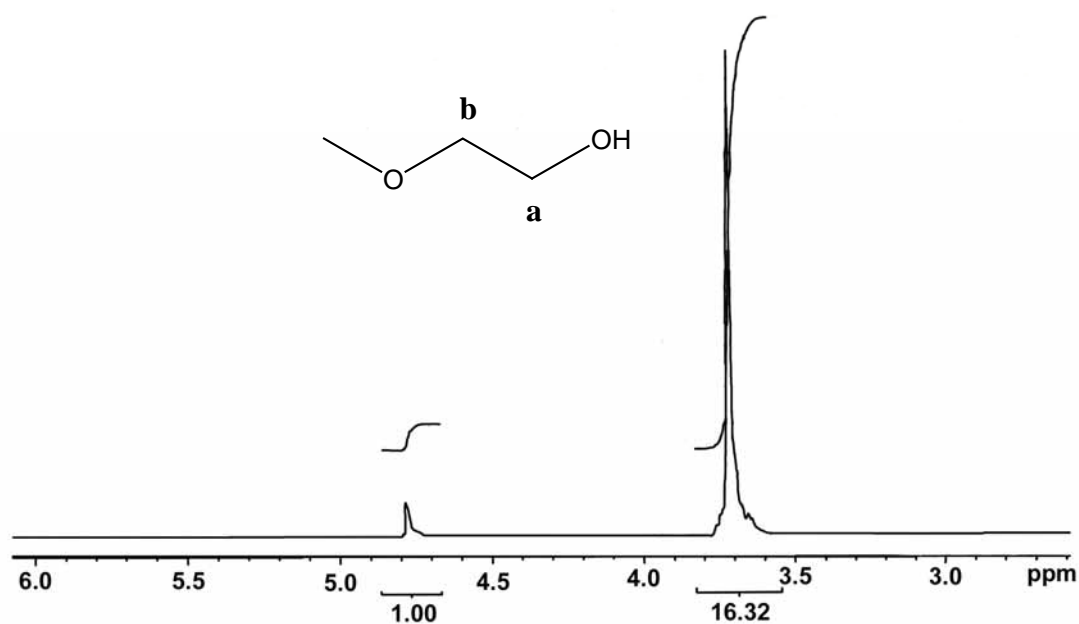
Figure 4.8 300 MHz ^{1}H NMR spectra for 5% wt of PEG in D$_2$O solution recorded at 25.0 °C.

Next, ^{13}C NMR spectra for 5% wt of PEG in D_2O solution were performed on a Varian Unity INOVA NMR spectrometer operating at 300 MHz (Figure 4.9). The NMR signals observed at 60.70 and 72.06 ppm are caused by carbon in terminal hydroxyethyl groups (**a**, 60.70 ppm and **b**, 72.06 ppm). The methylene (CH$_2$, **c**) in PEO split to three peaks at ~ 70 ppm.
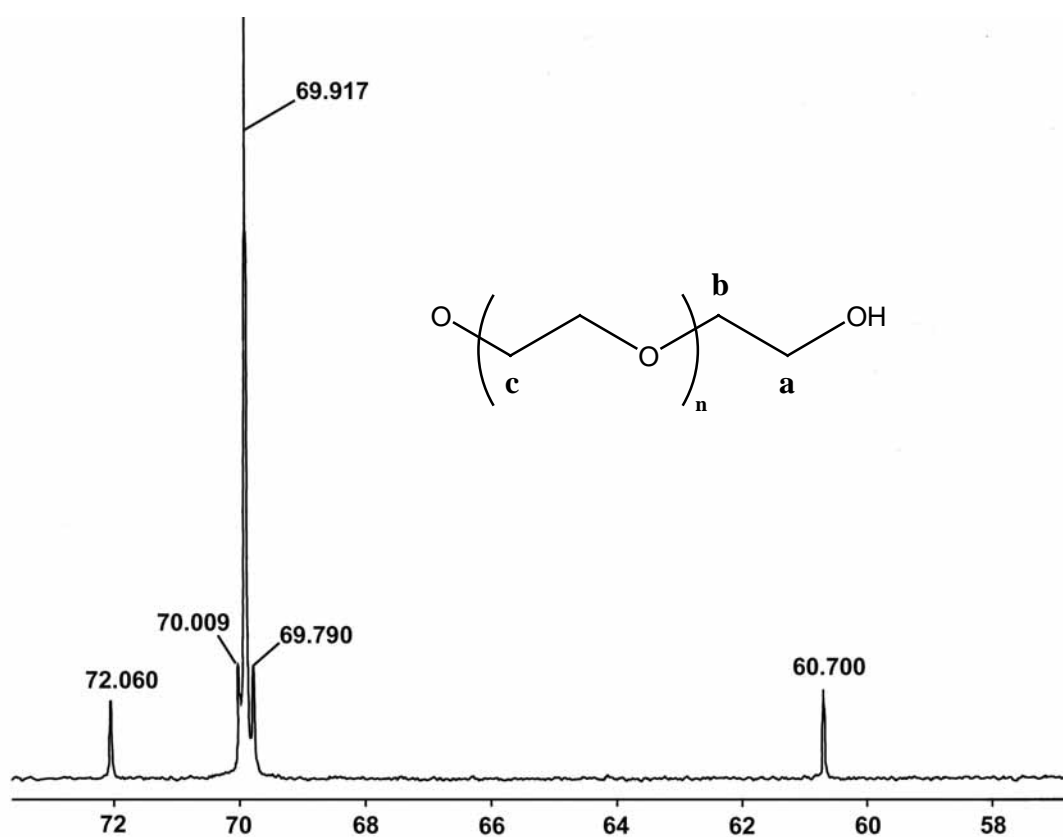
Figure 4.9 300 MHz ^{13}C NMR spectra for 5% wt of PEG in D_2O solution recorded at 25.0 °C.

Spin-Lattice Relaxation Times (T_1)

Proton spin-lattice relaxation times (T_1) for a 5 %wt solution of PEO in D_2O, measured over the temperature range 298-353 K are shown in Figure 4.10. The major contribution to proton relaxation in dilute solutions of PEO comes from the dipole-dipole interaction between the geminal protons in the methylene group. The observation that the temperature dependence of the PEO proton relaxation rate in dilute aqueous solution is accounted for by changes in the viscosity of the solvent is in agreement with the findings of Bieze (Bieze et al., 1994). This result came from measured deuteron relaxation rates in deuteriated PEO-H_2O solutions over the range 0-70 °C.

When K_2SO_4 is added to D_2O solutions of PEO, it has a pronounced effect on T_1. From experimental result T_1 values change from 0.71 sec without adding salt to 0.63 sec in 0.45 M K_2SO_4 solution at room temperature (298 K). It is speculated that the added salt drastically changes the solution viscosity of D_2O, through ion-solvent interactions, without interacting with PEO. Under these circumstances, a larger effective solvent viscosity would presumably impede polymer mobility, and lower the T_1 values.
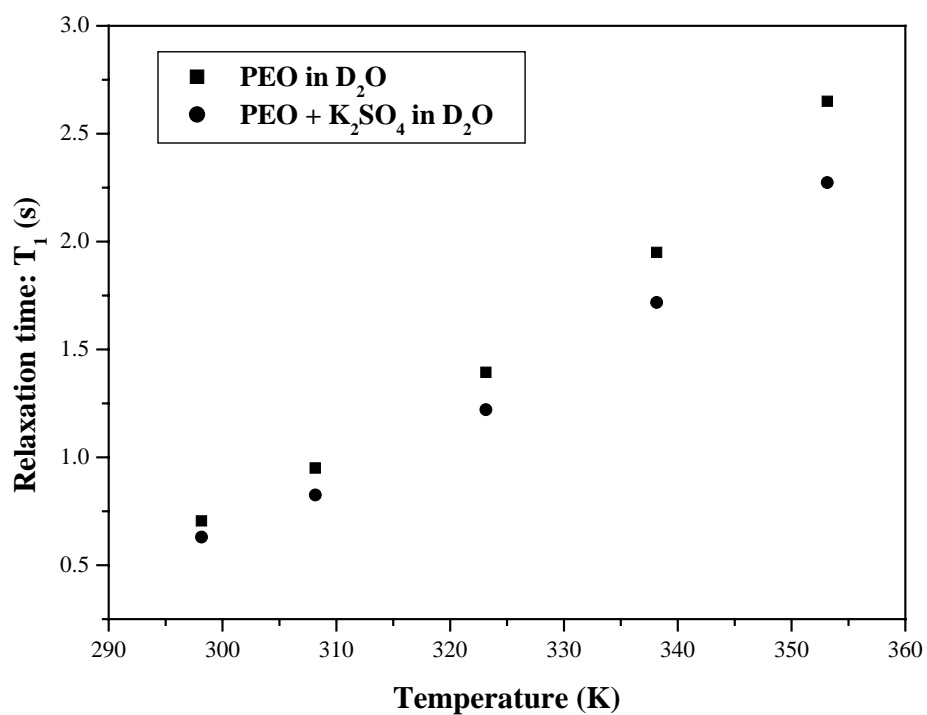
Figure 4.10 Temperature dependent of ^{1}H spin-lattice relaxation times for

(■) 5 %wt solution of PEO in D_2O (●) 5 %wt solution of PEO and 0.45

M K_2SO_4 in D_2O.

4.2.2 PEO-salt complexes (SPEs)

4.2.2.1 Effect of adding salt

SPEs are the materials of current interest due to ease of preparation in thin film, wide range of composition and mainly use in polymer batteries. Since the discovery of PEO-MX complexation, the complexes of PEO with alkali metal salts, divalent metal salts and transition metal salt ions have been studied. In the present study the polymer electrolytes belonging to the systems of $(PEO)_x LiCF_3SO_3$ and $(PEO)_x KSCN$ having oxygen to metal ion ratio (O:M) between 3 and 60 are studied by using the following techniques : FT-IR; XRD; DSC and conductivity measurement.

4.2.2.1.1 Infrared spectroscopy (IR)

I. $(PEO)_x LiCF_3SO_3$

The ionic transport in SPEs is strongly related to the cation-ether oxygen coordination bonds, to the freedom of polymer chains movements and to their rearrangements. Local relaxation and sequential motions of polymer host become essential to confer high ionic conductivity to the SPEs. Supporting evidence for ion association has been provided by vibrational spectroscopy studies. Different ionic species have been spectroscopically distinguished in polymer-salt system.

Ionic Association as a Function of Salt Concentration

Complexes of lithium triflate with poly(ethylene oxide) have been studied extensively by infrared spectroscopy in order to infer free ions, ion pairs and ion aggregates. The symmetric deformation mode of CF_3, $\delta_s(CF_3)$, is sensitive to ionic association in polymer-salt system. Figure 4.11 shows the spectra for $(PEO)_x LiCF_3SO_3$ systems as a function of O:M ratio in the $\delta_s(CF_3)$ spectral region, including pure PEO for comparison. At dilute salt concentrations, bands due to "free" triflate ion at 753 cm^{-1} and the ion pair at 757 cm^{-1} in 30:1 ratio are present. With increasing salt concentration, a band appears at 760 cm^{-1} attributed to the $(PEO)_x LiCF_3SO_3$ compound and the intensity grows until there is only a single band centered at this frequency for the 4:1 ratio. These assignments are consistent with an *ab initio* calculation and normal coordinate analysis (Huang et al., 1994).
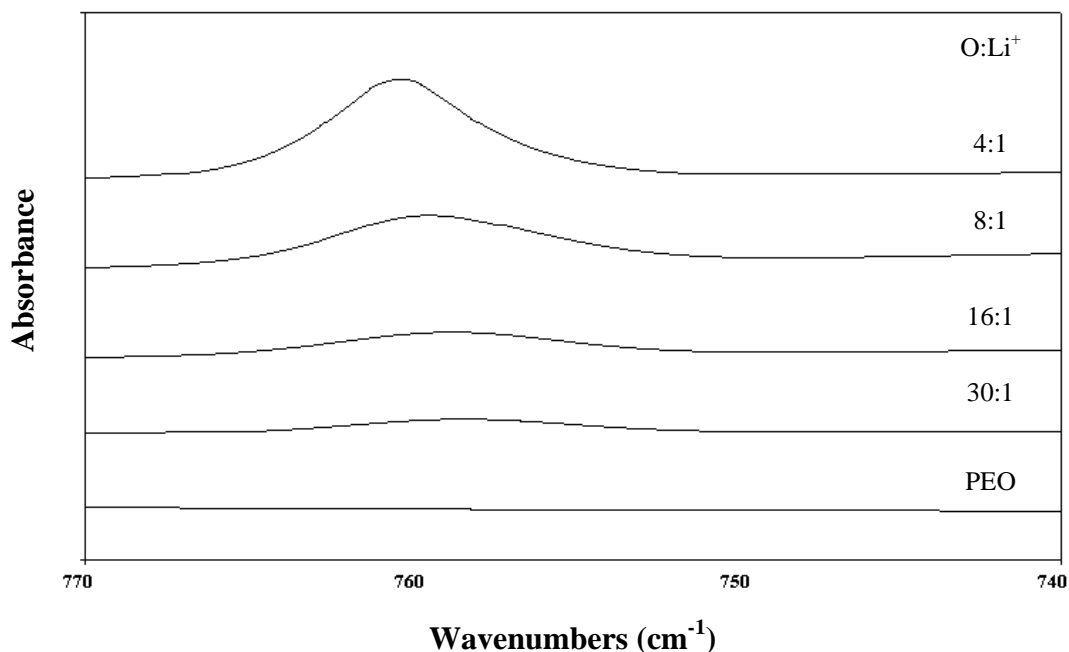
Figure 4.11 IR spectra of $(PEO)_xLiCF_3SO_3$ as a function of $O:Li^+$ ratio in the $\delta_s(CF_3)$ region.

Conformation of PEO Backbone

The 1000-800 cm^{-1} spectral region shown in Figure 4.12 is the characteristics of C-O stretching and CH$_2$ rocking modes. Spectral changes in this region reflect changes occurring in the local structure of the polymer backbone. The spectrum of pure PEO is also shown for comparison. The mode responsible for the band at 844 cm^{-1} is primarily due to the CH$_2$ rocking motion with a little C-O stretching motion mixed in, while the bands at 964 and 949 cm^{-1} originate primarily in the C-O stretching motion with some contribution from the CH$_2$ rocking motion. No significant changes are seen in the spectra of the dilute samples with $O:Li^+$ ratio of 50:1. When the salt concentration increases to 30:1, bands appear at 860, 834, 969,

956 and 952 cm^{-1}. The frequencies of these bands primarily due to CH$_2$ rocking motion are particularly sensitive to the local conformation of the polymer, specifically the O-C-C-O torsional angle. The appearance of one mode at a higher frequency and the second mode at a lower frequency than observed in pure PEO, originates from the interaction of lithium ion with ether oxygens. To coordinate the cation, the O-C-O-C torsional angle decreases in the compound relative to its value in pure PEO.
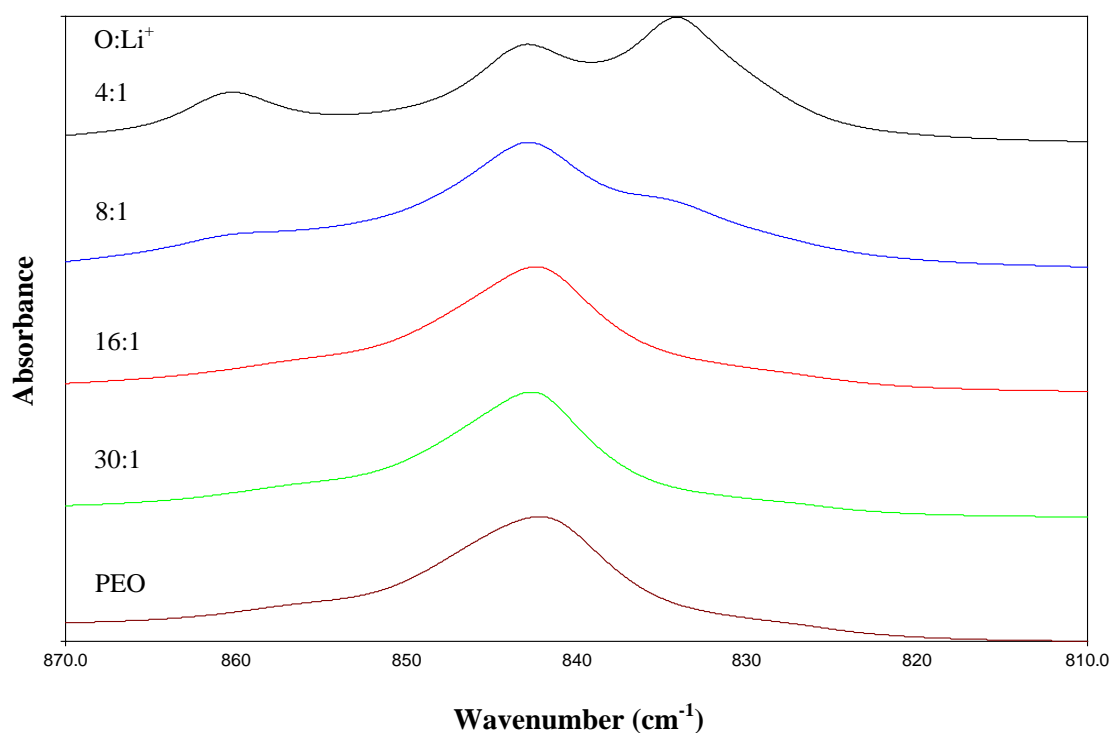
Figure 4.12 IR spectra of (PEO)$_x$LiCF$_3$SO$_3$ as a function of O:Li$^+$ ratio in the 900-800 cm^{-1} spectral region.

1400-1300 cm^{-1}

Figure 4.13 shows IR spectra in the 1400-1300 cm^{-1} region. The peaks at 1361 and 1342 cm^{-1} are CH$_2$ wagging modes which are the characteristic of crystalline PEO. With an increase in salt concentration, the intensity of 1361 cm^{-1} decreased drastically and replaced by a broad band at 1350 cm^{-1} for 4:1 compound, the broad band at 1350 cm^{-1} is assigned to crystalline content of PEO.
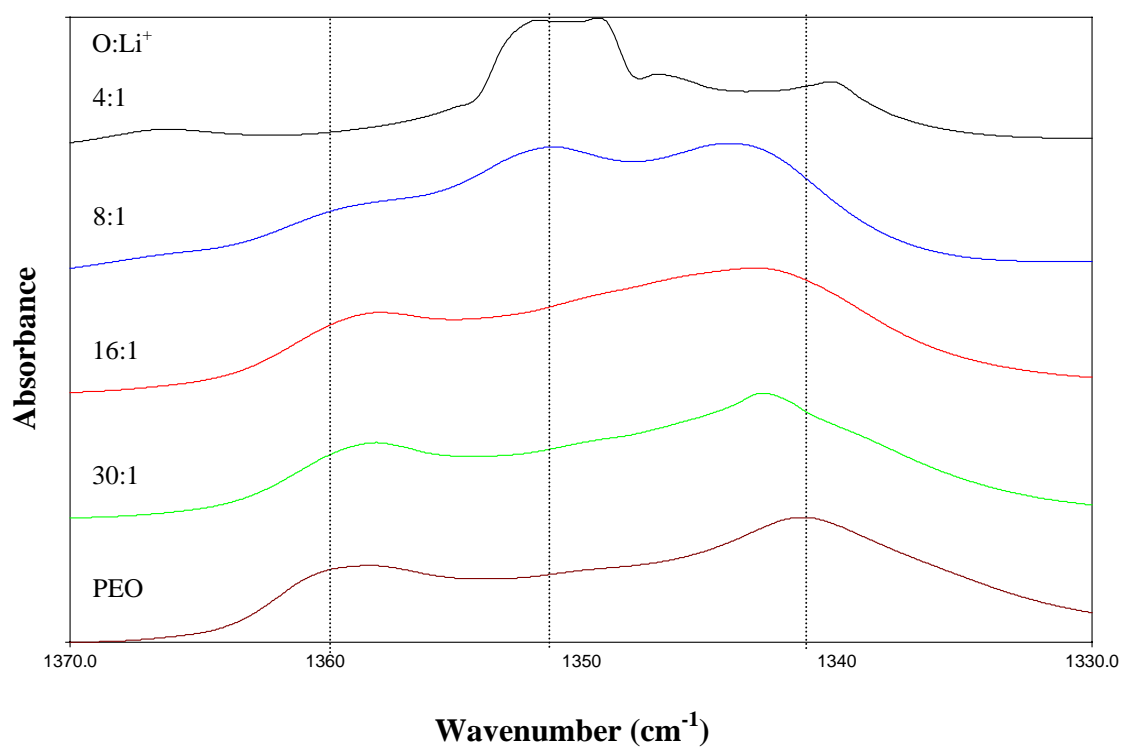
Figure 4.13 IR spectra of (PEO)$_x$LiCF$_3$SO$_3$ as a function of O:Li$^+$ ratio in the 1400-1300 cm^{-1} spectral region.

II. (PEO)$_x$KSCN

Polymer Backbone Conformation and CH$_2$ Twisting Mode

1400-1200 cm^{-1}

Figure 4.14 shows the IR spectra in the 1400-1260 cm^{-1} region. The peak at 1280 cm^{-1} is due to the CH$_2$ twisting mode in pure PEO. The intensity of these peaks decreases with increasing salt concentration. Although these modes between pure PEO and the compound shift very little, there are significant intensity differences as evident in the spectra. For (PEO)$_x$LiCF$_3$SO$_3$ system, peaks at 1361 and 1342 cm^{-1} are due to the CH$_2$ wagging of crystalline PEO. With increasing salt concentration, the peak at 1361 cm^{-1} is replaced by a broad band at 1350 cm^{-1} (amorphous PEO).
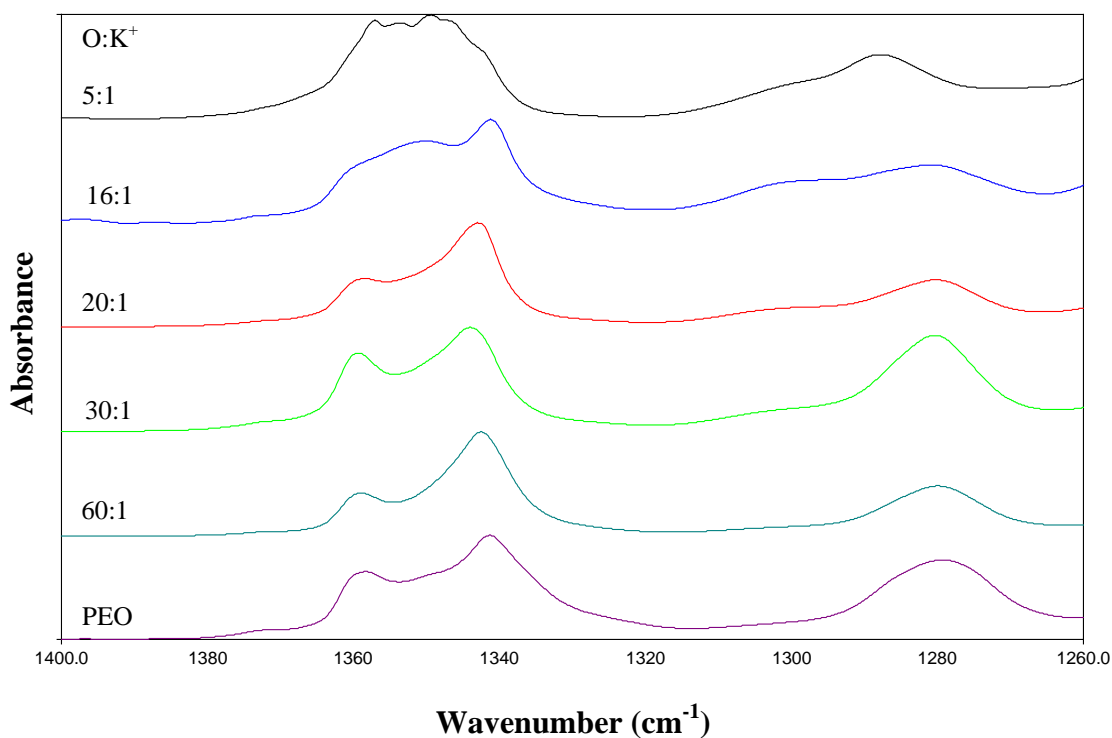
Figure 4.14 IR spectra of $(PEO)_xKSCN$ as a function of $O:K^+$ ratio in the 1400-1300 cm^{-1} spectral region.

Polymer Backbone Conformation

1000-800 cm^{-1}

The 1000-800 cm^{-1} region is the characteristics of the C-O stretching and CH_2 rocking mode. The bands in this region reflect the conformation of the polymer backbone and are sensitive to the interaction between cation and polymer backbone. Figure 4.15 shows the IR spectra of $(PEO)_xKSCN$ complex as a function of O:M ratio. The spectrum of pure PEO is also included for comparison. As described in $(PEO)_xLiCF_3SO_3$ system, peak at 844 cm^{-1} is ascribed primary to the rocking

motion of CH_2 units. With increasing salt concentration, several changes are visible. The peak at 844 cm^{-1} begins to decrease in its intensity and new peak appears at 833 cm^{-1}. The peak at 833 cm^{-1} is due to the compound of PEO and KSCN.
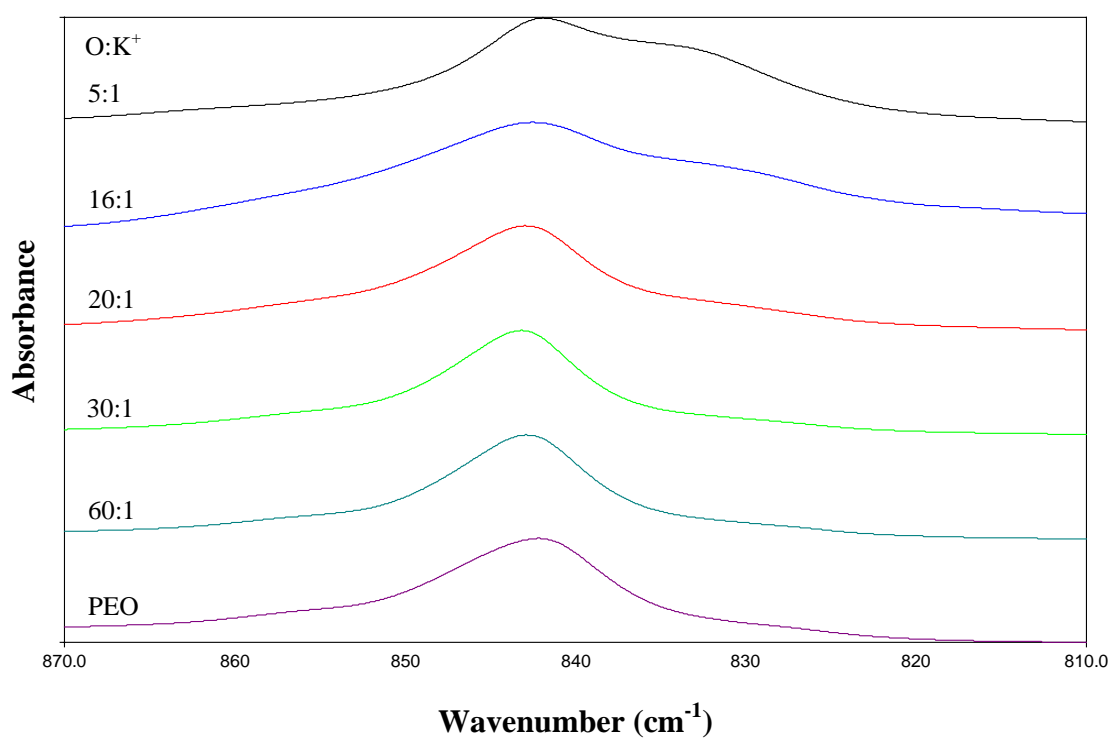
Figure 4.15 IR spectra of $(PEO)_x$KSCN as a function of $O:K^+$ ratio in

the 900-800 cm^{-1} spectral region.

Ionic Association as a Function of Salt Concentration

2400-1800 cm^{-1}

Figure 4.16 presents the IR spectra for pure PEO and (PEO)$_x$KSCN system in 2400-1800 cm^{-1} region. The bands in this region are related to ion-ion and ion-polymer interactions. The peak at ~2050 cm^{-1} characterizes C-N asymmetric stretching of SCN$^-$ anion. With an increase in salt concentration, this peak is sharper and it is more intensed for 16:1 and 5:1 complex. From these results, it suggests that an increase in salt concentration lead to ionic association increase.
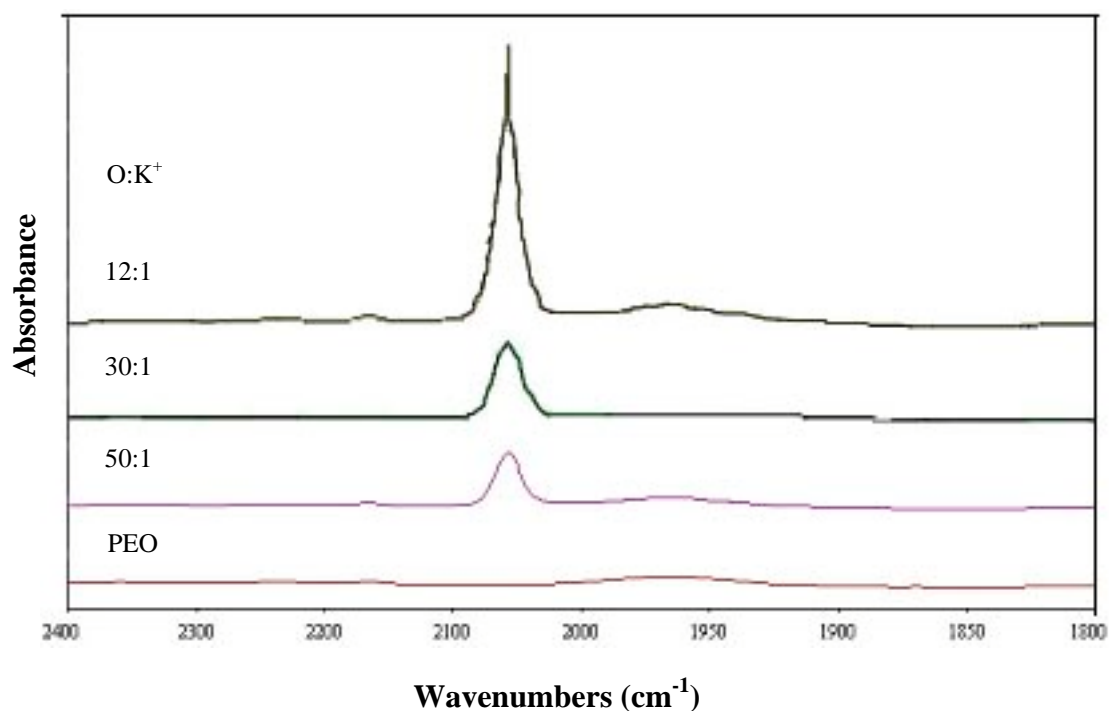
Figure 4.16 IR spectra of (PEO)$_x$KSCN as a function of O:K$^+$ ratio in the 2400-1800 cm^{-1} spectral region.

4.2.2.1.2 X-ray Diffraction (XRD)

Thermal and electrical behavior of PEO-salt systems can be better understood by characterization of the crystalline and amorphous phases of PEO and its complex. The XRD was performed to study the crystalline content. The results are described as follow

Figure 4.17 (a) and (b) shows the X-ray diffractograms in the 2θ region from 5° to 40° for the $(PEO)_x LiCF_3SO_3$ complexes with $O:Li^+$ ratios of 4:1, 8:1, 16:1 and 30:1. In addition, XRD patterns for pure PEO and $LiCF_3SO_3$ are also given for comparison. The XRD patterns for pure PEO gave two strong peaks, at 19° and 23°. The 30:1 and 16:1 complex also gave peaks at the same positions, but with lower intensities. This result is further evidence that the melting peak at 69.0 °C in DSC thermogram come from crystalline PEO, because the pure PEO phase still exist. It can be concluded that the crystalline phase in the film has the same structure as PEO, but at a lower percentage. Some portions of $(PEO)_x LiCF_3SO_3$ complex existed as an amorphous phase, and thus did not give a peak in the XRD pattern. The diffraction pattern of the 8:1 complex showed a completely amorphous phase. No peaks are observed in the XRD pattern, except a very broad humped baseline ranged from 17° to 30°. No peaks of pure $LiCF_3SO_3$ were observed, suggesting no free salt phase. The 4:1 complex showed absolutely different patterns from pure PEO. The peaks at 19 and 23° disappeared, suggesting that there was no free PEO crystalline phase. Many new peaks exist, implying that a new crystalline complex with well-defined structure is present.

Figure 4.18 shows X-ray diffractograms of $(PEO)_x KSCN$ complexes as a function of salt concentration in the 2θ region from $5°$ to $40°$ for the $(PEO)_x KSCN$ complexes, including pure PEO and pure KSCN for comparison. It can be seen that the 50:1, 30:1 and 16:1 complexes also gave peaks at the same positions corresponding to pure PEO (at 19 and 23°). The intensities of these peaks decrease while those due to PEO decrease (salt concentration increase) from 50:1 to the 30:1 complexes. It indicates that the crystalline phase of PEO still existed, but at a lower percentage. The peaks due to pure PEO are faintly visible in the 16:1 complexes and completely disappear in the 4:1 complexes.
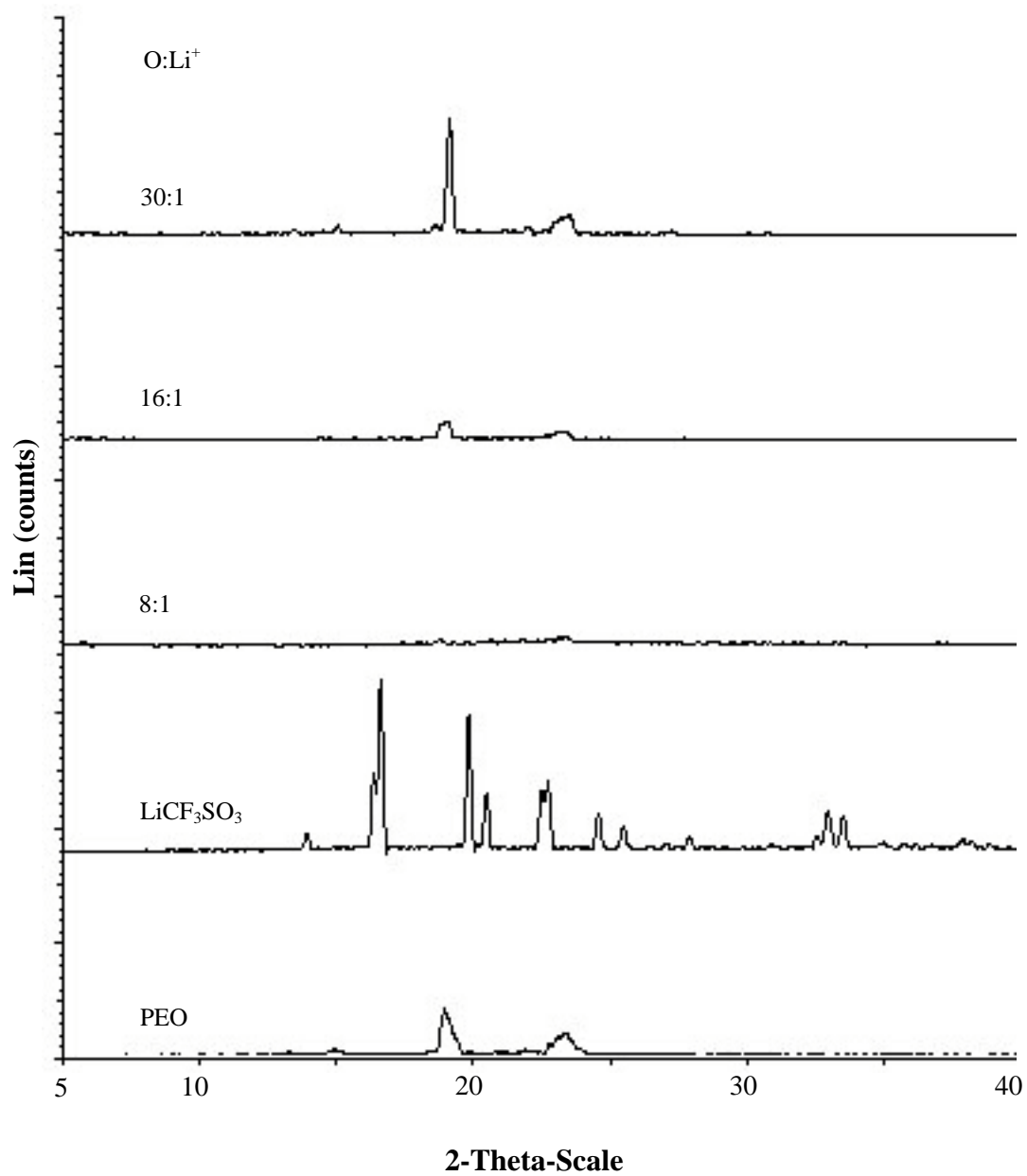
Figure 4.17(a) X-ray diffraction patterns of $(PEO)_x LiCF_3SO_3$ complex, including pure PEO and pure $LiCF_3SO_3$.
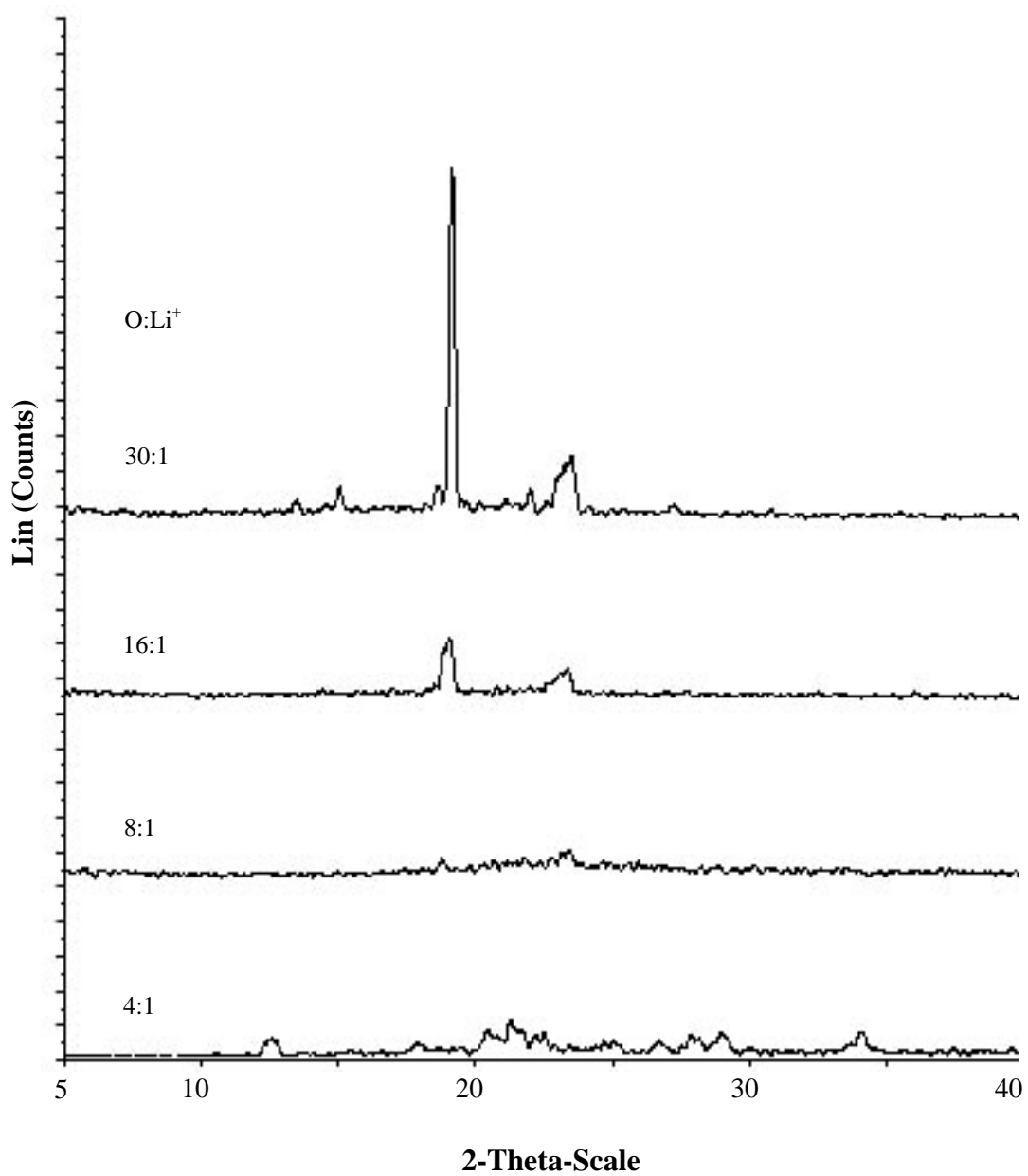
Figure 4.17(b) X-ray diffraction patterns of $(PEO)_xLiCF_3SO_3$ complex.
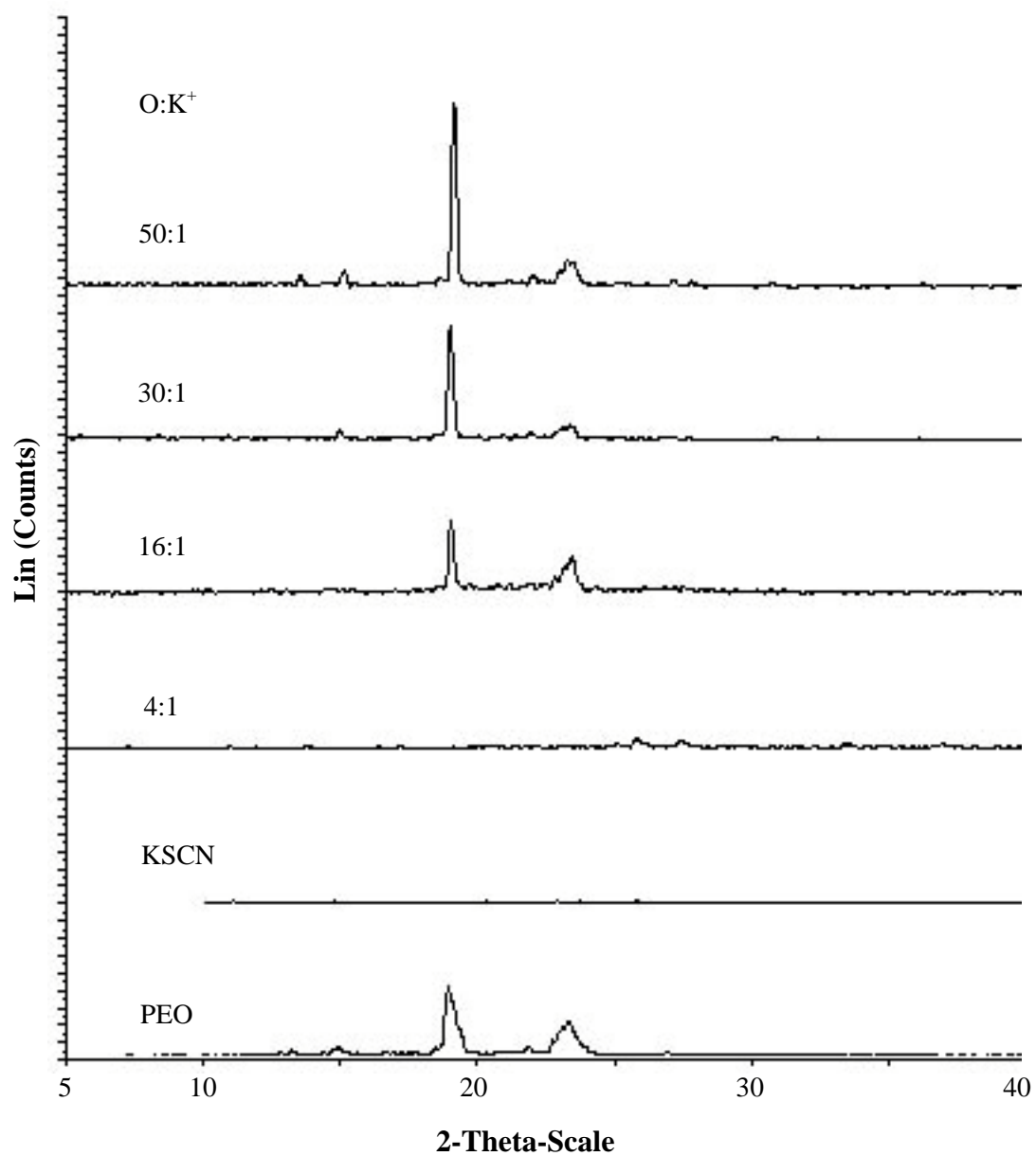
Figure 4.18 X-ray diffraction patterns of (PEO)$_x$KSCN complex, including

pure PEO and pure KSCN.

4.2.2.1.3 Differential Scanning Calorimeter (DSC)

Thermal behavior of PEO-salt complexes can be better understood by characterization of the crystalline and amorphous phase present in the complexes by using differential scanning calorimeter (DSC). The DSC thermograms of the PEO-salt complex give information on melting temperature (T_m), enthalpy of melting (ΔH) and percentage of crystallinity (%). The percentage of crystallinity can be calculated by integrating the area under the melting peak to obtain the endothermic energy change and comparing to a 100% crystalline PEO. The percentage of crystallinity was evaluated from the following equation.

$$\%\ \textbf{\textit{crystallinity}}\ \ =\ \ \frac{\Delta H_m}{\Delta H_m^0} \times 100$$

where ΔH_m is the enthalpy of melting of each sample and ΔH_m^0 is the enthalpy of melting of 100% crystalline PEO. The reported value of ΔH for 100% crystalline PEO is 45 cal g^{-1} or 188.1 J g^{-1} (Preechatiwong, et al., 1996).

The melting temperature and percentage crystallinity for each PEO-salt sample is summarized in Table 4.5. From DSC thermograms of pure PEO presented in Figure 4.19, the melting temperature of pure PEO is 69 °C and the percentage of crystallinity is approximately 70%. To compare DSC thermograms of pure PEO (Figure 4.19) with (PEO)$_x$LiCF$_3$SO$_3$ complex (Figure 4.20). In low salt concentration (16:1 ratio), the melting temperature of crystalline PEO is still observed with a lower crystallinity than pure PEO. In addition, 16:1 complex has a weak endotherm peak at

133 °C. From Rhodes et al. (2001), the 10:1 and 20:1 complex has a weak endotherm peak at 145 °C and 120 °C, respectively. They suggested that these peaks indicate very small amounts of the crystalline $(PEO)_3LiCF_3SO_3$ compound. In 3:1 complex, the melting temperature of crystalline PEO disappears, but show a high melting temperature at 189 °C of the fully complexed polymer-salt phase.

Table 4.5 Melting temperatures, enthalpy of melting and percentage crystallinity of $(PEO)_xLiCF_3SO_3$ and $(PEO)_xKSCN$ complexes.

Composition	T_m (°C)	ΔH_m (J g^{-1})	Crystallinity (%)
PEO	69.018	131.638	69.983
$LiCF_3SO_3$	226.100	-	-
KSCN	185.273	-	-
$(PEO)_xLiCF_3SO_3$ 16:1	69.041	65.566	34.857
$(PEO)_xLiCF_3SO_3$ 3:1	189.508	57.691	-
$(PEO)_xKSCN$ 50:1	74.136	84.844	39.413
$(PEO)_xKSCN$ 30:1	67.861	77.085	36.077
$(PEO)_xKSCN$ 16:1	63.070	39.958	21.243
$(PEO)_xKSCN$ 5:1	-[*]	-	-

[*] no peak observed in DSC thermogram

Figure 4.21 shows DSC thermograms for $(PEO)_xKSCN$ complex with $O:K^+$ ratios ranging from 30 to 5. The melting temperature, enthalpy of melting and percentage crystallinity of $(PEO)_xKSCN$ are similar to those of $(PEO)_xLiCF_3SO_3$ complex, i.e. when the salt concentration increases the percentage of crystallinity decrease. The complex at low salt concentration (30:1 and 16:1) result in lower crystallinity. It was assumed that the heat of fusion of the $(PEO)_xKSCN$ crystalline phase at the ratio 16:1 equals that of pure PEO (Preechatiwong et al., 1996). There is no strong peak in the DSC thermogram of the 5:1 complex; therefore, the mixture at this composition is completely amorphous.
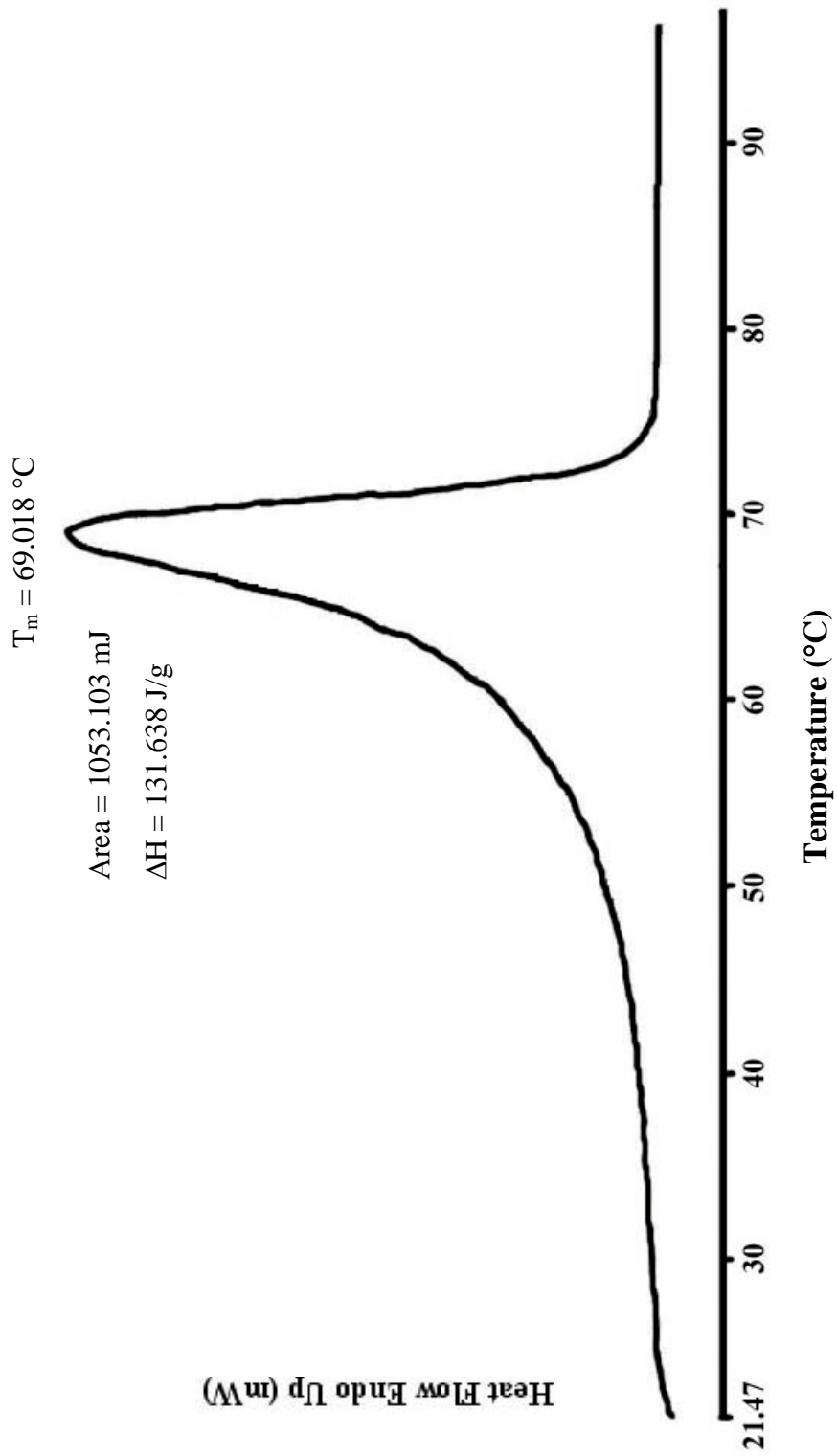
Figure 4.19 DSC thermogram for pure PEO.
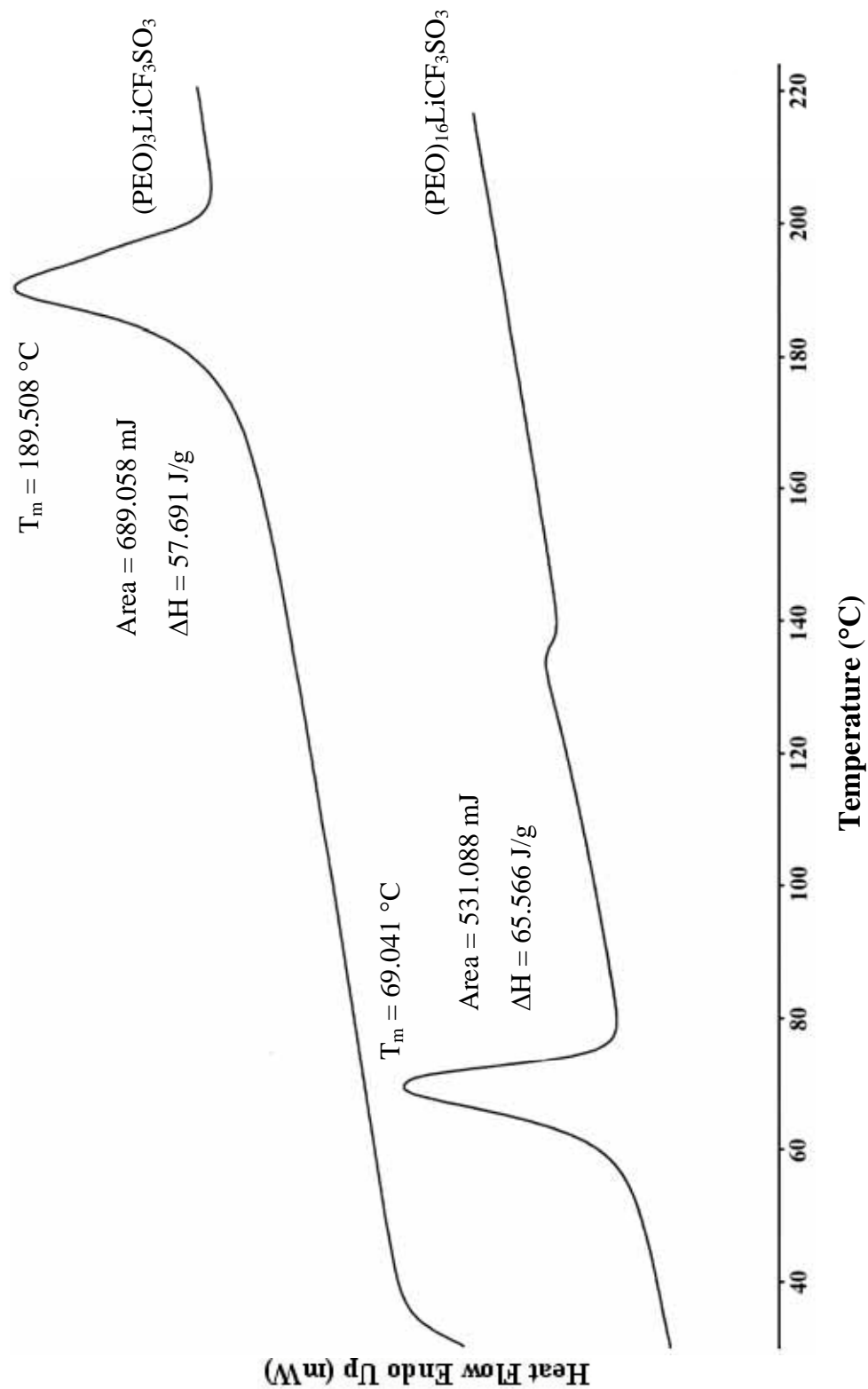
Figure 4.20 DSC thermogram for $(PEO)_xLiCF_3SO_3$ with different $O:Li^+$ ratio.
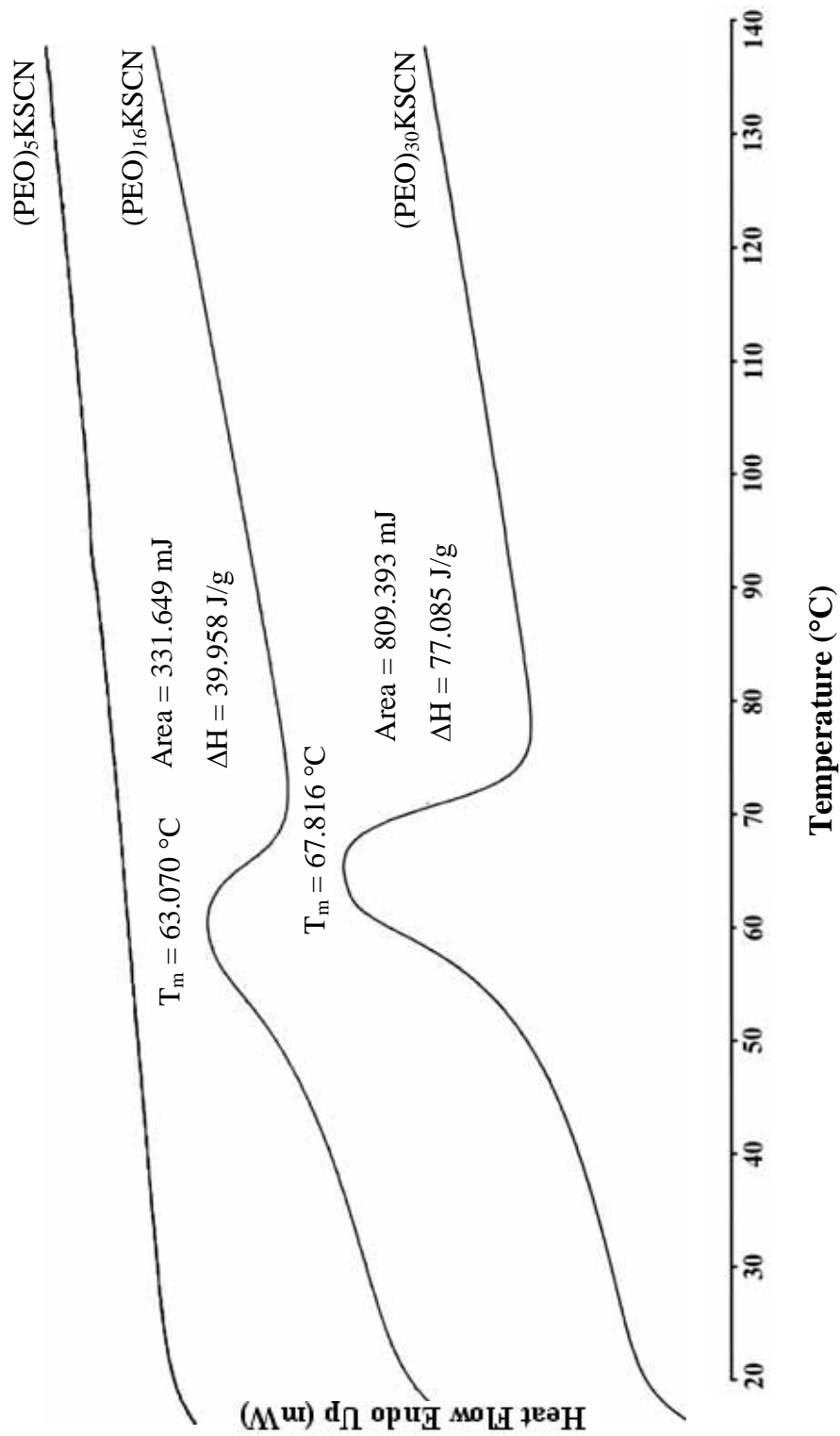
Figure 4.21 DSC thermogram for (PEO)$_x$KSCN with different O:K$^+$ ratio.

4.2.2.1.4 Conductivity Measurement

I. $(PEO)_xLiCF_3SO_3$

Comparison of the ionic conductivity for $(PEO)_xLiCF_3SO_3$ at room temperature with various salt concentrations is illustrated in Table 4.6 and Figure 4.22. A trend is observed in which conductivity increases with increasing salt concentration to a maximum (16:1), then it decreases at very high salt concentrations. The decrease in conductivity in $(PEO)_xLiCF_3SO_3$ was suggested to higher percentage of associated ions, ion pair and triple ions. This conclusion is supported by IR, XRD and DSC results. In IR spectra of $(PEO)_xLiCF_3SO_3$ (see Figure 4.11) at high salt concentrations (8:1 and 4:1 complexes), a band appears at 760 cm^{-1} attributed to ion pairs. XRD patterns and DSC thermogram at high salt concentrations suggest a new crystalline complex present.

Table 4.6 Ionic conductivity of pure PEO and $(PEO)_x LiCF_3SO_3$ electrolytes at room temperature.

O:Li$^+$ ratio	Weight Fraction of salt	Volume Fraction of salt	Conductivity (S cm^{-1})
3:1	0.542	0.347	0.385×10^{-9}
4:1	0.470	0.301	2.200×10^{-9}
8:1	0.307	0.197	4.800×10^{-9}
16:1	0.181	0.116	8.330×10^{-9}
20:1	0.151	0.097	2.270×10^{-9}
30:1	0.106	0.068	0.714×10^{-9}
40:1	0.081	0.052	0.330×10^{-9}
60:1	0.056	0.036	0.313×10^{-9}
Pure PEO	0.000	0.000	0.125×10^{-9}
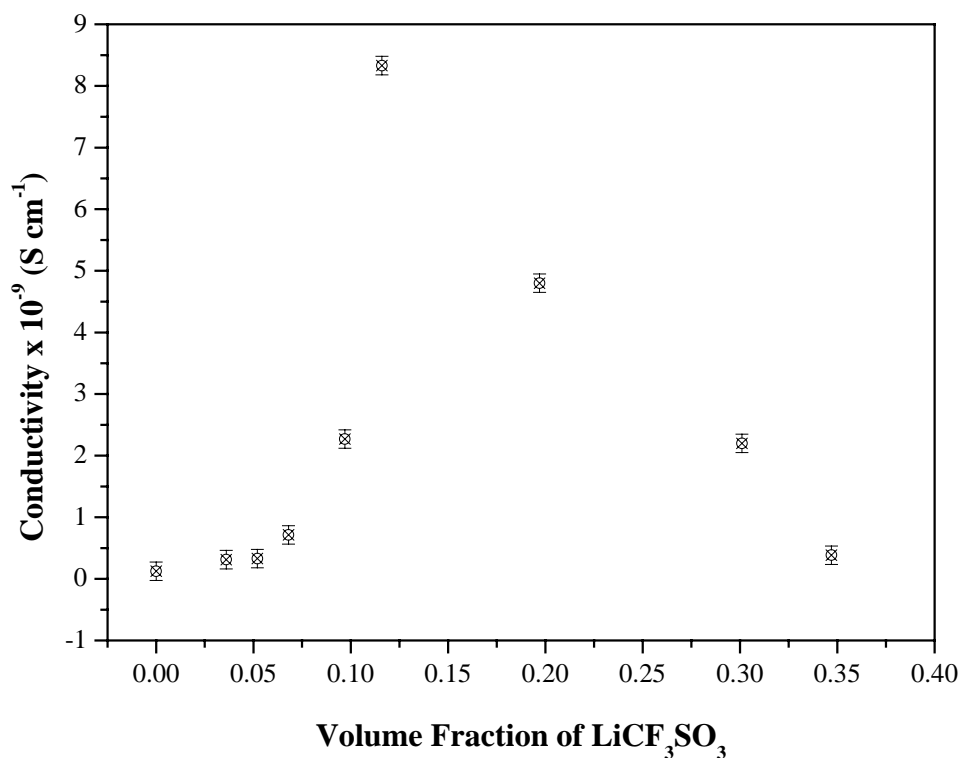
Figure 4.22 Ionic conductivity of pure PEO and $(PEO)_xLiCF_3SO_3$ complexes at various salt concentrations.

II. $(PEO)_xKSCN$

The ionic conductivity measurements carried out at room temperature of $(PEO)_xKSCN$ with various salt concentration are presented in Table 4.7 and Figure 4.23. Similar to $(PEO)_xLiCF_3SO_3$ complexes, the ionic conductivity increases when the salt concentration increases until the ratio $O:K^+$ equals to 16:1. After this point, the ionic conductivity decreases at high salt concentrations. A similar trend was also observed by Preechatiwong et al. (1996) and Zalewska et al. (2001). They found that the highest ionic conductivity of $(PEO)_xKSCN$ was at 8:1 complexes. In this work, the 8:1 complex could not be prepared because it was less soft.

Table 4.7 Ionic conductivity of pure PEO and $(PEO)_x KSCN$ electrolytes at room temperature.

O:K$^+$ ratio	Weight Fraction of salt	Volume Fraction of salt	Conductivity (S cm^{-1})
5:1	0.306	0.163	1.150×10^{-9}
16:1	0.121	0.064	1.430×10^{-9}
20:1	0.099	0.053	0.710×10^{-9}
30:1	0.068	0.036	0.400×10^{-9}
40:1	0.052	0.028	0.390×10^{-9}
50:1	0.042	0.022	0.350×10^{-9}
60:1	0.035	0.019	0.300×10^{-9}
Pure PEO	0.000	0.000	0.125×10^{-9}
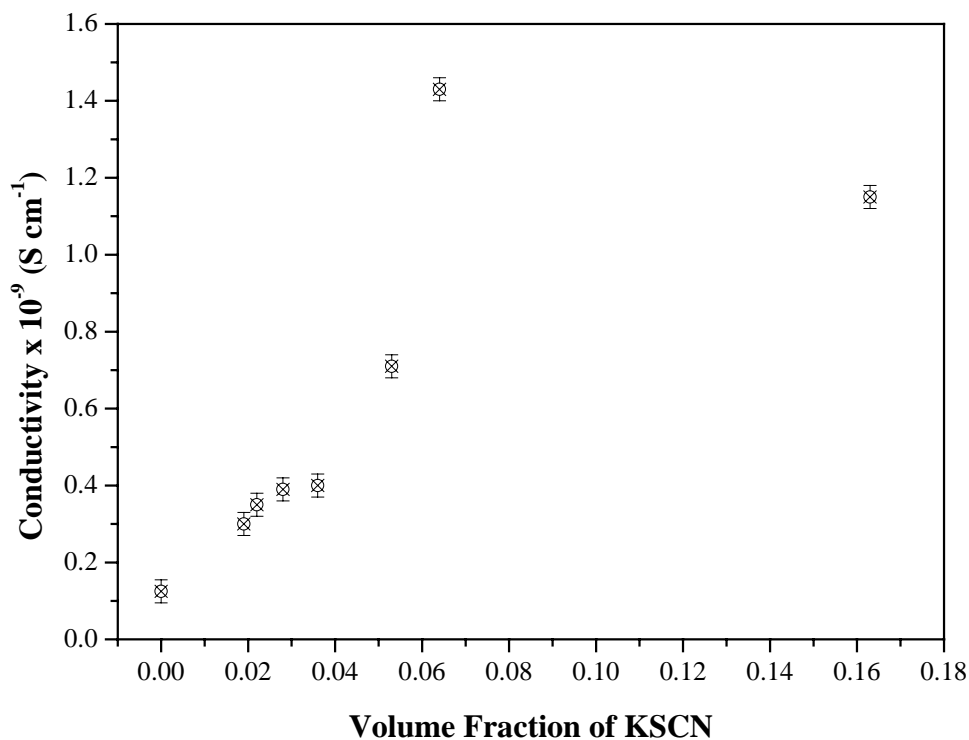
Figure 4.23 Ionic conductivity of pure PEO and $(PEO)_xKSCN$ complexes at various salt concentrations.

Our results suggest that $(PEO)_xLiCF_3SO_3$ complexes give higher ionic conductivity than that of $(PEO)_xKSCN$ complexes. Because the amount of charged species introduces on of the most complex features in the polymer-salt complex, which may result in the presence of ion pairs, triplets, or even higher degrees of association multiplets. As a result, the conductivity is reduced since neutral ion pairs or neutral multiplets do not contribute to the conductivity. In IR spectra of $(PEO)_xKSCN$ complex (Figure 4.16), ion association occurs at wavenumber ~2100 cm^{-1}. This interaction was stronger than $(PEO)_xLiCF_3SO_3$ complex (~760 cm^{-1}) and hence reduce the ion mobility for conduction.

Next the ionic conductivity as a function of salt concentration is presented. At low salt concentrations, increasing the salt concentration increases conductivity because there is more number of free carrier ions. At high salt concentrations, conductivity decreases because the crystalline complex between PEO and salt is formed.

4.2.2.2 Effect of adding plasticizer

PEO-salt complexes are the earliest and the most extensively studied system. There electrolytes commonly exhibit conductivities ranging from 10^{-8} to 10^{-4} S cm^{-1} at temperatures between 40 °C and 100 °C, which excludes practical applications at ambient temperature. This obstacle originates from, first, the high degree of crystallinity which is unfavourable for ion conduction in these complexes, and, second, the low solubility of salt in the amorphous phase (Berthier et al., 1983). Many valuable investigations have therefore focused primarily on the enhancement of the room temperature conductivity. The most striking advancements in the ionic conductivity of polymer electrolytes have been attained through the incorporation of substantial amounts of plasticizers. In addition to reducing the crystalline content and increasing the polymer segmental mobility, plasticizers can result in greater ion dissociation which allows greater numbers of charge carriers for ionic transport. Low-molecular-weight polyethers and polar organic solvents are two common plasticizers for these purposes. Yang and coworker studied the effect of adding dimethyl ether PEG (MW 750 g mol^{-1}) on PEO/LiClO$_4$ complex. They found that PEO/LiClO$_4$ electrolyte blended with 50 mass% of dimethyl ether PEG has an ionic conductivity close to 2 x 10^{-5} S cm^{-1} at 25 °C, which is about 200 times above that of the additive-free complex (Yang et al., 1990).

In this work, thermal and vibrational spectroscopic studies on the role of plasticizers in (PEO)$_x$LiCF$_3$SO$_3$ and (PEO)$_x$KSCN system are reported. The results of ionic conductivity measurements are also presented. The plasticizer used in this

study is low molecular weight poly(ethylene glycol) (PEG), which is –OH terminate and molecular weight equal 600 g mol^{-1}.

4.2.2.2.1 Infrared Spectroscopy (IR)

I. $(PEO)_xLiCF_3SO_3$ with different %wt of PEG

Ionic Association in Plasticized (PEG) SPEs

Ionic association is one of the main factors limiting ion conduction in solid polymer electrolytes (SPEs). This effect reduces the efficiency of the materials in any potential applications. One method of improving the conductivity of SPEs, without a great loss of their mechanical properties, is the addition of a low molecular weight co-solvent or plasticizer. The bands in the symmetric deformation of CF$_3$, δ (CF$_3$), spectra region are shown in Figure 4.24 for the $(PEO)_xLiCF_3SO_3$ system with different weight percent of PEG. As seen in the previous part (4.2.2.1.1), this band is sensitive to environmental changes around the triflate ion. There are three bands in the $\delta(CF_3)$ region: a small band at 753 cm^{-1} assigned to "free" triflate ions, a large band at 757 cm^{-1} assigned to ion pairs and a small band at 760 cm^{-1} assigned to a higher aggregate or $(PEO)_3LiCF_3SO_3$ compound. These assignments are based on numerous spectroscopic studies of the triflate ion vibrations in a variety of ethylene-oxide based solutions. Here, "free" triflate ion refers to the triflate species with no degree of ionic association but may exhibit weak interactions with the polymer host (PEO). In the 16:1 complex, after an addition of PEG, the band at 760 cm^{-1} due to the higher

aggregate is presented. There is a very slightly change in the intensity of this band. With increasing PEG content to 100 % weight PEG, the intensity of these band decrease and shift to 753 cm^{-1}. Chintapalli et al. (1996) also observed a similar trend in the PEO/LiCF$_3$SO$_3$ system plasticized with ethylene carbonate (EC) and propylene carbonate (PC). They found that, with an addition of EC or PC, the intensity of peaks at 753 and 757 cm^{-1} grow in both plasticized systems at the expense of the compound peak at 760 cm^{-1}. The intensity for the peaks of ion pair in the PC plasticized system increase and numbers of free ions are greater than that in the EC plasticized system.
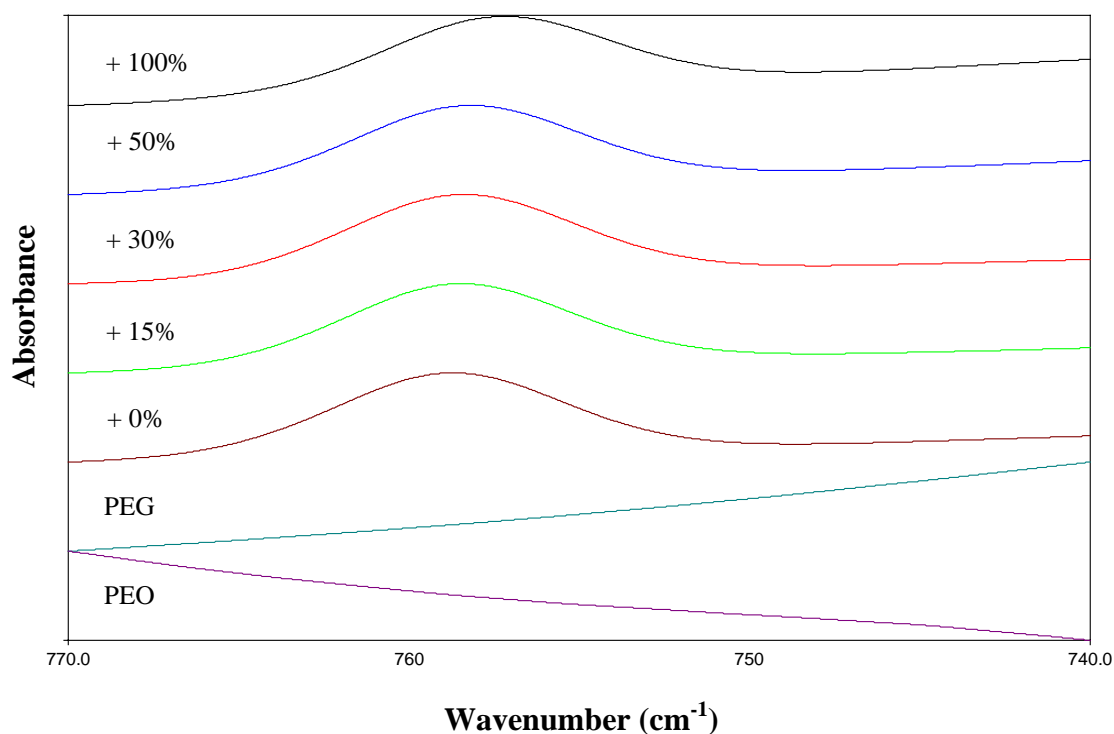
Figure 4.24 IR spectra of (PEO)$_{16}$LiCF$_3$SO$_3$ at different % weight PEG in the 800-700 cm^{-1} region

Conformation of PEO Backbone

In Figure 4.25, the infrared spectra of $(PEO)_{16}LiCF_3SO_3$ at different % weight of PEG compound are compared with the spectra of pure PEO and PEG in the 800-900 cm^{-1} region. Vibrational modes of this spectral region were assigned to a mixture of predominantly CH_2 rocking and C-O stretching motions. The frequencies and intensities of these modes are sensitive to the values of backbone torsional angles. Thus, this band is ideal for monitoring the changes in the conformation of PEO upon addition of PEG. In $(PEO)_xLiCF_3SO_3$ system, the band at 844 cm^{-1} is ascribed primarily to the CH_2 rocking motion mixed with C-O stretching. In the $(PEO)_{16}LiCF_3SO_3$ plasticized system, the coordination between cation and ether oxygen could be observed from the shift of C-O-C stretching peak, because of the strong positive effect of cation and plasticizer which decreases the electron density of C-O-C bond and weaken the C-O-C bond strength. Upon addition of plasticizer, there does not seem to be a very significant change in the conformation region.
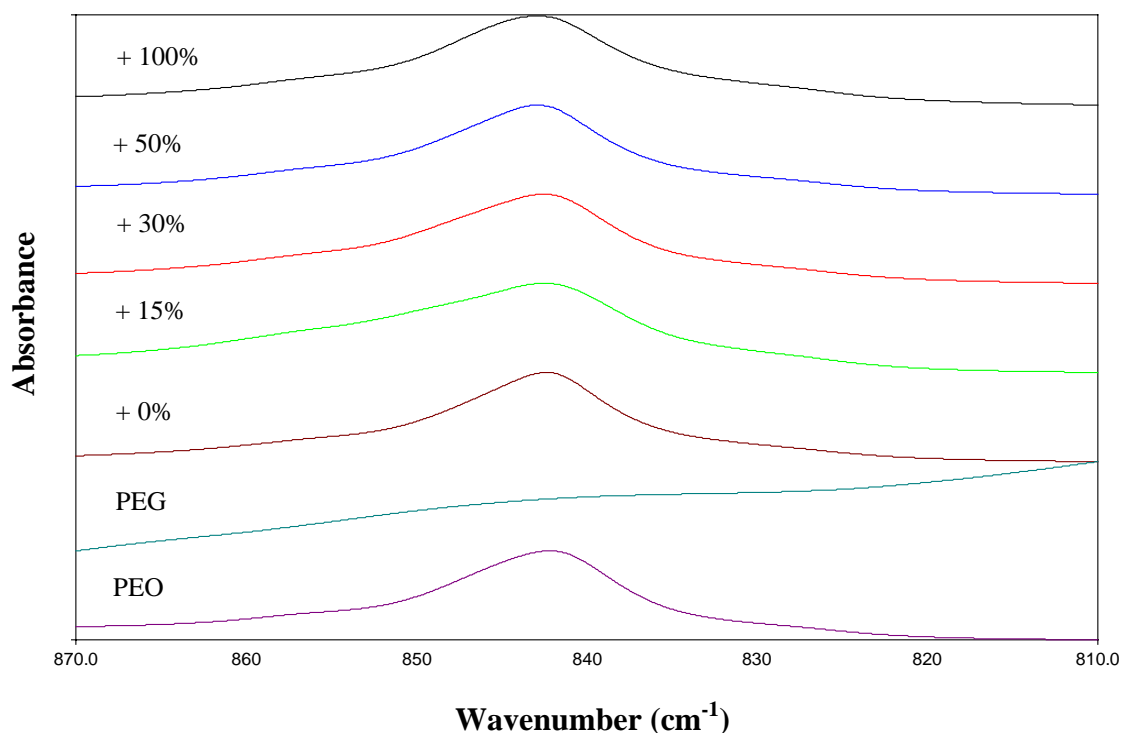
Figure 4.25 IR spectra of $(PEO)_{16}LiCF_3SO_3$ at different % weight PEG in the 900-800 cm^{-1} region

Interaction between Plasticizer and PEO

Further evidence for the preferential interaction of PEG with the crystalline PEO phase rather than $(PEO)_3LiCF_3SO_3$ compound can be seen in Figures 4.26, which shows infrared spectra in the CH$_2$ wagging region. As mentioned before, it is established that the bands at 1360 and 1343 cm^{-1} are due to the crystalline PEO phase, while the band at 1353 cm^{-1} originates in the $(PEO)_3LiCF_3SO_3$ compound. Upon addition of PEG, the intensity of bands due to crystalline PEO slightly decrease and then they are replaced by a broad band roughly centered at 1350 cm^{-1}.
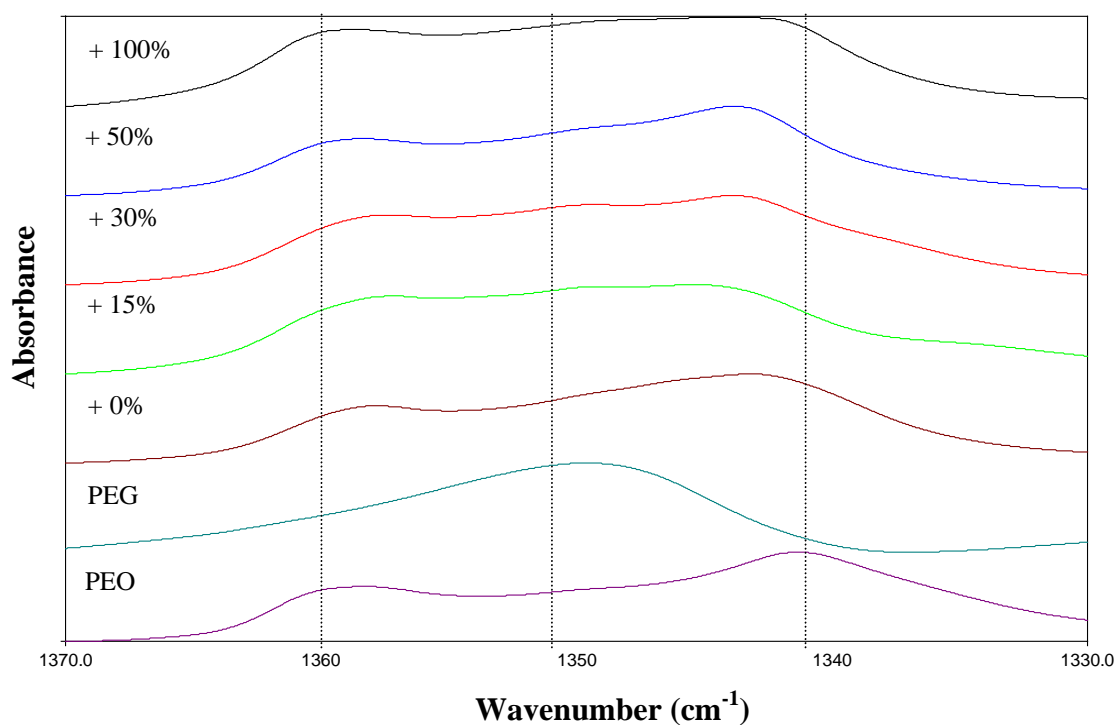
Figure 4.26 IR spectra of $(PEO)_{16}LiCF_3SO_3$ at different % weight PEG in the 1400-1300 cm^{-1} region

II. $(PEO)_xKSCN$ with different %wt of PEG

Ionic Association in Plasticized (PEG) SPEs

Infrared spectra in 2200-1900 cm^{-1} region for pure PEO and $(PEO)_{16}KSCN$ complex at different % weight of PEG are present in Figure 4.27. As mentioned before, the band at 2050 cm^{-1} is ascribed to the C-N asymmetric stretching vibrations of the SCN^- anion. The intensity of infrared spectra slightly changes with

an addition of PEG. From this result, it suggests that an increasing PEG content reduce ionic association.
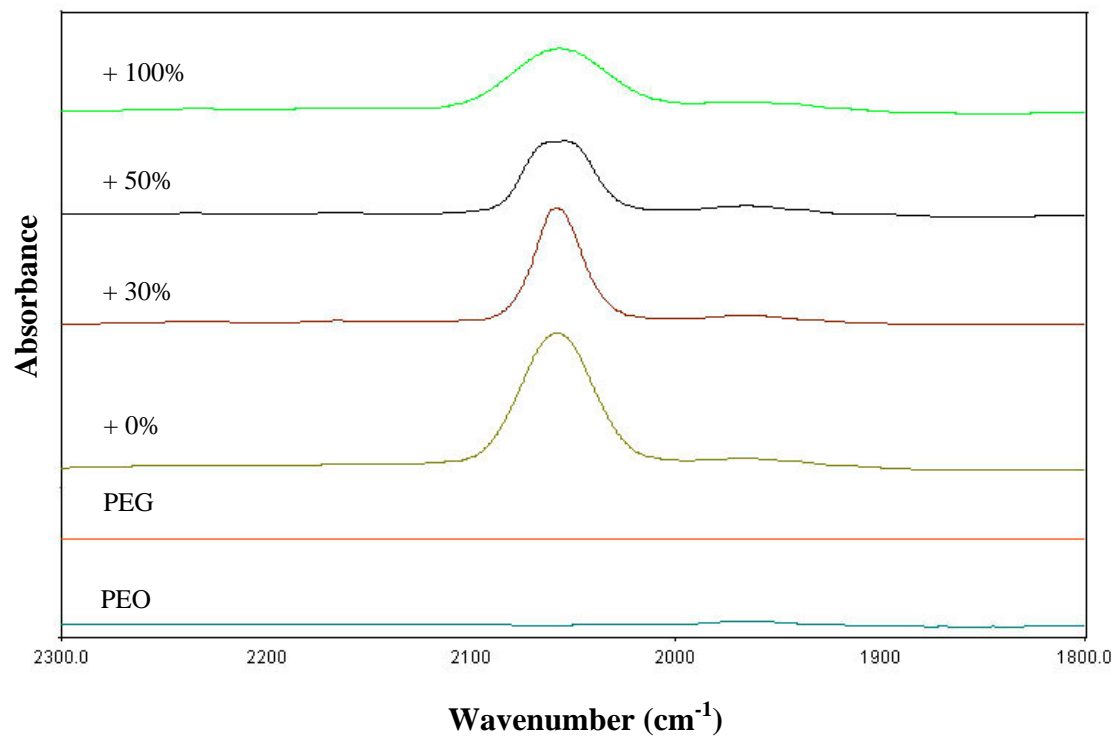
Figure 4.27 IR spectra of $(PEO)_{16}KSCN$ at different % weight PEG in the 2100-2000 cm^{-1} region

Conformation of PEO Backbone

Figure 4.28 shows infrared spectra of $(PEO)_{16}KSCN$ with different % weight of PEG in the 900 to 800 cm^{-1} region. This region is the characteristics of C-O stretching and CH_2 rocking modes. The peak at 844 cm^{-1} is the CH_2 rocking mode coupled with C-O stretching vibrations of PEO molecules. This band is sensitive to the interaction between the cation and polymer backbone. The band at 844 cm^{-1} slightly decreases in its intensity with increasing % weight of PEG.
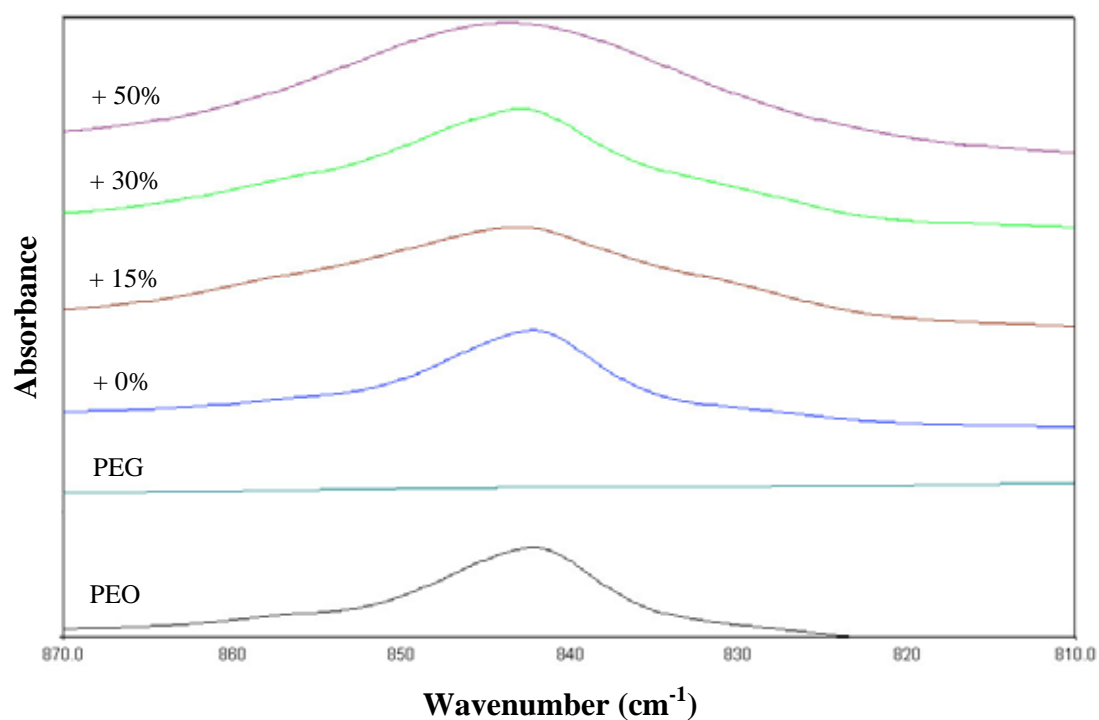
Figure 4.28 IR spectra of $(PEO)_{16}KSCN$ at different % weight PEG in the 900-800 cm^{-1} region.

Interaction between Plasticizer and PEO

Figure 4.29 shows infrared spectra of $(PEO)_{16}KSCN$ as a function of different % weight PEG in the 1400 to 1260 cm^{-1} region. A similar trend to $(PEO)_{16}LiCF_3SO_3$ is observed at different % weight PEG. The doublet peaks at 1360 and 1343 cm^{-1} are due to the CH_2 wagging of crystalline PEO. With increasing % weight of PEG, the peak at 1360 cm^{-1} is replaced by a broad band at 1353 cm^{-1}. This peak is arisen from an amorphous PEO.
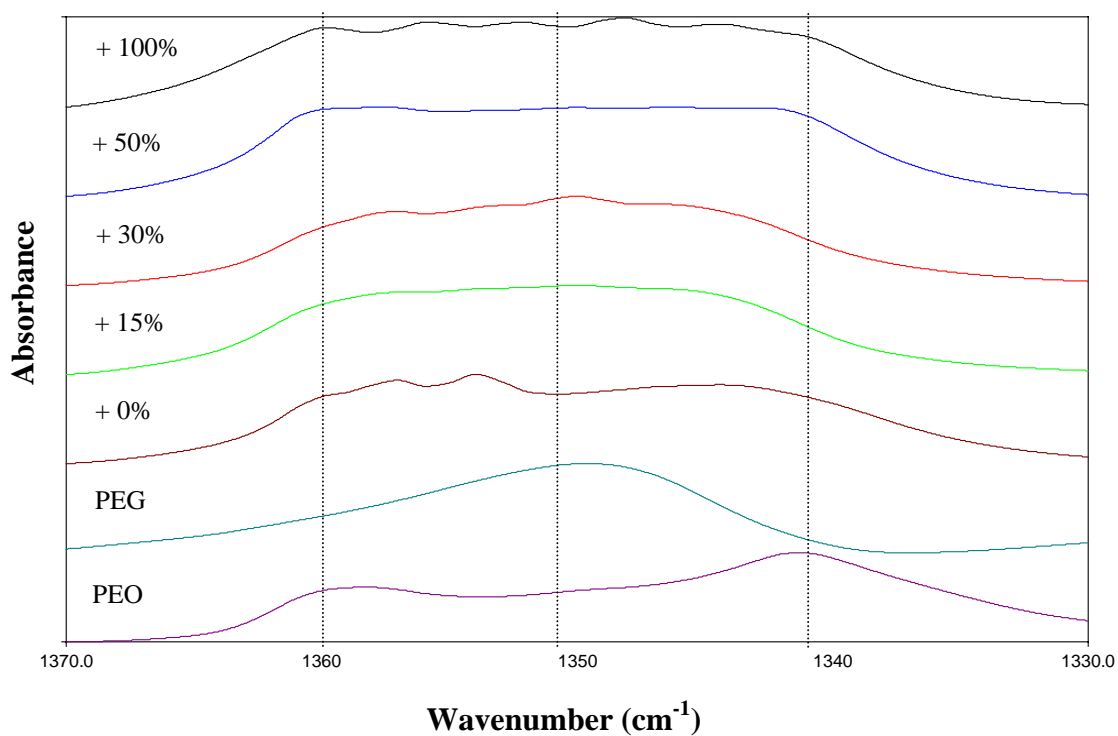
Figure 4.29 IR spectra of $(PEO)_{16}KSCN$ at different % weight PEG in the 1400-1300 cm^{-1} region

4.2.2.2.2 X-ray Diffraction (XRD)

The XRD patterns of the $(PEO)_{16}LiCF_3SO_3$ at different % weight of PEG for 2θ region between $5°$ to $40°$ are reproduced in Figure 4.30. The diffractograms of the $(PEO)_{16}LiCF_3SO_3$ with % weight of PEG ranging from 15% to 100% display a characteristic crystalline peak centered around 15, 19 and 23° which is ascribed to crystalline PEO. Addition PEG to the sample also gave peaks at the same positions but with lower intensities. It should be emphasized that $(PEO)_{16}LiCF_3SO_3$ at different % weight of PEG still have the crystalline phase but at a lower content than $(PEO)_{16}LiCF_3SO_3$. For the plasticized $(PEO)_{16}LiCF_3SO_3$, the intensity of crystalline PEO decreases with more PEG.

Figure 4.31 shows the XRD patterns of $(PEO)_{16}KSCN$ at different % weight of PEG in the 2θ region between $5°$ to $40°$. Similar result to Figure 4.30, the intensity of crystalline peak at 15% weight of PEG is higher than 50% weight of PEG. It suggests that with increasing PEG content, the intensity of crystalline PEO decreases.
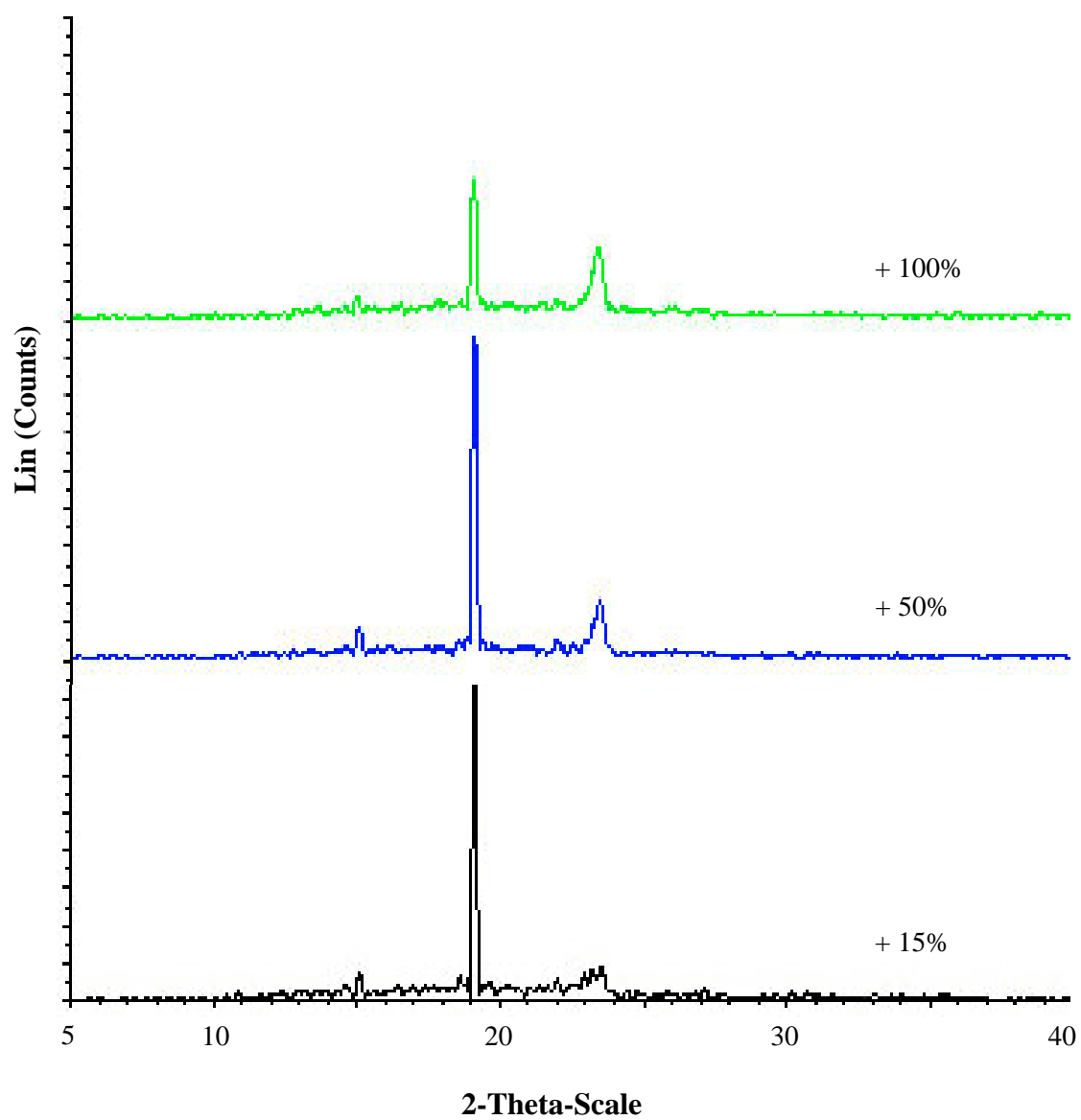
Figure 4.30 X-ray diffraction patterns of $(PEO)_{16}LiCF_3SO_3$ at different % weight of PEG.
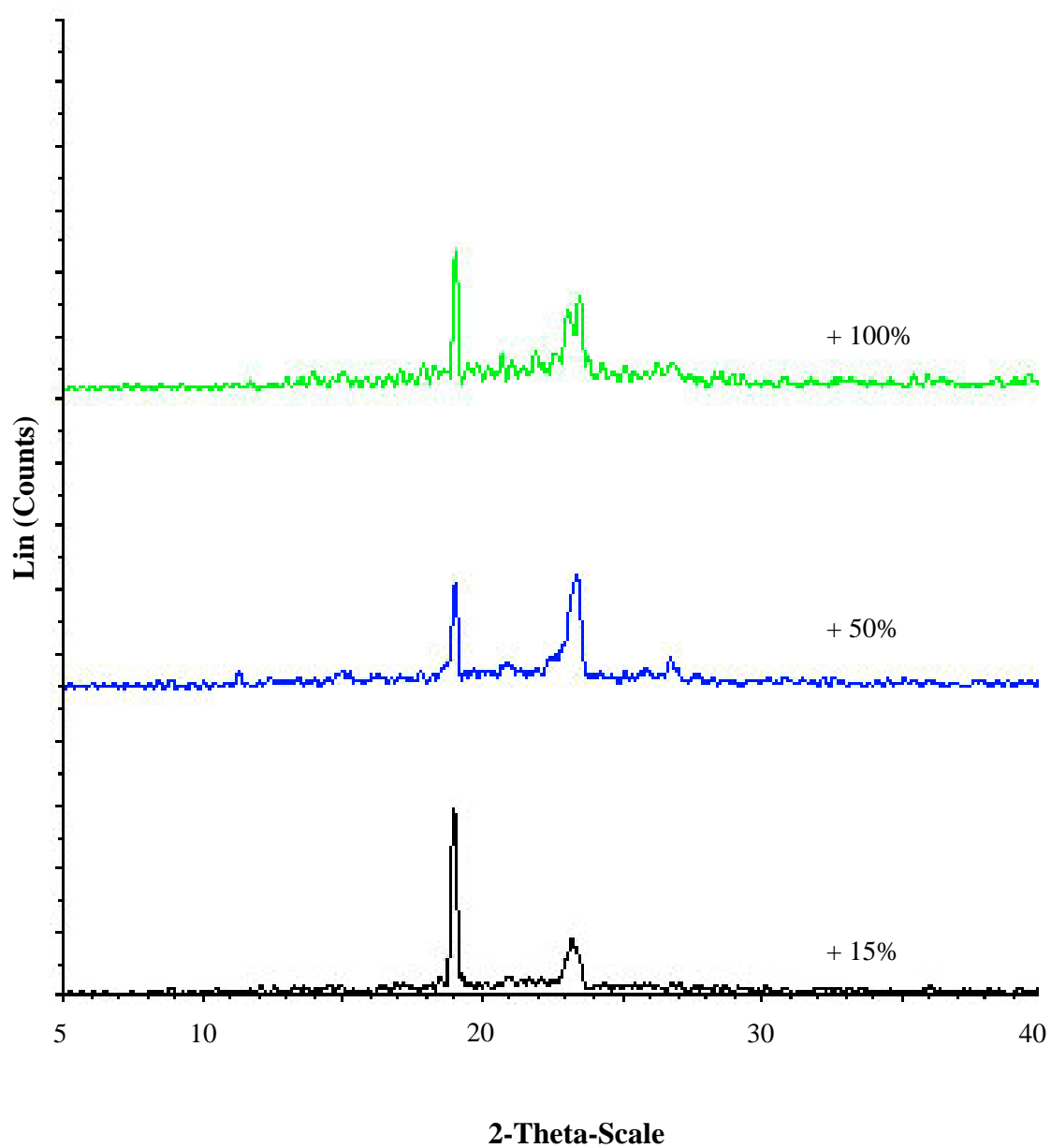
Figure 4.31 X-ray diffraction patterns of $(PEO)_{16}KSCN$ at different % weight of PEG.

4.2.2.2.3 Differential Scanning Calorimeter (DSC)

The effect of adding PEG on the changes of T_m and ΔH_m of PEO and PEO/LiCF$_3$SO$_3$ were investigated using DSC technique. T_m, ΔH_m and the percentage crystallinity for each specimen are shown in Table 4.8.

Figure 4.32 shows DSC thermograms of PEO + 100%PEG and (PEO)$_4$LiCF$_3$SO$_3$ + 100 %PEG specimens. The effect of adding PEG is seen as a shift in the melting temperature from 69.0 °C to 66.8 °C. It suggests that there is more amorphous domain in the complex due to the miscibility of PEG with PEO. ΔH_m and the percentages crystallinity of PEO + 100 %PEG are lower than that of PEO. It indicates that PEG is compatible with PEO and PEG reduces the crystallinity of PEO. XRD results of PEO + PEG system also support this idea.

From Table 4.8 and Figure 4.32, ΔH_m and the percentages crystallinity of (PEO)$_4$LiCF$_3$SO$_3$ are lower than pure PEO. For the PEO/LiCF$_3$SO$_3$ specimen at 4:1 ratios with 100 %wt PEG, there are two melting peaks at 57.6 °C (T_{m1}), and 137.5 °C (T_{m2}). The first peak is due to salt associated with pure PEO and the peak at high melting temperature (137.5 °C) suggests the presence of complex phase. Supportive evidence is obtained by XRD results for (PEO)$_{16}$LiCF$_3$SO$_3$ + %wt PEG shown in Figure 4.30. A reduction in T_{m1} of PEO/LiCF$_3$SO$_3$ 4:1 from 69.0 °C to 57.6 °C as the addition amount of PEG suggests that PEG is compatible with PEO and there is more amorphous domain in the complex.

Plasticized system of (PEO)$_x$KSCN at O:K$^+$ ratios 16:1 show the DSC results in Table 4.8 and Figure 4.33. From this thermogram, there is a shift in melting

temperature from 68.1 °C to 63.2 °C and a decrease in percentage crystallinity. From

these results, it indicates that there is more amorphous phase in the complex.

Table 4.8 Melting temperatures and percent crystallinity of polymer electrolytes as a

function of adding PEG.

Composition	T_m (°C)	ΔH_m (J g^{-1})	Crystallinity (%)
PEO	69.018	131.638	69.983
PEG	-	-[a]	-
LiCF$_3$SO$_3$	226.100	-	-
KSCN	185.273	-	-
PEO+100%PEG	66.888	71.472	37.997
PEO+15%PEG	68.136	90.908	48.330
(PEO)$_4$LiCF$_3$SO$_3$			
+ 100%PEG	57.563	24.812	13.191
(PEO)$_{16}$KSCN			
+15%PEG	63.177	51.421	27.337

[a] no peak observed in DSC thermogram

$T_m = 57.563$ °C

Area = 245.637 mJ

$\Delta H = 24.812$ J/g

$T_m = 137.509$ °C

Area = 126.960 mJ

$\Delta H = 12.824$ J/g

$(PEO)_4LiCF_3SO_3 + 100\%$ wt PEG

$T_m = 66.888$ °C

Area = 750.457 mJ

$\Delta H = 71.472$ J/g

PEO $+100\%$ wt PEG

Heat Flow Endo Up (mW)

Temperature (°C)
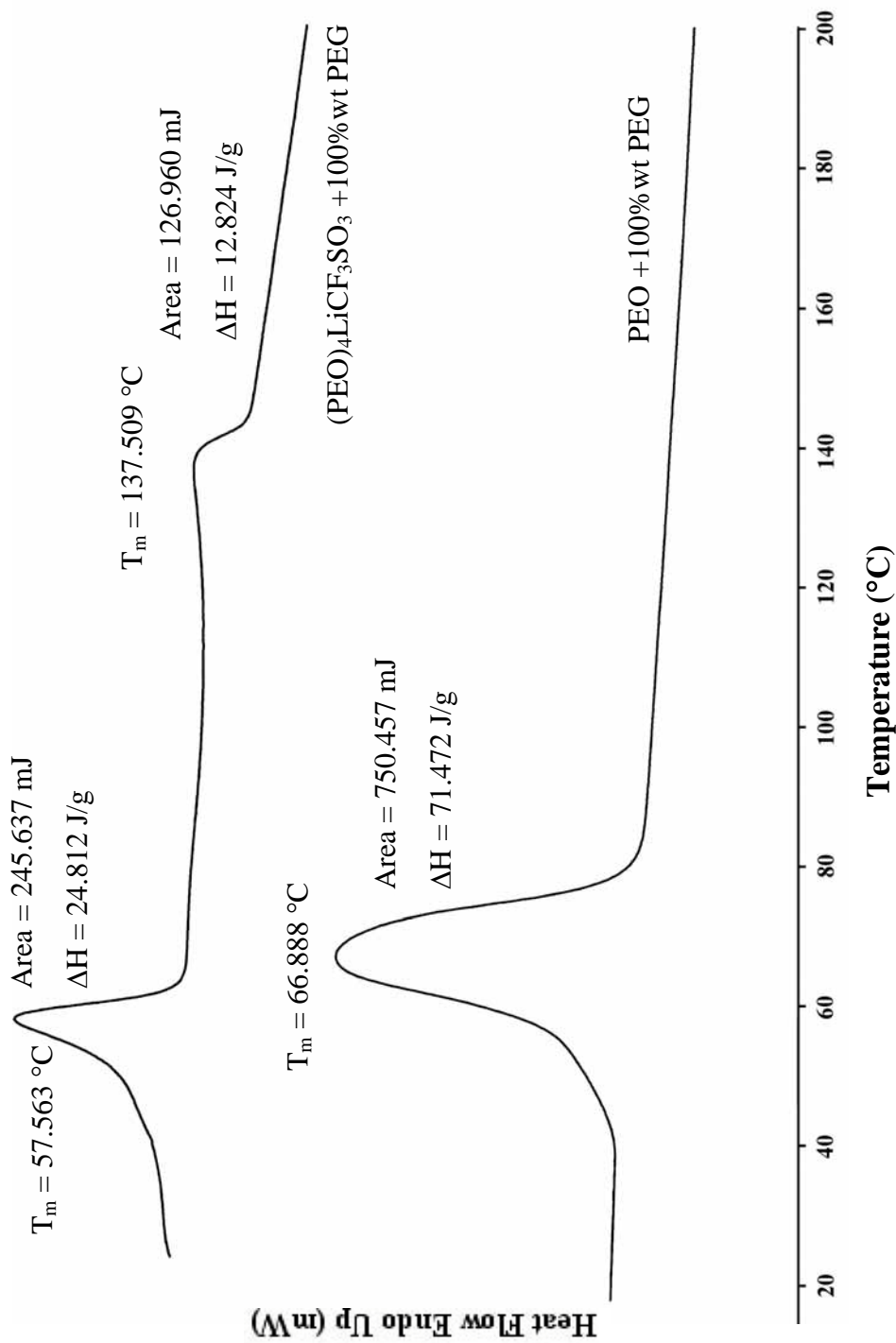
Figure 4.32 DSC thermogram for PEO + 100% wt PEG and $(PEO)_4LiCF_3SO_3$ + 100% wt PEG.
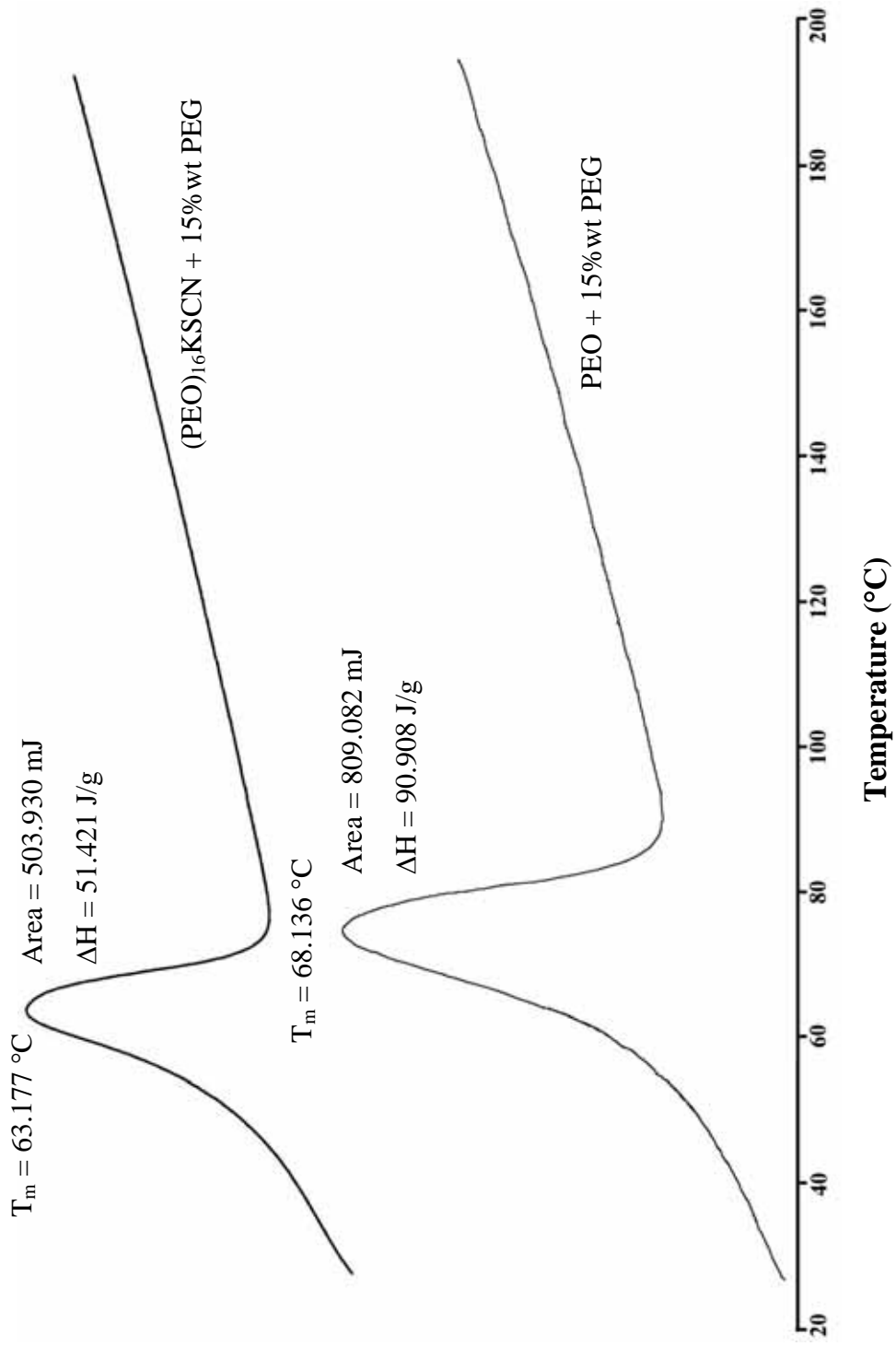
Figure 4.33 DSC thermogram for PEO + 15%wt PEG and(PEO)$_{16}$KSCN + 15%wt PEG.

4.2.2.2.4 Conductivity Measurement

I. (PEO)$_x$LiCF$_3$SO$_3$

Table 4.9 and Figure 4.34 show ionic conductivity measurements carried out at room temperature of (PEO)$_x$LiCF$_3$SO$_3$ with various O:Li$^+$ ratio and % weight PEG. It can be seen that ionic conductivity increases with LiCF$_3$SO$_3$ concentration (O:Li$^+$ ratio) up to 16:1 and then decreases at high LiCF$_3$SO$_3$ concentration. A trend that observed with increasing salt concentration at high content suggested to higher percentage of associated ions. This conclusion is supported by results from IR, XRD and DSC experiments.

In plasticized system, adding of PEG shows better ionic conductivity. The ionic conductivity of (PEO)$_x$LiCF$_3$SO$_3$ varying % weight PEG (~10^{-8} S cm^{-1}) is about an order of magnitude higher than (PEO)$_x$LiCF$_3$SO$_3$ (~10^{-9} S cm^{-1}) that are not plasticized. The increasing ionic conductivity, which may be explained by the following factors. Firstly, with addition PEG as plasticizer the ionic conductivity is enhanced because PEG induces more amorphous phase. Secondly, adding PEG decreases the effect from ionic association. This conclusion is consistent with earlier results from IR, XRD and DSC. The highest ionic conductivity was at O:Li$^+$ ratio 16:1 and 100 % weight PEG.

Table 4.9 Ionic conductivity of $(PEO)_xLiCF_3SO_3$ and $(PEO)_xLiCF_3SO_3$ + % weight

PEG electrolytes.

% wt PEG	Conductivity (S cm^{-1}) at O:Li$^+$ ratio			
	4:1	8:1	16:1	20:1
0 %	0.220×10^{-8}	0.480×10^{-8}	0.833×10^{-8}	0.227×10^{-8}
15 %	0.278×10^{-8}	0.570×10^{-8}	1.330×10^{-8}	0.288×10^{-8}
30 %	0.335×10^{-8}	0.910×10^{-8}	1.600×10^{-8}	0.367×10^{-8}
50 %	0.810×10^{-8}	1.200×10^{-8}	1.800×10^{-8}	0.645×10^{-8}
100 %	0.710×10^{-8}	1.300×10^{-8}	2.150×10^{-8}	0.676×10^{-8}
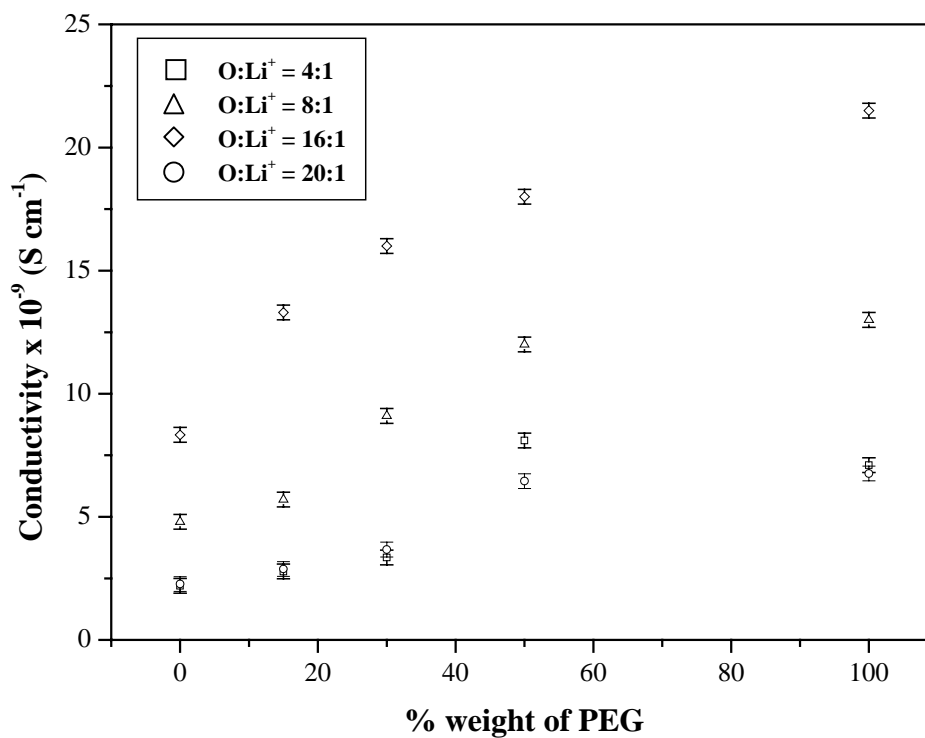
Figure 4.34 Ionic conductivity against % weight PEG of $(PEO)_xLiCF_3SO_3$.

A plot of room temperature ionic conductivity versus % weight PEG for the $(PEO)_x$KSCN system is shown in Table 4.10 and Figure 4.35. It can be seen that for given % weight PEG, it exhibits an enhanced conductivity that is at least 2 order higher than unplasticized $(PEO)_x$KSCN. This can be explained on the basis that the plasticizer interacts with the crystalline PEO rendering the complexes amorphous and hence the conductivity increases. The maximum value of an ionic conductivity is seen when $O:K^+$ ratio is 16:1 with 50 % weight PEG.

The conductivities of PEO/PEG/LiCF$_3$SO$_3$ complexes are found to be higher than the corresponding PEO/PEG/KSCN complexes. In general, ionic conduction in polymer complexes depends on the number of carriers, ionic mobility and phase relation.

Table 4.10 Ionic conductivity of $(PEO)_x$KSCN and $(PEO)_x$KSCN + % weight PEG electrolytes.

% wt PEG	Conductivity $(S\ cm^{-1})$ at $O:K^+$ ratio		
	16:1	30:1	50:1
0	1.43×10^{-9}	0.40×10^{-9}	0.35×10^{-9}
15	1.90×10^{-9}	1.20×10^{-9}	1.30×10^{-9}
30	2.20×10^{-9}	1.55×10^{-9}	1.50×10^{-9}
50	2.53×10^{-9}	1.63×10^{-9}	1.59×10^{-9}
100	2.41×10^{-9}	1.51×10^{-9}	1.43×10^{-9}
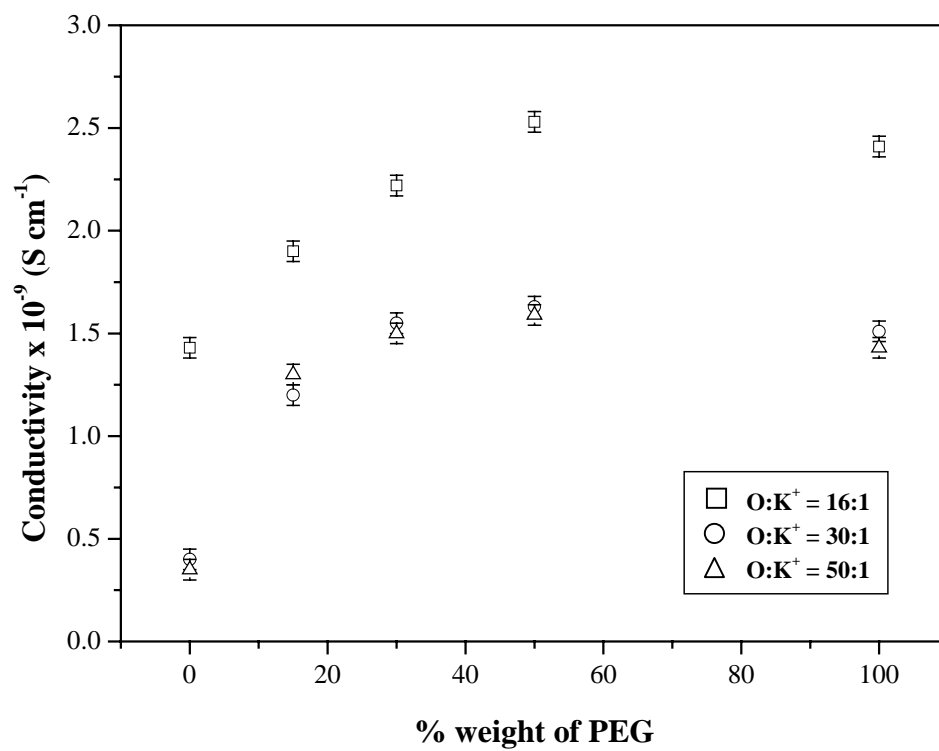
Figure 4.35 Ionic conductivity against % weight PEG of $(PEO)_x$KSCN.

4.3 Theoretical Part

4.3.1 Ionic conductivity based on Adam-Gibbs configuration entropy model

Figure 4.36 shows the composition dependence of the conductivity for PEO/LiCF$_3$SO$_3$ system. The conductivity (dark square) is measured by high resistance meter. Solid line is calculated from the proposed model in section 3.3.1. The properties of the chosen model systems are listed in Table 4.11. By substituting values of 4×10^6 g mol^{-1} (MW$_2$), 156 g mol^{-1} (MW$_1$), $r_1 = 1$, $r_2 = 33,057.9$, and $z = 6$ into Eqs. (3.48-3.50), the best fit to the curvature of the conductivity plot (the solid line in Figure 4.36) was obtained. Adjustable model parameters (A, B', and λ_s) are listed in Table 4.12. The pre-exponential factor A is regarded as being inversely proportional to charge carriers in the system and decreases as the number of charge carriers increase. If the temperature of the system increases, A is observed to decrease for the model systems. B' can be explained in terms of $\Delta\mu$, the activation energy required to rearrange a small side-chain segment at a given salt concentration. The degree of specific interaction ($-\lambda_s$) is related to a small entropy loss with increasing salt concentrations.
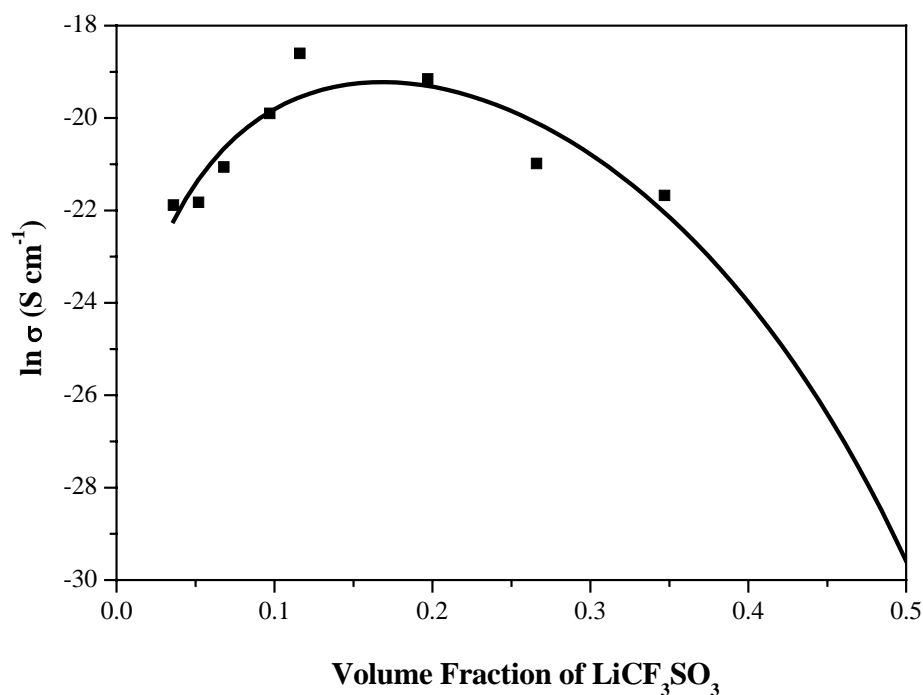
Figure 4.36 The conductivity dependence on salt concentrations for the PEO/LiCF$_3$SO$_3$ system. The conductivity (dark square) is measured by Hewlett-Packard 4339B high resistance meter. Solid line is calculated by Eqs. (3.48-3.50).

When more salt is added to the system, the short-range specific interaction between salt ions and the polymer leads to the loose complex formation, raises the T$_g$ and makes the segmental motion more difficult. The proposed model predicts a maximum conductivity at the volume fraction of LiCF$_3$SO$_3$ $\approx$ 0.15.

Table 4.11 List of Molecular Weight, Density and Molar Volume for a Model System.

System	MW (g mol^{-1})	Density (g cm^{-3})	Molar Volume (cm^3 mol^{-1})
PEO	4,000,000	1.21	3,305,785
LiCF$_3$SO$_3$	156	1.56	100
KSCN	97	1.88	51.6
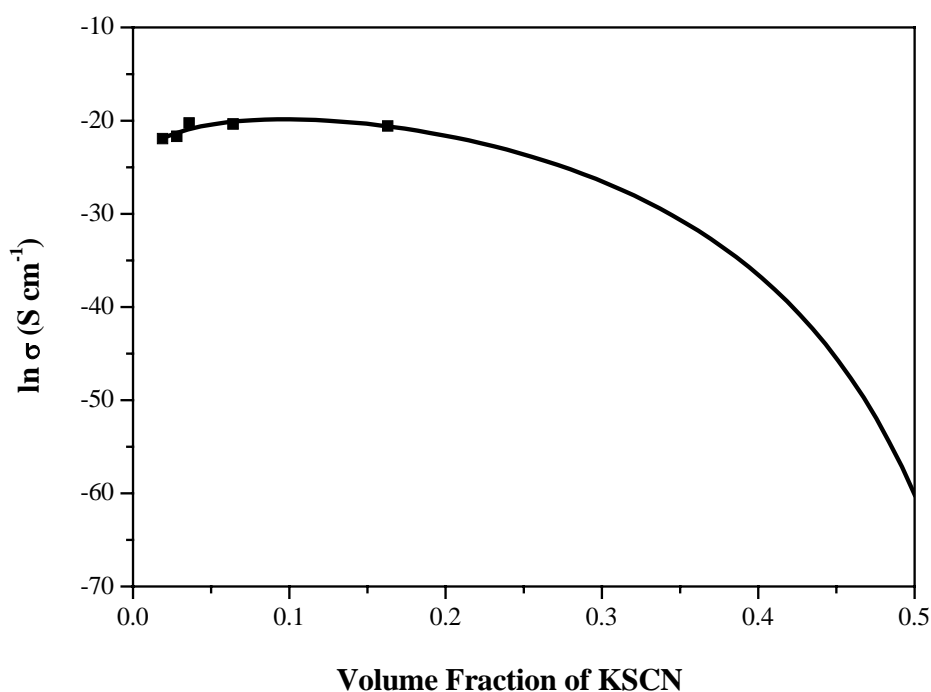
Figure 4.37 The conductivity dependence on salt concentrations for the PEO/KSCN system. The dark square is measured by Hewlett-Packard 4339B high resistance meter. Solid line is calculated by Eqs.(3.48-3.50).

Figure 4.37 shows the conductivity dependence on salt concentrations for PEO/KSCN system. The proposed model predicts a maximum of conductivity at volume fraction of KSCN $\approx$ 0.10. As shown in Figure 4.37, the conductivity of PEO/KSCN systems is lower than that of PEO/LiCF$_3$SO$_3$ system. This is consistent with the analysis of three adjustable model parameters: A = 4081, B' = 21.430, and λ_s = -1.283 for the PEO/LiCF$_3$SO$_3$ system, and A = 4445, B' = 23.981, and λ_s = -1.181 for the PEO/KSCN system, respectively. The proposed model describes very well the conductivity behavior of the complexes, including the maximum of conductivity at the volume fraction of salt $\approx$ 0.15 and $\approx$ 0.1 for PEO/LiCF$_3$SO$_3$ and PEO/KSCN, respectively.

Table 4.12 List of Adjustable Parameters for the Configurational Entropy Model.

Polymer host	salt	A	B'	λ_s
PEO	LiCF$_3$SO$_3$	4.081×10^3	21.430	-1.283
PEO	KSCN	4.445×10^3	23.981	-1.181

4.3.2 Phase Diagram based on Flory-Huggins theory

Figure 4.38 shows phase behaviours of the PEO/LiCF$_3$SO$_3$ system. Dark circles ($\bullet$) were measured by DSC and Solid lines were calculated from Eqs. (3.63) and (3.64). Other experimental data were obtained by DTA or DSC (+, $\times$) (Minier et al., 1984; Weston et al., 1981), conductivity (Δ) (Robitaille et al., 1986) and thermo-optical analysis (∇) (Kim et al., 1998). The melting points obtained by DSC ($\bullet$) are consistent with data measured by others. From the proposed model which describes the thermo-dynamic equilibrium of the amorphous phase with the crystalline phase, Eq. (3.63) was used for the calculation of the polymer-rich liquidus curve, and Eq. (3.64) for the calculation of the salt-rich one. The density of PEO and LiCF$_3$SO$_3$ was taken as 1.21 g cm^{-3} and 2.69 g cm^{-3}. By substituting values of R = 1.98 cal K^{-1} mol^{-1}, ΔH_1 = 2513.5 cal mol^{-1}, r_1 = 1, r_2 = 2594.92, and $T_{m,1}^o$ = 499.29 K into Eq. (3.64), the best fit to the salt-rich liquidus curve (solid line on the right-hand side) was obtained. Adjustable model parameters are d_o = -4.523, d_1 = 2304.7, and b = -0.253. Substituting the same adjustable model parameters, ΔH_u = 1980 cal mol^{-1}, V_u = 36.6 cm^3 mol^{-1}, V_1 = 57.99 cm^3 mol^{-1} and $T_{m,2}^o$ = 338.15 K into Eq. (3.63) give the solid line on the left-hand side. As shown in Fig. 4.38, the theoretical prediction not only gives an excellent agreement with experimental results but also identifies the eutectic point at the intersection of the two liquidus curves at a weight of LiCF$_3$SO$_3$ $\approx$ 0.05.
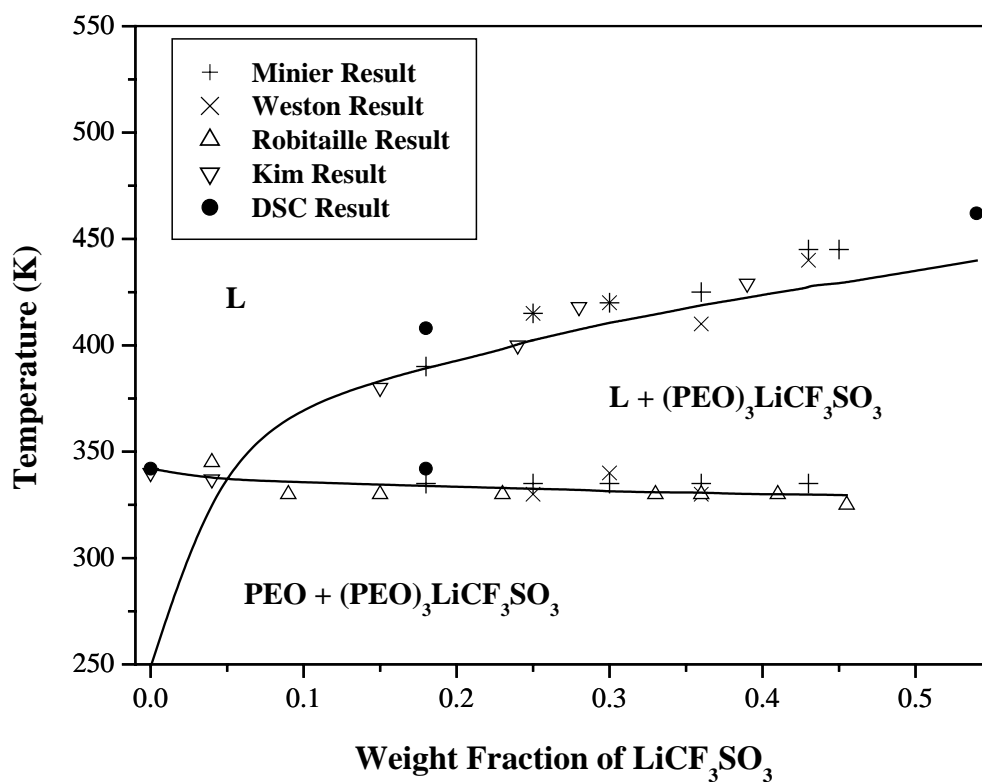
Figure 4.38 Phase diagram of the PEO/LiCF$_3$SO$_3$ system. The transition temperatures were obtained using various experimental-techniques: DSC or DTA (+, ×), conductivity (Δ) and thermo-optical analysis technique (∇). This study: DSC ($\bullet$) and theory (solid lines).

CHAPTER V

CONCLUSION

The characterization of the PEO chain was investigated using molecular modeling technique and the Rotational Isomeric State (RIS) model. Conformational-dependent properties calculated values are in excellent agreement with those values obtained from experimental results. For example, the characteristic ratio and dipole moment ratios obtained from measurement are 4.0 ± 0.4 at 313 K and 0.62 at 293 K, respectively. The concurrence of these values with experimental results proposes that the conformation energy obtained from the Molecular Mechanics (MM) calculation by the default force field in Chem3D software can be used to construct the statistical weight matrices for the RIS model with a reasonable accuracy.

The effect of plasticizer (PEG) has been studied in the PEO/salt (LiCF$_3$SO$_3$ or KSCN) system using infrared spectroscopy, x-ray diffraction and differential scanning calorimeter augmented with measurements of conductivity. Plasticizers affect the crystalline content and ionic conductivity in the PEO/salt complexes. This study shows that the PEG is able to decrease crystalline content and can enhance ionic conductivity. The ionic conductivity is increased by an order of magnitude compare to the non-plasticized system. The ionic conductivity of PEO/LiCF$_3$SO$_3$ complexes is higher than the corresponding PEO/KSCN complexes. The maximum value of ionic conductivity was seen when O:M ratio (ether oxygen in the PEO to metal cation of

salt) equals to 16:1 with 100%wt PEG for PEO/PEG/LiCF$_3$SO$_3$ complexes and 16:1 with 50%wt PEG for PEO/PEG/KSCN complexes.

The theory based on the Adam-Gibbs configurational entropy model describes the composition dependence of the conductivity for the semicrystalline PEO/salt systems very well. Three adjustable model parameters are sufficient for elucidating the conductivity behavior of chosen systems without losing the physical meaning of the model parameters. The phase diagrams of SPEs systems composed of PEO and LiCF$_3$SO$_3$ were constructed and the liquidus curves between crystalline phase and amorphous phase were calculated from Flory-Huggins equation based on Flory's melting depression concept. The proposed model describes very well the phase behaviours and also predicts remarkably well a eutectic point at the intersection of two liquidus curves for PEO/LiCF$_3$SO$_3$ system.

REFERENCE

REFERENCES

Abe, A., Furuya, H., Mitra, M. K. and Hiejima, T. (1998). The polyoxyethylene chain on the origin of its conformational flexibility. Comp. **Computational and Theoretical Polymer Science.** 8: 253.

Andreev, Y. G., Lightfoot, P. and Bruce, P. G. (1996) Chem. Commun. 18: 2169 Quoted in Johansson, P. (1998) **Conformations and Vibrations in Polymer Electrolytes** [On-line]. Available: http://fy.chalmers.se/~patrikj/thesis.htm.

Armand, M. B. (1979). **Fast Ion Transport in Solids**. Elsevier North-Halland. Quoted in Puatrakul, T. (2000). **Studies of Ionic Conductivity of Uniaxially Stretched Polymer Electrolytes Films.** Ph.D. Thesis, University of Akron, USA.

Aylwad, G. and Findlay T. (1994) **SI Chemical Data.** J. Wiley &Sons: Brisbane.

Bak, K., Elefante, G. and Mark, J. E. (1967) Configurational Properties of Poly (ethylene oxide) and Poly(tetramethylene oxide). **J. Phys. Chem.** 71: 4007.

Bakker, A. (1995) Comprehensive Summaries of Uppsala Dissertations from the Faculty of Science and Technology, Uppsala. Quoted in Johansson, P. (1998) **Conformations and Vibrations in Polymer Electrolytes** [On-line]. Available: http://fy.chalmers.se/~patrikj/thesis.htm.

Baril, D., Michot, C. and Armand, M. (1997). Electrochemistry of liquids vs. solids: Polymer electrolytes. **Solid State Ionics** 94: 35.

Berson, A., Lindgren, J. Huang, W. and Frech, R. (1995) Polymer 36:4471. Quoted in Johansson, P. (1998) **Conformations and Vibrations in Polymer Electrolytes** [On-line]. Available: http://fy.chalmers.se/~patrikj/thesis.htm.

Berthier, C., Gorecki, W., Minier, M., Armand, M. B. and Chabagno, P. (1983) Microscopic investigation of ionic conductivity in alkali metal salts-poly (ethylene oxide) adducts. **Solid State Ionic** 11: 91.

Bieze, T. W. N., van der Maarel, J. R. C., Eisenbach, C. D. and Leyte, J. C. (1994). Polymer Dynamics in Aqueous Poly(ethylene oxide) Solutions. An NMR Study. **Macromolecule** 27: 1355.

Bluestone, S., Mark, J. E. and Flory, P. J. (1974). The Interpretation of Viscosity-Temperature Coefficient for Poly(oxyethylene) Chain in a Thermodynamically Good Solvent. **Macromolecules** 7: 325 - 328.

Blythe, A. R. (1979). **Electrical Properties of polymers**. United Kingdom: Cambridge University Press.

Brown, B. D. and deLong, D. J. (1982). Kirk-Othmer Encyclopedia of Chemical Technology Vol. 18. Joh Wiley & Sons: New York.

Bruce, P. G. (1992). NATO ASI Series. 250: 87. Quoted in Chintapalli, S. (1996). **Structural characterization of polymer – salt complexes and the role of plasticizers in ionic transport.** Ph. D. Dissertation, University of Oklahoma Graduate College, USA.

Bruce, P.G. and Vincent, C.A. (1993). J. Chem. Soc. Faraday Trans. 89: 3187 Quoted in Johansson, P. (1998) **Conformations and Vibrations in Polymer Electrolytes** [On-line]. Available: http://fy.chalmers.se/~patrikj/thesis.htm

Bruce, P. G. (1995). **Solid state electrochemistry.** United Kingdom: Cambridge University Press.

Bruce, P. G. (1995). Structure and electrochemistry of polymer electrolytes. **Electrochim. Acta.** 40: 2077.

CambridgeSoft Corporation. (1986-2000). CS Chem3D Molecular Modeling and analysis User'Guide   [computer softwere]. USA: Cambridge Scientific Computing.

Candia, F. de, Vittoria, V., Bianchi, U. and Patrone, E. (1972). **Macromolecules** 5:493 Quoted in Bluestone, S., Mark, J. E. and Flory, P. J. (1974). The Interpretation of Viscosity-Temperature Coefficient for Poly(oxyethylene) Chain in a Thermodynamically Good Solvent. **Macromolecules** 7: 325 - 328.

Chatani, Y. and Okamura, S. (1987). Crystal structure of poly(ethylene oxide)-sodium iodide complex. **Polymer** 28: 1815.

Chatani, Y., Fujji, Y., Takayanagi, T. and Honma, A. (1990). Structures of two crystal forms of poly(ethylene oxide)-sodium thiocyanate complex with molar ratios of 3:1 and 1:1. **Polymer** 31: 2238.

Chintapalli, S. (1996). **Structural characterization of polymer – salt complexes and the role of plasticizers in ionic transport.** Ph. D. Dissertation, University of Oklahoma Graduate College, USA.

Doeff, M. M., Visco, S. J., Ma, Y., Peng, M., Ding, L. and De Jonghe, L. C. (1995). Thin film solid state sodium batteries for electric vehicles. **Electrochimica Acta**. 40: 2205.

Duke, C. B. and Gibson, H. W. (1978). **Encyclopedia of Chemical Technology** (Vol. 18). 3rd ed. New York: John Wiley & Sons.

Fauteux, D., Lupien, M. D. and Robitaille, C. D. (1987). J. Electrochem. Soc. 134: 2761. Quoted in Chintapalli, S. (1996). **Structural characterization of polymer – salt complexes and the role of plasticizers in ionic transport.** Ph. D. Dissertation, University of Oklahoma Graduate College, USA.

Flory, P. J. (1953). **Principles of Polymer Chemistry.** New York: Cornell University Press.

Flory, P. J. (1969). **Statistical mechanics of chain molecules.** New York: Interscience.

Fenton, D. E., Parker, J. M. and Wright, P. V. (1973) **Polymer** 14: 589 Quoted in Bruce, P. G. (1995). **Solid state electrochemistry.** United Kingdom: Cambridge University Press.

Frech, R., Chintapalli, S., Bruce, P. G. and Vincent, C. A. (1997) Chem. Commun. 6:157. Quoted in Johansson, P. (1998) **Conformations and Vibrations in Polymer Electrolytes** [On-line]. Available: http://fy.chalmers.se/~patrikj/thesis.htm.

Gutmann, F. and Lyons, L. E. (1976). **Organic Semiconductors**. (n.p.) John Wiley & Sons.

Hardy, L. C. and Shriver, D. F. (1985). Preparation and electrical response of solid polymer electrolytes with only one mobile species. **J. Am. Chem. Soc.** 107: 3823.

Ito, Y., Kanehori, K., Miyauchi, K. and Kudo, T. (1987) J. Mater. Sci. 22: 1845. Quoted in Mendolia, M. S. and Farrington, G. C. (1995). High-Conductivity, Solid Polymeric Electrolytes. **Materials Chemistry: An Emerging Discipline** (108). American Chemical Society.

Iwamoto, R., Saito, Y., Ishihara, H. and Tadokoro, H. (1968). J. Polym. Sci., A-2, 6: 1509. Quoted in Chintapalli, S. (1996). **Structural characterization of polymer – salt complexes and the role of plasticizers in ionic transport.** Ph. D. Dissertation, University of Oklahoma Graduate College, USA.

Iwatsuki, S., Kubo, S. and Ohtake, M. (1992). Chem. Lett. 519. Quoted in Mendolia, M. S. and Farrington, G. C. (1995). High-Conductivity, Solid Polymeric Electrolytes. **Materials Chemistry: An Emerging Discipline** (108). American Chemical Society.

Johansson, P., Wendsjo, A. and Tegenfeldt, J. (1992). NMR spectroscopy of peo-based polymer electrolytes. **Electrochimica Acta.** 37:1487.

Johansson, P. (1998) **Conformations and Vibrations in Polymer Electrolytes** [On-line]. Available: http://fy.chalmers.se/~patrikj/thesis.htm

Jones, G. K., Farrington, G. C. and McGhie, A. R. (1990). Proc. Second Int. Symp. on Polymer Electrolytes. Quoted in Johansson, P. (1998) **Conformations and Vibrations in Polymer Electrolytes** [On-line]. Available: http://fy.chalmers.se/~patrikj/thesis.htm

Kelly, I. E., Owen, J. R. and Steele, B. C. H. (1985). Poly(ethylene oxide) electrolytes for operation at near room temperature. **J. Power Source.** 14: 13.

Kim, J. Y., Noh, S. and Bae, Y. C. (1998). Phase behaviors of solid polymer electrolytes: applicability of the melting point depression. **Polymer** 39: 3473-3477.

Kim, J. Y. and Bae, Y. C. (1999). Configurational entropy effect for the conductivity of semicrystalline polymer/salt systems. **Fluid Phase Equilibria** 163: 291-302.

Kim, J. Y. and Bae, Y. C. (1999). Phase behaviors of solid polymer electrolytes: applicability of an extended Dybye-Hückel theory. **Polymer** 40: 1979-1984.

Kramers, H. A. and Wannier, G. H. (1941) Phys. Rev. 60: 252. Quoted in Akten, E. D. (2001). **Computer simulation of polyolefins and monte carlo simulation of RIS chains on a high-coordination diamond.** Ph.D. Thesis, University of Akron, USA.

Lee, Y. L. and Crist, B. (1986) J. Appl. Phys. 60: 2683. Quoted in Chintapalli, S. (1996). **Structural characterization of polymer – salt complexes and the role of plasticizers in ionic transport.** Ph. D. Dissertation, University of Oklahoma Graduate College, USA.

Lightfoot, P., Metha, M. A. and Bruce, P. G. (1992). **J. Mater. Chem.** 2: 379. Quoted in Chintapalli, S. (1996). **Structural characterization of polymer – salt complexes and the role of plasticizers in ionic transport.** Ph. D. Dissertation, University of Oklahoma Graduate College, USA.

Lightfoot, P., Metha, M. A. and Bruce, P. G. (1993). **Science** 262: 883. Quoted in Puatrakul, T. (2000). **Studies of Ionic Conductivity of Uniaxially Stretched Polymer Electrolytes Films.** Ph.D. Thesis, University of Akron, USA.

Lightfoot, P., Nowinski, J. L. and Bruce, P. G. (1994). Crystal Structures of the Polymer Electrolytes Poly(ethylene oxide)4:MSCN (M = NH₄, K). **J. Am. Chem. Soc.** 116:7469.

Mark, J. E. and Flory, P. J. (1965). The Configuration of the Polyoxyethylene Chain. **J. Am. Chem. Soc.** 87: 1415.

Mendolia, M. S. and Farrington, G. C. (1995). High-Conductivity, Solid Polymeric Electrolytes. **Materials Chemistry: An Emerging Discipline** (108). American Chemical Society.

Minier, M. Berthier, C. and Gorecki, W. (1984) J. Phys. 45: 739. Quoted in Kim, J. Y., Noh, S. and Bae, Y. C. (1998). Phase behaviors of solid polymer electrolytes: applicability of the melting point depression. **Polymer** 39: 3473-3477

Preechatiwong, W. and Schultz, J. M., (1996). Electrical conductivity of poly (ethylene oxide)- alkali metal salts systems and effects of mixed salts and mixed molecular weights. **Polymer** 37: 5109 – 5116.

Qian, C., Munby, SJ. and Eichnger, BE. (1991). Phase diagrams of binary polymer solutions and blends. **Macromolecules** 24: 1655.

Quartarone, E., Mustarelli, P. and Magistris, A. (1998). PEO – based composite polymer electrolytes. **Solid State Ionics** 110: 1 – 14.

Rhodes, C. P. and Frech, R. (2001). Local structures in crystalline and amorphous phases of Diglyme-LiCF₃SO₃ and poly(ethylene oxide)- LiCF₃SO₃ systems: Implications for the mechanism of ionic transport. **Macromolecules** 34: 2660-2666.

Robitaille, C. D. and Fauteux, D. (1986). J. Electrochem. Soc. 133: 315. Quoted in Chintapalli, S. (1996). **Structural characterization of polymer – salt complexes and the role of plasticizers in ionic transport.** Ph. D. Dissertation, University of Oklahoma Graduate College, USA.

Robitaille, C., Marques, S., Boils, D. and Prud'homme, J. (1987). Thermal properties of poly(ethylene oxide) complexed with NaSCN and KSCN. **Macromolecules** 20: 3023-3034.

Sandner, B., Steurich, T., Wiesner, K. and Bischoff, H. (1992). Polym. Bull. 28: 355. Quoted in Mendolia, M. S. and Farrington, G. C. (1995). High-Conductivity, Solid Polymeric Electrolytes. **Materials Chemistry: An Emerging Discipline** (108). American Chemical Society.

Song, J. Y., Wang, Y. Y. and Wan, C. C. (1999). Review of gel – type polymer – electrolytes for lithium – ion batteries. **J. Power Sources** 77: 183 – 197.

Spindler, R. and Shriver, D. F. (1986). Physical and spectroscopic properties of ternary polymer electrolytes composed of poly(vinylpyrrolidinone), polyethylene glycol, and lithium trifluoromethanesulfonate. **Macromolecules.** 19: 347.

Stainer, M., Hardy, L. C., Whitmore, D. H. and Shriver, D. F. (1984), J Electrochem. Soc. 131: 784. Quoted in Bruce, P. G. (1995). **Solid state electrochemistry.** United Kingdom: Cambridge University Press.

Stowe, M. K. (2001). **PEO-Based Polymer Electrolytes for Secondary Lithium Batteries.** Ph.D. Dissertation, Michigan State University, USA.

Sukeshini, A. M., Kulkarni, A. R. and Sharma, A. (1998). PEO based solid polymer electrolyte plasticized by dibutyl phthalate. **Solid State Ionics.** 113-115: 179-186.

Takahashi, Y. and Tadokoro, H. (1973). Structural Studies of Polyethers, (-(CH$_2$)m-O-)$_n$. X. Crystal Structure of Poly(ethylene oxide). **Macromolecules** 6: 672.

Takeoka, S., Horiuchi, K., Yamagata, S. and Tsuchida, E. (1991). Sodium ion conduction of perfluorosulfonate ionomer/poly(oxyethylene) composite films. **Macromolecules.** 24: 2003.

Thomson, J. B., Lightfoot, P. and Bruce, P. G. (1996). Structure of polymer electrolytes: the crystal structure of poly(ethylene oxide)$_4$:RbSCN. **Solid State Ionics**. 85: 203.

Vellee, A., Besner, S. and Prud'homme, J. (1992). Comparative study of poly (ethylene oxide) electrolytes made with LiN(CF$_3$SO$_2$)$_2$, LiCF$_3$SO$_3$ and LiClO$_4$: Thermal properties and conductivity behavior. **Electrochimica Acta.** 37: 1579.

Volkenstein, M. V. (1951). **Dokl. Akad. Nauk SSSR.** 78:879. Quoted in Akten, E. D. (2001). **Computer simulation of polyolefins and monte carlo simulation of RIS chains on a high-coordination diamond.** Ph.D. Thesis, University of Akron, USA.

Wahg, C., Yu, D., Liu, Q., Yang, L. and Wang, Z. (1990). In Recent Advances in Fast Ion Conducting Materials and Devices. 237. Quoted in Mendolia, M. S. and Farrington, G. C. (1995). High-Conductivity, Solid Polymeric Electrolytes. **Materials Chemistry: An Emerging Discipline** (108). American Chemical Society.

Wendsjo, A., Lingren, J. and Paluszkiewicz, C. (1992) Electrochimica Acta. 37:1689. Quoted in Johansson, P. (1998) **Conformations and Vibrations in Polymer Electrolytes** [On-line]. Available: http://fy.chalmers.se/~patrikj/thesis.htm.

Weston, J. E. and Steele, B. C. H. (1981) Solid State Ionics 2: 347. Quoted in Kim, J. Y., Noh, S. and Bae, Y. C. (1998). Phase behaviors of solid polymer electrolytes: applicability of the melting point depression. **Polymer** 39: 3473-3477.

Wright, P. V.,Br. (1975). **Polym. J**. 7:319. Quoted in Puatrakul, T. (2000). **Studies of Ionic Conductivity of Uniaxially Stretched Polymer Electrolytes Films.** Ph.D. Thesis, University of Akron, USA.

Yang, L., Lin, J., Wang, Z., Wang, C., Zhou, R. and Liu, Q. (1990). Effects of plasticizers on properties of poly(ethylene oxide) complex electrolytes. **Solid State Ionics** 40/41: 616.

Zalewska, A., Stygar, J., Ciszewska, E., Wiktorko, M. and Wieczorek, W. (2001). The Effect of Type of Cation and Salt Concentration on Ion-Ion and Ion-Polymer Interactions in PEG-MSCN (M = Li, Na, K) Polymer Electrolytes. **J. Phys. Chem. B.** 105: 5847.

APPENDICES

APPENDIX A

Supplementary Infrared Active Bands Of PEO In The Amorphous Phase (A), The Crystalline Phase (X) And The Polymer-Salt Complex ((PEO)$_x$LiCF$_3$SO$_3$ and (PEO)$_x$KSCN).

PEO (A)	PEO (X)	(PEO)$_9$ LiCF$_3$SO$_3$	(PEO)$_x$ KSCN	Peak assignment
			2090-2020	-SCN asym. stretching
		1367 (C)		
	1361	1361 (P)		$w_s(CH_2) + v(CC)$
1350				
		1353 (C)		
	1343	1343 (P)		$w_{as}(CH_2)$
		1340 (C)		
1325				
		1309 (C)		
		1298 (C)		$v_{as}(SO_3)$
1294				
		1288 (C)		$v_{as}(SO_3)$
	1280	1280 (P)		$t_{as}(CH_2) + t_s(CH_2)$

PEO (A)	PEO (X)	(PEO)$_9$ LiCF$_3$SO$_3$	(PEO)$_x$ KSCN	Peak assignment
1250		1263 (C)		$v_{as}(SO_3)$
	1244	1244 (P)		$t_{as}(CH_2)$
	1236			$t_{as}(CH_2) - t_s(CH_2)$
		1233 (C)		$v_s(CF_3)$
		1179 (C)		
		1160 (C)		$v_{as}(CF_3)$
	1150	1150 (P)		$v(CC) - v_{as}(COC)$
	1144	1144 (C, P)		$v(CC) - v_{as}(COC)$
1142				
		1138 (C)		
	1113			$v_s(COC)$ or $v_{as}(COC)$
1110	1111	1111		$v_s(COC)$ or $v_{as}(COC)$
		1092 (C)		
		1082 (C)		
	1061	1061 (P)		$v_{as}(COC) + r_s (CH_2)$
		1045 (C)		$v_s(SO_3)$
1040				
993				
		969 (C)		
	963	964 (P)		$r_{as} (CH_2)$

PEO (A)	PEO (X)	(PEO)$_9$ LiCF$_3$SO$_3$	(PEO)$_x$ KSCN	Peak assignment
948	949	952 (C)		r_s (CH$_2$) $-$ v_{as}(COC)
		940 (C)		
	934			
		927 (C)		
		860 (C)		
856	857			
	844	844 (P)		r_{as} (CH$_2$)
		833 (C)		
	828	828 (P)		
		760 (C)		δ_s(CF$_3$)
			746	SCN sym. stretching
			470	SCN bending

APPENDIX B

Abstract of Presentation at the 3rd National Symposium on Graduated Research,
Suranaree University of Technology, Thailand, 18-19 July 2002.

ชื่อบทความ : ภาษาไทย	การศึกษาเชิงกายภาพของโครงรูปพอลิเอทธิลีนออกไซด์
: ภาษาอังกฤษ	Conformational dependent physical properties of Poly(ethylene oxide)
ผู้แต่ง :	Jittima Chaodamrongsakul[1] and Visit Vao-soongnern[2]
ผู้นำเสนอบทความ :	Jittima Chaodamrongsakul
สังกัด :	Computational Chemistry Research Group, School of Chemistry, Institute of Science, Suranaree University of Technology, Nakhon Ratchasima 30000 Thailand
อีเมล์ :	[1]jeaborchid@hotmail.com **โทร:** (044) 223153
กลุ่มวิชา :	Science, Engineering and Technology

Solid Polymer Electrolytes (SPEs) are subject to intense study because they are vital components of modern electronic devices. SPEs consist of salts dissolved in solid high molecular weight polymer. Poly(ethylene oxide) (PEO) is the most interesting base material because of its high chemical and thermal stability, PEO can also solvate a wide variety of salts, even at very high salt concentrations. Theoretical studies based on statistical thermodynamics have been extensively performed for macromolecules in order to interpret and to understand their physical properties which strongly depend on the spatial arrangement of chain molecules. The Rotational Isomeric State (RIS) theory is an excellent calculation technique to predict the conformation-dependent physical properties of polymeric chains. RIS theory assumes that each skeletal bond has a small number of discrete rotational states and considers interactions between atoms on a chain separated by only a small number of bonds (short-range interactions). Interaction appearing upon a rotation around a single bond and two consecutive bonds is called *the first-order interaction* and *the second-order interaction*, respectively. These interactions are then parameterized and grouped into the matrix called *the statistical weight matrix.* Then the conformational dependent physical properties can be computed from these statistical weight matrices. The most frequently calculated properties are the mean-square end-to-end distance $\left\langle r^2 \right\rangle_0$, the mean-square radius of gyration $\left\langle s^2 \right\rangle_0$ and the characteristic ratio (C_n).

In this present work, RIS theory was developed in order to describe the conformational characteristics of PEO and compared their conformational dependent properties with those obtained from experiment.

Paper of Presentation at The 10th Tri-University International Joint Seminar & Symposium, Mie University, Japan, 17-21 October 2003.

Solid Polymer Electrolytes for an Application as Novel Energy Storage Materials

Jittima Chaodamrongsakul
Panita Decha
Visit Vao-soongnern

School of Chemistry,
Institute of Science,
Suranaree University of
Technology, Nakhon
Ratchasima 30000
THAILAND

ABSTRACT The research in solid polymer electrolytes (SPEs) for an application as novel energy storage materials has been performed at the School of Chemistry, Institute of Science, Suranaree University of Technology during the past 3 years. The system of interest is the plasticized PEO based electrolyte film of various compositions PEO/PEG/salt where PEO, PEG and salt act as a polymer host, a plasticizer and ionic charge, respectively. In this paper, we present the results from the system xPEO/LiCF$_3$SO$_3$/PEG, where x varies from 4 to 20 which were prepared by solution casting. The thermal properties, X-ray diffraction, vibrational spectra and electrical conductivity were studied. In addition, both DSC and XRD indicate a decrease in the percent of crystallinity for the plasticized system. Complexation of salt to polymer was substantiated by the appearance of new bands not present in PEO/PEG and also broadening of the C–O–C vibrations as the salt content increased. Room temperature conductivity changed increasing from 1.33×10^{-8} S cm^{-1} for 15 %wt PEG to 2.15×10^{-8} S cm^{-1} for 100 %wt PEG. This conductivity is much higher than in similar PEO/LiCF$_3$SO$_3$ systems that are not plasticized. The plasticizer seems to play a catalytic role in dissociating the salt and increasing the carrier concentration.

1. INTRODUCTION

The rapid development of portable electronic devices and electric/hybrid vehicles has increased the demand for compact, lightweight, high capacity batteries. Polymers are widely studied due to their significant potential for an application as a medium in rechargeable batteries. One of the earliest example involved complexes of alkali salts with poly(ethylene oxide) (PEO) studied in details by Wright and co-workers [1, 2]. However, it was particularly Armand and co-worker who pointed out and explored the usefulness of ion-conducting polymer electrolytes in high energy storage materials [3]. Since then, the application of this polymer-salt comlex or Solid Polymer Electrolyte (SPEs) to lithium batteries has been much interest. The research and development effort has been made throughout the world, the United States, Japan and Europe in particular. In these countries, such work is quite active in national projects such as USABC in the USA, NEDO in Japan and JOULE in Europe.

There are several advantages from replacing the aqueous electrolytes of conventional batteries with SPEs. First, polymers have good chemical stability and are generally unreactive with lithium, which is a very attractive battery anode because of its high reducing power and low equivalent weight. Second, SPEs can be used as thin layer; thus, the battery volume and weight devoted to the electrolyte are decreased. In addition, their mechanical properties are very attractive: polymer electrolytes are deformable, flexible, and easily fabricated by conventional manufacturing processes. The typical polymer-based battery is a layered thin-film structure in which a thin polymer electrolyte (~20-50 mm thick) is sandwiched between a lithium anode and an intercalation cathode (e.g., V$_6$O$_{13}$) (Figure 1). The entire cell can be produced as a continuous tape and can be rolled or folded into its finished shape [4].

Solid Polymer Electrolytes (SPEs) consist of salts dissolved in high molecular weight polymer. Polymer, which can dissolve salt must be comprise of O, N or S atoms because these atoms can interact with cation, and dissociate to have a better ionic conductivity. A considerable scientific effort has been dedicated to exploring and understanding the characteristics of these

electrolyte systems. Many investigations have focused on developing SPEs with high ionic conductivities (10^{-3} S/cm or higher) at ambient temperature. In majority of reported systems [5, 6], an alkali or alkaline earth metal salt is solubilized in a polymer, generally through complex formation with ion-chelating monomer units or with pendant moieties of the macromolecule.
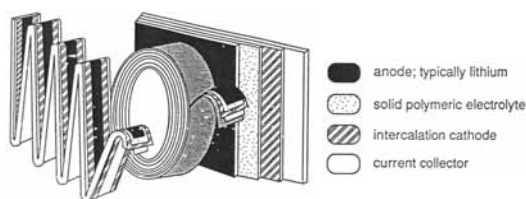
Figure 1 Schematic of polymer-based batteries. The thin-film composites are very flexible and can be folded or rolled into various geometries [4].

Poly(ethylene oxide) (PEO) is the most interesting base material because of its high chemical and thermal stability. PEO is a semicrystalline polymer, possessing both an amorphous and a crystalline phase at room temperature. It can also solvate a wide variety of salts, even at very high salt concentrations. The solvation of salts occurs through the association of the metallic cations with the oxygen atoms in the backbone. Several other polymers or copolymer are regarded as possible fruitful alternatives. However, none of them appears to have the same ability to solvate salts as PEO.

The multi-phase nature of PEO is most often regarded as a major problem in real working systems, since the ionic conduction has been shown to take place mainly in the amorphous phase. Furthermore, the same is true for the study of specific properties, where the effect of a variable can be concealed by the changes in the relative amounts of each phase. Many investigations have been done to reduce the crystalline content, via various approaches such as using blends, copolymers, comb-branch polymers and cross-linked polymer networks [4, 7-9]. The most dramatic improvement in the ionic conductivity of SPEs, with reduction of their crystalline content, is the addition of a low molecular weight or plasticizer. The conductivities were enhanced by producing systems with less crystallinity and lower glass-transtion temperatures than those found in simple PEO-salt systems. Plasticizers, in addition to

reducing the crystalline content and increasing the polymer segmental mobility, can result in greater ion dissociation, thus allowing large numbers of charge carriers for ionic transport; in addition, the cationic transport may be enhanced.

In this research work, we are interested in polymer electrolytes based on PEO/PEG/salt system at various plasticizer content and salt concentrations. In particular, PEO, PEG and salt act as a polymer host, plasticizer and ionic charge, respectively. PEG is selected because it has the same backbone structure as PEO and it is a suitable model to study experimentally and theoretically for the role of plasticizer on structures and properties of SPEs. Adding PEG to the system is expected to increase the proportion of amorphous region and consequently enhance the conductivity.

2. EXPERIMENTAL

2.1 Sample Preparation

PEO (MW 4 x 10^6 g mol^{-1}, Aldrich) and PEG (MW 600 g mol^{-1}, Fluka) were used as received. The salts, lithium trifluoromethanesulfonate (LiCF$_3$SO$_3$, Fluka), were dried in the vacuum oven at ~ 100-140 °C for 48 hours. Stoichiometric amount of PEO and the desired salt (different salt concentration and percent PEG) were dissolved in methanol and stirred continuously for 24 hours at room temperature. After continuous stirring, the solution was allowed to stand at room temperature for 24 h to facilitate degassing. To obtain thin film of the sample, the gelatinous polymer solution was cast on the glass plate. The films were dried in vacuum oven at 50 °C for 24 hours to remove solvent.

2.2 Sample Characterization

The interactions between salt and polymer in PEO/PEG/LiCF$_3$SO$_3$ complexes and salt association were investigated by FTIR. The study was carried out with FT-IR spectrometer Perkin-Elmer model: spectrum GX. The numbers of scans were 4 at the resolution of 4 cm^{-1}. The range of measurement was between 4000 cm^{-1} and 400 cm^{-1}. The diffraction patterns were recorded with a Bruker D5005 X-ray generator at room temperature between 2θ values 10 ° to 60 °. DSC data were collected with Perkin-Elmer DSC-7 of 8 – 10 mg from 25 to 100 °C at heating rate of 10 °C min^{-1} under N$_2$ atmosphere with the flow rate ~ 87 mL min^{-1}. Conductivity measurement was performed using a Hewlett-

Packard 4339B high resistance meter. The samples were sandwiched between the stainless steel blocking electrodes in sample holder (4 cm in diameter).

3. RESULT AND DISCUSSION

3.1 Fourier Transform Infrared Spectroscopy (FT-IR)

3.1.1 Ionic Association

Ionic association is one of the main factors limiting ion conduction in SPEs. This effect reduces the efficiency of the materials in any potential applications. One method of improving the conductivity of SPEs, without a great loss of their mechanical properties, is the addition of a low molecular weight co-solvent or plasticizer. The bands in the symmetric deformation of CF_3, $\delta(CF_3)$, spectra region are shown in Figure 2 for the $PEO/LiCF_3SO_3$ system with different weight percent of PEG. This band is sensitive to environmental changes around the triflate ion (CF_3SO_3). There are three bands in the $\delta(CF_3)$ region: a small band at 753 cm^{-1} assigned to "free" triflate ions, a large band at 757 cm^{-1} assigned to ion pairs and a small band at 760 cm^{-1} assigned to a higher aggregate or (PEO) $_3LiCF_3SO_3$ compound. These assignments are based on numerous spectroscopic studies of the triflate ion vibrations in a variety of ethylene-oxide based solutions. Here, "free" triflate ion refers to the triflate species with no degree of ionic association but may exhibit weak interactions with the polymer host (PEO). In the 16:1 complex, after addition of PEG, the band at 760 cm^{-1} due to the higher aggregate is presented. There is a very slightly change in the intensity of this band. With increasing PEG content to 100% weight PEG, the intensity of these band decrease and shift to 753 cm^{-1}.

Figure 3 IR spectra of 16:1 $PEO/LiCF_3SO_3$ at different % weight PEG in 900-800 cm^{-1} region.

3.1.2 Conformation of PEO Backbone

In Figure 3 the infrared spectra of the 16:1 $PEO/LiCF_3SO_3$ at different % weight PEG compound are compared with the spectra of pure PEO and PEG in the 800-900 cm^{-1} region. Vibrational modes of this spectral region were assigned to a mixture of predominantly CH_2 rocking and C-O stretching motions. The frequencies and intensities of these modes are sensitive to the values of backbone torsional angles. Thus, this band is ideal for monitoring the changes in the conformation of PEO upon addition of PEG. In $PEO/LiCF_3SO_3$ system, the band at 844 cm^{-1} is ascribed primarily to the CH_2 rocking mixed with C-O stretching. In the 16:1 $PEOLiCF_3SO_3$ plasticized system, the coordination between cation and ether oxygen could be observed from the shift of C-O-C stretching peak because of the strong positive effect of cation and plasticizer which decrease the electron density of C-O-C bond and weaken the C-O-C bond strength. Upon additon of plasticizer, there does not seem to be a very significant change in the conformation region.

Figure 2 IR spectra of 16:1 $PEO/LiCF_3SO_3$ at different % weight PEG in 800-700 cm^{-1} region.
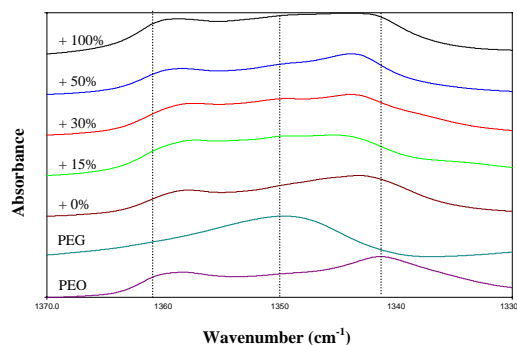
Figure 4 IR spectra of 16:1 $PEO/LiCF_3SO_3$ at different % weight PEG in 1400-1300 cm^{-1} region.

3.1.3 Interaction between plasticizer and PEO

Further evidence for the preferential interaction of the PEG with the crystalline PEO phase rather than $(PEO)_3LiCF_3SO_3$ compound can be seen in Figures 4, which shows infrared spectra in the CH_2 wagging region. It is established that the bands at 1360 and 1343 cm^{-1} are due to the crystalline PEO phase, while the band at 1353 cm^{-1} originate in the $(PEO)_3LiCF_3SO_3$ compound. Upon addition of PEG, the bands due to crystalline PEO slightly decrease in intensity, while replaced by a broad band roughly centered at 1350 cm^{-1}.

3.2 X-Ray Diffraction (XRD)

The XRD patterns of the 16:1 $PEO/LiCF_3SO_3$ at different % weight of PEG for 2θ region between 5° to 40° are reproduced in Figure 5. The diffractograms of the 16:1 $PEO/LiCF_3SO_3$ with % weight of PEG ranging from 15% to 100% display characteristic crystalline peaks centered around 15°, 19° and 23° which is ascribed to crystalline PEO. Addition PEG to the sample also gives peaks at the same positions but with lower intensities. It should be emphasized that 16:1 $PEO/LiCF_3SO_3$ at different % weight of PEG crystalline phase still existed but at a lower crystalline content than 16:1 $PEO/LiCF_3SO_3$. For the 16:1 $PEO/LiCF_3SO_3$ at 15 % and 100% weight of PEG, the intensity of crystalline PEO decreases more with addition 100% than 15% weight of PEG.

3.3 Differential Scanning Calorimeter (DSC)

The effect of adding PEG on the changes of T_m and ΔH_m of PEO and $PEO/LiCF_3SO_3$ were investigated using DSC technique. T_m, ΔH_m and the percentages crystallinity for each specimen are shown in Table 1.

The DSC thermograms of PEO + PEG and $PEO-LiCF_3SO_3$ 4:1 + 100 %wt PEG specimens are shown in Figure 6. The plasticizing effect of PEG is clearly seen as a shift in the melting temperature of PEO from 69.0 °C to 66.8 °C. It suggests that there is more amorphous domain in the complex due to the miscibility of PEG with PEO. ΔH_m and the percentages crystallinity of PEO + 100 %wt PEG are lower than that of PEO. It reveals that PEG is compatible with PEO and PEG reduces the crystallinity of PEO. XRD results of PEO + PEG system also support this idea.
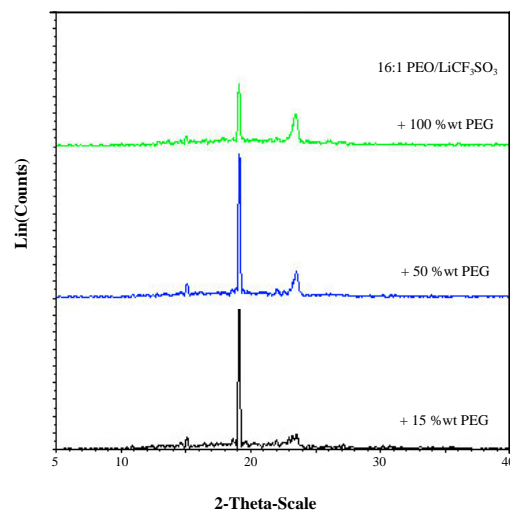
Figure 5 X-ray diffraction patterns of 16:1 $PEO/LiCF_3SO_3$

Table 1 Melting temperatures and percent crystallinity of polymer electrolytes as a function of adding PEG.

Composition	T_m (°C)	ΔH_m (J g^{-1})	Crystallinity (%)
PEO	69.018	131.638	69.983
PEG		$-$[a]	
$LiCF_3SO_3$	226.100	$-$	$-$
PEO+100%PEG	66.888	71.472	37.997
4:1 $PEO/LiCF_3SO_3$ +100%PEG	57.563	24.812	13.191

[a] no peak observed in DSC thermogram

However, ΔH_m and the percentages crystallinity of $PEO/LiCF_3SO_3$ 4:1 are lower than those of pure PEO. For the $PEO/LiCF_3SO_3$ specimen at ratios of 4:1 with 100 %wt PEG, there are two melting peaks at 57.6 °C (T_{m1}), and 137.5 °C (T_{m2}). The first peak is due to salt associated with pure PEO and a new endotherm peak at high melting temperature (137.5 °C) suggests the presence of complex phase. Supportive evidence is obtained by XRD results for $PEO/LiCF_3SO_3$ + %wt PEG shown in Figure 5. A reduction in T_{m1} of $PEO/LiCF_3SO_3$ 4:1 from 69.0 °C to 57.6 °C as the addition amount of PEG suggests that PEG is compatible with PEO and there is more amorphous domain in the complex.

3.4 Conductivity measurement

Comparisons of the ionic conductivity for $PEO/LiCF_3SO_3$ at room temperature with various $LiCF_3SO_3$ concentration and %wt PEG content are presented in Figure 7. The results display the ionic conductivity against %wt PEG, which ionic

conductivity increases with the $LiCF_3SO_3$ concentration upto $O:Li^+$ ratio equal to 16:1 and then decreases at very high $LiCF_3SO_3$ concentration. A decrease in ionic conductivity at high salt concentration was suggested to higher percentage of associated ions, ion pairs or ions acting as a transient cross-linking agent [10,11]. The FTIR, XRD, and DSC results shown earlier also confirm this discussion.
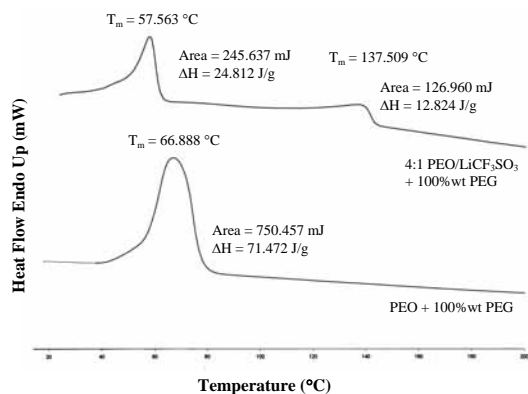
Figure 6 DSC thermogram of PEO+100 %wt PEG and 4:1 $PEO/LiCF_3SO_3$+100 %wt PEG.

In plasticized system, adding PEG shows better ionic conductivity. The ionic conductivity of $PEO/LiCF_3SO_3$ + %wt PEG (~10^{-8} S cm^{-1}) is about 10 times higher than $PEO/LiCF_3SO_3$ (~10^{-9} S cm^{-1}). The conductivity is improved due to an increase in the amorphous phase, which enhance the ion mobility. The FTIR, XRD, and DSC results also support this conclusion as a substantial amount of PEG plasticizer is incorporated in SPEs films. PEG reduces the crystallinity of PEO and $PEO/LiCF_3SO_3$ system by more than 45% and 80%, respectively. The ionic conductivity increases with increasing %wt PEG content and then it decreases at very high PEG content. It should be noted that the increase in an ionic conductivity to a maximum point for each sample depended on the amount of salt and PEG. The maximum value of an ionic conductivity is seen when O:Li ratio is 16:1. In our work, $PEO/PEG/LiCF_3SO_3$ electrolyte has the highest ionic conductivity when $O:Li^+$ ratio is 16:1 with 100 %wt PEG.

4. CONCLUSION

The FTIR, XRD and DSC results showed that the PEG was able to decrease the crystalline content and improve the ionic conductivity of $PEO/LiCF_3SO_3$ systems. A trend was observed in which the conductivity increased with increasing

salt concentration to a maximum $O:Li^+$ ratio equal 16:1, then decreased at very high salt concentration. The best composition that gave the highest ionic conductivity in this work was 16:1 $PEO/LiCF_3SO_3$ with 100 %wt PEG.
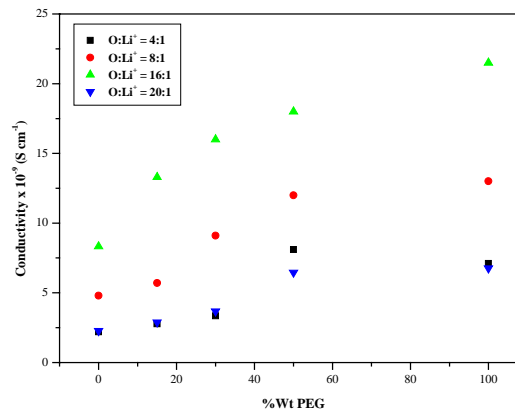
Figure 7 Ionic conductivity against % wt PEG of $O:Li^+$ ratio.

6. REFERENCES

[1] Fenton D. E., Parker J. M., Wright P. V. *Polymer.* 14, 1973. p589.
[2] Wright P. V. *Br. Polym. J.* 7, 1975. p319.
[3] Armand, M. B., Chabagno J. M., Duclot J. M. *Fast Ion Transport in Solids.* Elsevier North-Holland. 1979. p131.
[4] Mendolia M. S., Farrington G. C. Materials Chemistry: An Emerging Discipline 1995. p108.
[5] Chintapalli, S. Ph. D. Dissertation, University of Oklahoma Graduate College, USA 1996.
[6] Bruce, P. G. Solid state electrochemistry. United Kingdom: Cambridge University Press 1995.
[7] Quartarone E., Mustarelli P., Magistris A. *Solid State Ionics* 110, 1998. p1. p14.
[8] Song J. Y., Wang Y. Y., Wan, C. C. *J. Power Sources* 77, 1999. p183. p197.
[9] Sukeshini A. M., Kulkarni A. R., Sharma, A. *Solid State Ionics.* 113-115, 1998. p179. p186.
[10] Preechatiwong W., Schultz J. M. *Polymer.* 37, 1996. p5109. p5116.
[11] Sekhon S. S., Singh G., Agnihotry S. A., Chandra S. *Solid State Ionics.* 80, 1995. p37. p44.

CURRICULUM VITAE

JITTIMA CHAODAMRONGSAKUL

Born: March 14, 1978, Nakhon Ratchasima

Citizenship: Thailand

Education

1996 – 1999   B.Sc. Chemistry

Burapha University, Chonburi, Thailand

Experience

1999   Training in Operation Center Laboratory, Chonburi, Petroleum

Authority Thailand.

1999-2002   Teaching Asistance, School of Chemistry, Institute of Science,

Suranaree University of Technology, Nakhon Ratchasima.

Presentation

1. "Conformational dependent physical properties of Poly(ethylene oxide)" The 3rd National Symposium on Graduated Research, 18-19 July 2002, Suranaree University of Technology, Thailand.

2. "Solid Polymer Electrolytes for an Application as Novel Energy Storage Materials" The 10th Tri-University International Joint Seminar & Symposium 2003, 18-21 October 2003, Mie University, Japan.